Role of Cannabinoid Receptor 2 in Adult Neurogenesis and cyclic AMP Signalling detected with Live Cell FRET Imaging in a Cell Model and Microglia

Dissertation

zur Erlangung der Würde des Doktors der Naturwissenschaften
der Fakultät für Mathematik, Informatik und
Naturwissenschaften, Fachbereich Chemie
der Universität Hamburg

vorlegt von

Leonore Mensching-Johnson

aus Hannover

Hamburg, 2019

Dissertationsgutachter / *dissertation reviewers* :

1. Gutachterin / *first reviewer* : **Prof. Dr. Meliha Karsak**
Center for Molecular Neurobiology Hamburg (ZMNH), University Medical Center Hamburg-Eppendorf, Germany

2. Gutachterin / *second reviewer* : **Prof. Dr. Zoya Ignatova**
Institute for Biochemistry and Molecular Biology, University of Hamburg, Germany

Datum der Disputation / *disputation date* : **08.11.2019**

Diese Arbeit wurde im Zeitraum vom 1. Juni 2015 bis zum 31. Oktober 2018 am Zentrum für Molekulare Neurobiologie Hamburg (ZMNH) im Universitätsklinikum Hamburg-Eppendorf in der Arbeitsgruppe Neuronale und Zelluläre Signal Transduktion (Leitung: Prof. Dr. Meliha Karsak) angefertigt.

This work was done from June, 1st 2015 to October, 31st 2018 at the Center for Molecular Neurobiology Hamburg (ZMNH) at the University Medical Center Hamburg-Eppendorf in the research group Neuronal and Cellular Signal Transduction (Head: Prof. Dr. Meliha Karsak).

Contents

List of Figures

Acronyms

α_{2A}**AR** α_{2A}-adrenergic receptor

β**AR** β-adrenergic receptors

β_1**AR** β_1-adrenergic receptor

β_2**AR** β_2-adrenergic receptor

β_3**AR** β_3-adrenergic receptor

2-AG 2-arachidonoyl glycerol

AA arachidonic acid

Ab antibody

AC adenylyl cyclase

AD Alzheimer's disease

AEA anandamide

AKAP A kinase anchor protein

ATP adenosine triphosphate

BCP β-caryophyllene

BrdU 5-bromo-2'-deoxyuridine

CaM calmodulin

cAMP 3',5'-cyclic adenosine monophosphate

Cas9 CRISPR associated protein 9

CB2 cannabinoid receptor 2

CFP cyan fluorescent protein

CNGC cyclic-nucleotide gated ion channels

CNS central nervous system

cpm counts per million

CR calretinin

CREB cAMP response element-binding protein

CRISPR clustered regularly interspaced short palindromic repeats

CX3CR1 C-X3-C chemokine receptor 1

CXCR4 C-X-C chemokine receptor type 4

DAG 1,2-diacylglycerol

DAGL DAG lipase

DAMGO [D-Ala^2, N-MePhe^4, Gly-ol]-enkephalin

DCX doublecortin

DDM n-dodecyl β-D-maltoside

DG dentate gyrus

DMSO dimethyl sulfoxide

DNA desoxyribonucleic acid

DPBS Dulbecco's phosphate-buffered saline

EAE experimental autoimmune encephalitis

EC$_{50}$ half maximal effective concentration

ECS endocannabinoid system

Epac exchange protein directly activated by cAMP

ER endoplasmatic reticulum

ERK total ERK

ERK1/2 extracellular signal-regulated kinase

FAAH fatty acid amide hydrolase

FBS fetal bovine serum

FRET Förster resonance energy transfer

FSK forskolin

GCL granular cell layer

GDP guanosine diphosphate

GEF guanine nucleotide exchange factor

GFAP glial fibrillary acidic protein

GFP green fluorescent protein

GIRK G-protein-gated inwardly rectifying potassium

GPCR G-protein coupled receptor

GPR55 G-protein coupled receptor 55

GRK GPCR kinases

GTP guanosine triphosphate

HEK293 human embryonal kidney cells 293

HIV-1 human immunodeficiency virus 1

Iba-1 ionized calcium-binding adapter molecule 1

IBMX 3-isobutyl-1-methylxanthine

ICC immunocytochemistry

IFNγ interferon γ

IL-1β interleukin 1β

iNOS induced nitric oxide synthase

IP imunoprecipitation

IP$_3$ inositol trisphosphate

IQR interquartile range

IRES internal ribosome entry site

ISO isoprenaline

K$_i$ association constant

Ki67 antigen KI-67

LPS lipopolysaccharides

MAGL monoacylglycerol lipase

MAPK mitogen-activated protein kinase

MED median

mRNA messenger RNA

mTORC1 mammalian target of rapamycin complex 1

NAM negative allosteric modulator

NAPE-PLD N-acetyl phosphatidyl ethanolamine-hydrolysing phospholipase D

NArPE N-arachidonoyl phosphatidyl ethanolamine

NeuroD1 neurogenic differentiation 1

NF-κB nuclear factor kappa-light-chain-enhancer of activated B cells

NLP3 NLR family, pyrin domain containing 3

NPC neural progenitor cells

P/S penicillin/streptomycin

P2YR$_{12}$ P2Y receptor 12

PAM positive allosteric modulator

PC12 pepcan-12

PDE phosphodiesterase

pERK phosphorylated ERK

PFA phosphate-buffered formaldehyde

PI3K phosphatidylinositol 3-kinase

PKA protein kinase A

PKB protein kinase B

PKC protein kinase C

PLC phospholipase C

PLL poly-L-lysin

Prox1 prospero homeobox protein 1

PSD-95 postsynaptic density protein 95

Ras rat sarcoma

RET resonance energy transfer

RGC radial glia-like type 1 cells

RGS regulators of G-protein signalling

Rho Ras homolog gene family

RhoA Rho, member A

RNA ribonucleic acid

RNAseq RNA sequencing

scRNAseq single cell RNA sequencing

SDS-PAGE sodium dodecyl sulfate polyacrylamide gel electrophoresis

SGZ subgranular zone

Sox2 sex determining region Y-box 2

STAT signal transducer and activator of transcription

SVZ subventricular zone

Tbr2 T-box brain protein 2

TGFβ transforming growth factor β

THC *trans*-Δ^9-tetrahydrocannabinol

TNFα tumour necrosis factor α

TREM2 triggering receptor expressed on myeloid cells 2

TRP transient receptor potential

TRPA1 TRP cation channel, subfamily A, member 1

YFP yellow fluorescent protein

1 Zusammenfassung

Der G-Protein-gekoppelte Cannabinoid Rezeptor 2 (CB2) hat sich in den letzten zwei Jahrzehnten zu einem vielversprechenden Ziel in der Behandlung pathophysiologischer Prozesse im zentralen Nervensystem entwickelt. Wichtige Aspekte, auf die sich diese Arbeit fokussiert, sind hierbei die Rolle von CB2-Signalwegen für anti-inflammatorische Funktionen von Mikroglia, seine Relevanz in der Regulation adulter Neurogenese (AN) im Hippocampus, sowie die Aktivierung von cAMP- und MAPK-Signalkaskaden durch CB2 und seinen möglichen Interaktionspartnern, den β-adrenergen Rezeptoren (βAR). Zunächst war das Ziel, den Beitrag von basaler CB2-Aktivität an AN in der Maus zu quantifizieren. Anschließend sollte ein HEK293-Zellmodel generiert werden, welches es erlaubt, die Dynamiken intrazellulären cAMPs nach CB2-Stimulation in lebenden Zellen und in Echtzeit zu messen. Die Untersuchung eines möglichen funktionellen Crosstalks mit βAR in cAMP- und MAPK-Signalwegen, sowie die Rezeptorinteraktion zwischen CB2 und dem β_2-adrenergen Rezeptor (β_2AR) sollten ebenso untersucht werden, wie Echtzeit-cAMP-Dynamiken in adulten Mikroglia der Maus nach der Stimulation von CB2 und βAR.

Mithilfe von Immunfluoreszenzfärbung für den Proliferationsmarker Ki67 und Markern für neuronale Progenitorzellen, Doublecortin (DCX) und Calretinin (CR), in Gehirnschnitten von 16 bis 17 Wochen alten CB2-defizienten und Kontroll-Mäusen wurde AN in der subgranulären Zone des Gyrus Dentatus quantifiziert. Die Quantifizierung von AN in CB2-defizienten Mäusen zeigte, dass CB2 keinen Einfluss auf die Zellproliferation ($\sim 1 \times 10^5$ Ki67+ pro mm^3 der Körnerzellschicht (GCL)) und die Größe der DCX+ ($\sim 4.5 \times 10^5$ DCX+ pro mm^3 GCL) und DCX+/CR+ ($\sim 75\%$ aller DCX+ Zellen) Zellpopulationen im Gyrus Dentatus hatte.

In HEK293-Zellen, die den FRET-basierten cAMP-Biosensor Epac1-camps stabil exprimieren, wurde ebenso FLAG-hCB2 stabil integriert (Epac1-CB2-HEK-Zellen), um Effekte von CB2 und endogenen βAR auf den cAMP-Signalweg über die Detektion von FRET in Echtzeit an lebenden Zellen zu messen. FLAG-hCB2 und HA-hβ_2AR wurden in HEK293 Zellen ko-transfiziert, um per Ko-Immunopräzipitation eine mögliche Komplexbildung zu untersuchen und um per Immunfärbung und Fluoreszenzdetektion eine Ko-Lokalisierung der Rezeptoren an der Plasmamembran zu zeigen. Zelllysate von stimulierten Epac1-CB2-HEK-Zellen wurden per Western Blot analysiert und die Phosphorylierung von ERK1/2 wurde quantifiziert.

Mit dem generierten Zellmodell Epac1-CB2-HEK, welches auf Einzelzellebene Heterogenität aufweist, war es möglich, die Inhibition von cAMP-Produktion durch $G\alpha_i$-Proteine nach CB2-Stimulation mit unterschiedlichen CB2-Liganden in Echtzeit zu messen, sowie diese mit CB2-spezifischen inversen Agonisten/Antagonisten AM630 zu blocken. Epac1-CB2-HEK-Zellen zeigten ebenso ein negatives cAMP-Feedback nach initialer cAMP-Produktion durch den βAR-Agonisten Isoprenalin, welches durch Stimulation mit AM630 geblockt werden konnte. Ko-Stimulation von CB2 und βAR führte zu einer doppelt so starken Aktivierung von ERK1/2 in Epac1-CB2-HEK-Zellen verglichen mit der Einzelstimulation der Rezeptoren. Die Komplexbildung von CB2 und β_2AR wurde durch die gegenseitige Ko-Präzipitation von CB2 und HA-hβ_2AR gezeigt und ebenso konnte die Ko-Lokalisierung von ca. 24% aller positiven Fluoreszenzsignale der markierten Rezeptoren an der Zellmembran detektiert werden.

RNAseq-Expressionsdaten aus murinen adulten Mikroglia wurden in einer Meta-Analyse mit Bezug auf GPCR-assoziierte cAMP-Signalkaskaden zusammengefasst und die FRET-Echtzeitmessung von CB2- und βAR-Effekten auf die intrazelluläre cAMP-Konzentration in adulten Mikroglia von Wildtyp und CB2-defizienten Mäusen mit Epac1-camps-Expression wurde durchgeführt. Obwohl es nicht möglich war, CB2-Effekte auf cAMP-Signalwege in adulten Mikroglia zu messen, konnte ein negatives cAMP-Feedback nach Stimulation von βAR, ähnlich zu Epac1-CB2-HEK-Zellen, auch in Mikroglia festgestellt werden.

In dieser Arbeit wurde gezeigt, dass sich der Verlust von CB2 nicht auf die basale AN im Hippocampus auswirkt, und, dass das generierte Zellmodell Epac1-CB2-HEK die Möglichkeit zur Echtzeitmessung von CB2-Effekten auf die intrazelluläre cAMP-Konzentration möglich macht. Mit dieser Methode konnte ebenso ein funktioneller Rezeptor-Crosstalk mit βAR detektiert werden, der auch im MAPK-Signalweg gezeigt wurde. Die Interaktion zwischen CB2- und β_2AR konnte in ko-transfizierten HEK293-Zellen gezeigt werden.
Im Gegensatz zu CB2-Effekten, konnten das negative cAMP-Feedback nach cAMP-Produktion durch βAR-Stimulation in lebenden adulten heterogenen Mikroglia und in Echtzeit gemessen werden. Die Resultate dieser Arbeit haben Auswirkungen auf die Sicht der Rolle von CB2 in adulter Neurogenese und auf generelle Aspekte von CB2 und seinen Interaktionspartnern. Ebenso liefern sie Erkenntnisse zu cAMP-Signalkaskaden in Mikroglia, die wichtig für CB2-Effekte während neuroinflammatorischer Prozesse sein könnten.

2 Abstract

In the last two decades, the G-protein coupled cannabinoid receptor 2 (CB2) has emerged as a target for treating pathophysiological processes in the central nervous system. The role of CB2 signalling in anti-inflammatory functions of microglia, its relevance for the regulation of adult hippocampal neurogenesis (AN) and the activation of cyclic AMP and MAPK pathways by CB2 and its putative interaction partners, β-adrenergic receptors (βAR), are the main aspects this work is focused on. First, the aim was to quantify the contribution of basal CB2 signalling to AN in mice. Second, the goal was to generate a HEK293 cell model that allows for the live measurement of CB2-mediated cAMP dynamics and the investigation of possible functional crosstalk with βAR in cAMP but also in MAPK pathways. The possible interaction between CB2 and β_2AR was specifically investigated. Finally, CB2- and βAR-mediated cAMP signalling and functional crosstalk were studied in primary adult mouse microglia.

AN in the subgranular zone of the dentate gyrus was quantified in 16 to 17-week-old wildtype and CB2-deficient mice using immunostaining of brain sections for the cell proliferation marker Ki67 and neural progenitor markers doublecortin (DCX) and calretinin (CR). Quantification of AN revealed that CB2-deficiency did not impair cell proliferation ($\sim 1 \times 10^5$ Ki67+ per mm^3 granule cell layer (GCL)) or the size of the DCX+ ($\sim 4.5 \times 10^5$ DCX+ per mm^3 GCL) or DCX+/CR+ cell population ($\sim 75\,\%$ of all DCX+ cells) in the dentate gyrus.

Using HEK293 cells that stably express the FRET-based cAMP biosensor Epac1-camps, cells with additional stable heterologous expression of FLAG-hCB2 were generated (Epac1-CB2-HEK) and CB2- and endogenous βAR-mediated effects on intracellular cAMP levels were measured via live cell FRET imaging. Co-immunoprecipitation (IP) and immunocytochemistry in FLAG-hCB2 and HA-hβ_2AR co-transfected HEK293 cells were used to investigate complex formation and co-localisation of the two receptors at the cell membrane and activation of the MAPK pathway was determined by detecting the phosphorylation of ERK1/2 in stimulated Epac1-CB2-HEK cell lysates via immunoblotting.
With the generated cell model Epac1-CB2-HEK, it was possible to measure live CB2-mediated inhibition of cAMP production by Gα_i subunits and its blockage using different CB2 ligands despite the heterogeneity of the cell model on a single cell level. Epac1-CB2-HEK cells also showed a negative cAMP feedback after Gα_s-mediated cAMP production elicited by βAR agonist isoprenaline, which was reversible by the CB2 inverse agonist/antagonist AM630. Co-stimulation of CB2 and βAR led to a two-fold stronger acti-

vation of ERK1/2 in Epac1-CB2-HEK cells compared to the activation of a single receptor. Complex formation of CB2 and β_2AR was demonstrated by showing the co-precipitation of HA-hβ_2AR in FLAG-hCB2-IP samples and vice versa in HEK293 cells transiently transfected with both receptors. Co-localisation at the cell membrane was seen for around 24% of all positive fluorescent signals from both labelled receptors.

In a meta-analysis of mouse microglia RNAseq data, previously published research was summarised regarding the expression of GPCRs and the cAMP signalling machinery. To study endogenous CB2 and βAR effects on cAMP signalling, adult microglia from wildtype and CB2-deficient mice ubiquitously expressing Epac1-camps were isolated and live cell FRET imaging was conducted. Detection of CB2 effects on cAMP signalling in adult microglia was not possible with the present approach, however, endogenous βAR signalling was detectable and displayed a negative cAMP feedback after initial cAMP production similar to Epac1-CB2-HEK cells with variability on a single cell level.

In this work, it was shown that CB2 deficiency did not impair basal levels of AN in mice and that using a newly generated Epac1-CB2-HEK cell line to measure live cell dynamics of CB2-mediated cAMP signalling, functional crosstalk with βAR was seen, that was also detected for the MAPK pathway ERK1/2. Evidence for the interaction between CB2 and β_2AR was shown in co-transfected HEK293 cells. Detection of live cAMP changes after CB2 stimulation in adult mouse microglia failed, but live cAMP signalling from βAR showed a negative cAMP feedback after initial cAMP production and heterogeneity on a single cell level. These results have implications for the role of CB2 in AN as well as for general aspects of CB2 signalling and possible interaction partners. They also provide insights into microglial cAMP signalling which may be of importance for CB2-mediated effects during neuroinflammatory processes.

3 Introduction

This work focuses on the cannabinoid receptor 2 (CB2), a G-protein coupled receptor (GPCR) that is part of the endocannabinoid system (ECS). In the following introductory chapters selected aspects of CB2-mediated signalling, functional implications and theoretical background on GPCR signalling are reviewed to give the reader an overview of the research field.

3.1 G-protein Coupled Receptors

G-protein coupled receptors are diverse transmembrane proteins found in all eukaryotes that integrate extracellular cues into cellular responses. Their important involvement in physiological and pathophysiological biological processes in humans makes them an important target for biomedical research and drug development (Sriram and Insel, 2018). To date, it is estimated that 35 % of all drugs approved in the European Union and the United States target GPCRs, establishing them as the most frequently drug-targeted proteins (Sriram and Insel, 2018; Campbell and Smrcka, 2018).

In humans, the GPCR superfamily consists of at least 810 different genes and is categorised into different classes. Class A rhodopsin-like GPCRs are the largest group with more than 700 receptors (Stevens et al., 2012). Class B secretin-like and class C glutamate-like receptors each have 15 receptors and the classes E and F (adhesion and frizzled) receptors each consist of 24 receptors in humans (Stevens et al., 2012). Olfactory receptors are the most abundant class A GPCRs with almost 400 receptors (Stevens et al., 2012), and from the remaining receptors more than 100 are so-called orphan receptors where endogenous ligands have not yet been identified (Wacker et al., 2017). Structurally, a GPCR has seven transmembrane domains (α-helices) that are highly conserved, an extracellular N-terminus and an intracellular C-terminus exposing three interhelical loops towards each side of the membrane (Venkatakrishnan et al., 2013). Depending on the GPCR-ligand pairing, binding to the ligand can involve the N-terminus, the transmembrane domains and/or the loops (Venkatakrishnan et al., 2013).

GPCRs trigger G-protein dependent and independent intracellular signalling cascades. G-protein dependent pathways are activated via the heterotrimeric G-protein complex that consists of the three G-protein subunits, α, β, and γ, and binds to cytoplasmic domains of a GPCR (Flock et al., 2017). When the Gα subunit is bound to guanosine diphosphate (GDP), it associates with the G$\beta\gamma$-heterodimer. Upon ligand activation of a GPCR,

conformational changes enable it to act as a guanine nucleotide exchange factor (GEF), exchanging the GDP from the Gα to a guanosine triphosphate (GTP) after receptor association with the G-protein complex. This leads to further conformational changes causing the GTP-bound Gα and G$\beta\gamma$ to dissociate from the receptor (Oldham and Hamm, 2008). Both, Gα and G$\beta\gamma$, then affect their downstream targets and transduce the extracellular signal onto intracellular effectors (Wettschureck and Offermanns, 2005; Gurevich and Gurevich, 2018). The Gα subunit has an intrinsic GTPase activity that hydrolyses GTP to GDP and inorganic phosphate and therefore self-deactivates it to start a new activation cycle (Oldham and Hamm, 2008).

Following ligand activation of a GPCR, its phosphorylation by GPCR kinases (GRK) causes the scaffold-protein β-arrestin to bind the receptor and initiate its internalisation. Internalisation of GPCRs via clathrin-dependent endocytosis is an important step in the desensitisation of G-protein dependent signalling and their trafficking to intracellular sites, such as endosomes or the Golgi (Wang et al., 2018). Recent evidence supports the continued signalling of internalised ligand- and scaffold-bound GPCRs at these sites that significantly influences the cellular response as it has been shown for the β_2-adrenergic receptor (β_2AR) (Calebiro et al., 2009).

It has been accepted that GPCR β-arrestin dependent signalling is important for the prolonged activation of the mitogen-activated protein kinase (MAPK) ERK1/2 (extracellular signal-regulated kinase), a signalling pathway integral to cell survival, proliferation and differentiation (Wang et al., 2018; Shenoy et al., 2005). Using β-arrestin or G-protein knockout cell lines and pharmacological tools, several studies have questioned the importance of β-arrestin in activating ERK1/2 while showing that this activation can rely solely on the heterotrimeric G-protein complex (Grundmann et al., 2018). On the other hand, Luttrell et al. (2018) show that both β-arrestin and G-protein dependent pathways contribute to the activation of MAPK and that the deletion of either pathway may increase the dependence on the remaining signalling proteins. Further research may resolve this controversy (Wootten et al., 2018) but it illustrates that the abundance or absence of intracellular proteins binding GPCRs modulates engaged signalling pathways and that experimental designs must account for this.

In addition to β-arrestin, there are PDZ- and Non-PDZ scaffold proteins that bind GPCRs at their C-terminus or at intracellular loops, respectively (Wootten et al., 2018). PDZ scaffolds, like postsynaptic density protein 95 (PSD-95) or Homer1 associate with kinases and phospholipases, like phospholipase C (PLC) and protein kinase A (PKA), as well as ion channels to modulate the activation of these downstream pathways. They may also directly influence the interaction of G-proteins or β-arrestin with a GPCR regulating G-protein dependent signalling and internalisation rates (Wootten et al., 2018). Signalling regulation can also be achieved by the engagement of a GPCR with Non-PDZ scaffolds, like the A kinase anchor protein (AKAP), that can bind the kinases PKA and

protein kinase C (PKC) in addition to phosphatases and intracellular receptors. AKAPs have also been shown to bind the small G-protein Ras (rat sarcoma) and STAT (signal transducer and activator of transcription) (Wootten et al., 2018). The coupling of GPCRs to these regulatory proteins is highly dynamic and may be modulated by the cell's general state or the conformation of the receptor.

Another layer of complexity added to GPCR signalling is the capability of some receptors to form homo- and/or heterodimers. Class C glutamate receptors e.g. are frequently present in dimers, however, for class A rhodopsin-like GPCRs dimerisation seems to be less frequent (Felce et al., 2017). It has been shown by Felce et al. (2017) that the ancestor of all rhodopsin-like receptors was and a majority of GPCRs on HEK293 is monomeric and that only around 20 % of the tested GPCRs may form dimers.
Especially GPCR heterodimers may have profound impact on cellular signalling as receptor cross-agonism, cross-antagonism, and crosstalk can lead to unexpected signalling behaviour *in vivo*, where endogenous ligands are dynamically released and/or continuingly present (Gomes et al., 2016).
Three criteria for the classification of a functional GPCR heterodimer have been reviewed by Gomes et al. (2016) and entail that heteromers should physically interact and colocalise (1) and show distinct signalling properties compared to each single receptor (2, unique biochemical fingerprint). Additionally, the disruption of the heteromer via antibodies, specific ligands or mutated receptor variants should lead to the loss of unique heteromer-signalling and protein complexes (3).
The characterisation of these protein-protein interactions has been facilitated using resonance energy transfer (RET) methods allowing the live imaging of GPCR complex formation (Goddard and Watts, 2012). Still, *in vivo* studies on the functional impact of GPCR heterodimers are rare. Among the best described heterodimers, that fulfill all three criteria, is the δ-μ opioid receptor heterodimer that shows enhanced ligand potency and efficacy as a heterodimer and is of importance for the treatment of pain with opiate analgetics (Gomes et al., 2000).

There are many reported GPCR heterodimers that show the presence of one or two criteria for functional heterodimerisation in heterologous expression systems, however, impact and relevance of these receptor pairings in a physiological setting must be further investigated.
The temporal and spatial compartmentalisation of GPCR signalling by the complexity of regulatory proteins, ligands and GPCR interactions has important implications on the manipulation of GPCRs via drugs and is continuing to make understanding GPCR physiology in health and disease a challenging task.

3.1.1 Heterotrimeric G-Protein Subunits and GPCR Signal Transduction

Although GPCRs show a high diversity, they couple with a relatively limited number of Gα and G$\beta\gamma$ subunits to activate distinct signalling pathways. Among downstream effector proteins of Gα and G$\beta\gamma$ subunits are adenylyl cyclases (AC), the enzymes that produce the ubiquitous second messenger 3',5'-cyclic adenosine monophosphate (cAMP) from adenosine triphosphate (ATP), ion channels and protein kinases.

Gα subtypes are encoded by 16 genes in humans, are functionally diverse and classified into four groups, Gα_s, G$\alpha_{i/o}$, G$\alpha_{q/11}$, and G$\alpha_{12/13}$, according to their downstream effectors. Members of one group are structurally similar but can have very different expression patterns (Wettschureck and Offermanns, 2005).
The Gα_s group with its members Gα_s, a longer version of Gα_s named Gα_{sXL} and Gα_{olf} targets all nine membrane-bound isoforms of the cAMP-producing enzyme AC. The binding of Gα_s leads to an increased enzymatic activity of ACs and therefore to an increase in cAMP production (Wettschureck and Offermanns, 2005; Northup et al., 1980).

Gα_{i1}, Gα_{i2}, and Gα_{i3} belong to the G$\alpha_{i/o}$ group and are subunit isoforms that inhibit ACs and their production of cAMP (Taussig et al., 1993). Interestingly, not all AC isoforms are targeted by Gα_i. It has been shown that only AC$_1$, AC$_5$, and AC$_6$ are directly inhibited by Gα_i (Sunahara, 2002; Taussig et al., 1994). Gα_o and Gα_z are less abundant G$\alpha_{i/o}$ proteins. Gα_z has been shown to affect the Rap1 GTPase activating protein and to inhibit AC$_1$, AC$_5$, and AC$_6$ (Campbell and Smrcka, 2018; Meng et al., 1999), whereas AC inhibition by Gα_o has only been reported for AC$_1$ (Sadana and Dessauer, 2009). The more specialised G$\alpha_{i/o}$ proteins are Gα_{gust}, Gα_{t-r} and Gα_{t-c} and are only found in taste cells, rods, and cones (Wettschureck and Offermanns, 2005).

The smallest Gα group consists of Gα_{12} and Gα_{13} and links GPCRs to the activation of Rho (Ras homolog gene family) signalling pathways. They are abundantly expressed and can directly interact with different RhoGEFs to mediate the assembly of cytoskeleton structures as well as cell adhesion molecules (Wettschureck and Offermanns, 2005; Siehler, 2009). It has also been reported that AC$_7$ is a downstream effector of G$\alpha_{12/13}$ and is synergistically regulated when additionally stimulated with Gα_s (Jiang et al., 2008, 2012).

The two ubiquitously expressed G$\alpha_{q/11}$ group members, Gα_q and Gα_{11} , are implicated in the activation of PLCβ-mediated release of intracellular Ca^{2+} and PKC activation (Campbell and Smrcka, 2018). Gα_q and Gα_{11} have 90 % sequence similarity and seem to have identical biological functions. GPCRs that couple these Gα subunits can also interchange them (Offermanns et al., 1994; Wettschureck and Offermanns, 2005). Another effector of Gα_q and Gα_{11} is p63RhoGEF that further activates Rho, and for Gα_q, PKCζ has been reported as a downstream effector (Campbell and Smrcka, 2018). Besides activating

PLCβ, no other functions are reliably associated with Gα_{14} and G$\alpha_{15/16}$, the other members of the G$\alpha_{q/11}$ group. It has been reported, though, that mutations in the Gα_{14} gene can cause childhood vascular tumours (Lim et al., 2016).

The intrinstic GTPase activity of all Gα subunits that recycles Gα for a new GPCR activation cycle can be regulated by around 30 different regulators of G-protein signalling (RGS). Several RGS show selective targeting of different Gα subunits and are therefore able to specifically regulate Gα-turnover and signalling rates (Syrovatkina et al., 2016).

The second part of the heterotrimeric G-protein complex, the G$\beta\gamma$ subunit, interacts with and affects a large variety of downstream effectors. Gβ subunits are less diverse, with five different isoforms compared to 12 variants of Gγ in mammals. Gβ_{1-4} share a high homology and are most likely functionally interchangeable as they couple to any Gγ subunit (Davis et al., 2005). Gβ_5 is mainly expressed in the brain and there is no evidence that it interacts with either Gγ or Gα *in vivo*. However, it has been shown that Gβ_5 forms complexes with RGS proteins possibly modulating their binding to Gα subunits (Witherow et al., 2000).
Different G$\beta\gamma$ combinations do not seem to have different functional effects although the knockout or knockdown of specific subunit isoforms can lead to severe phenotypes (Campbell and Smrcka, 2018). After GPCR activation, G$\beta\gamma$ subunits regulate ion channels, stimulate specific AC variants (2, 4, 5, 6, and 7) or inhibit them(1, 8, and 3). They also activate PLC and phosphatidylinositol 3-kinases (PI3K) that further activate protein kinase B (PKB) (also called Akt) (Sadana and Dessauer, 2009; Wettschureck and Offermanns, 2005).

Most GPCRs are predominantly coupled to a particular Gα subunit, however, for some receptors coupling to different Gα has been shown in heterologous cell models as well as endogenous systems (Wacker et al., 2017). In 2017, Flock et al. (2017) revealed that GPCR-Gα selectivity is achieved via barcode sequences in the Gα proteins that are recognised by different receptor regions in different GPCRs. This could explain the development of the vast diversity of GPCRs that bind a small set of highly conserved Gα proteins and help to understand observations like the Gα-switching or the pre-coupling of multi-complexes including GPCR, G-proteins and downstream effectors, like ACs (Campbell and Smrcka, 2018).

3.1.2 Activation of GPCRs

GPCRs respond to a variety of ligands that ranges from small and large peptides, such as cytokines and hormones, to lipids, ions, odorants or photons (Wettschureck and Offermanns, 2005). Ligands are pharmacologically characterised according to their efficacy to produce GPCR activity relative to their concentration (half maximal effective concentration (EC_{50})) and according to their affinity to bind the receptor (association constant (K_i)). Endogenous ligands that elicit maximal receptor activation for a signalling pathway are termed full agonists, whereas agonists that fail to fully activate the GPCR are partial agonists. A neutral antagonist binds the receptor but does not initiate changes in signalling and an inverse agonist can inhibit receptor activation below basal levels that are maintained by constitutive receptor activity (Wacker et al., 2017).

Agonists, antagonists and inverse agonist bind the orthosteric binding pocket of a receptor that represents the site of endogenous ligand binding. Ligands that not only bind the orthosteric site but additionally bind an alternative allosteric site are called bitopic ligands.

Allosteric sites may also be used by positive (PAM) or negative (NAM) allosteric modulators. These small molecules can facilitate or hinder the binding of an orthosteric ligand affecting its receptor affinity (Wacker et al., 2017).

In the multi-state GPCR model (Hill, 2006), it is stated that GPCRs exist in various spontaneously or constitutively active and inactive conformations that form an activity equilibrium. Ligands may have different affinities towards a receptor conformation and then stabilise the GPCR in a particular conformation, shifting the equilibrium to elicit biological effects (de Ligt et al., 2000; Milligan, 2003; Sato et al., 2016). Additionally, protean ligands may act as an agonist in systems with low receptor activity but show inverse agonism when a receptor exhibits a high degree of constitutive activity (Kenakin, 2001). Using heterologous expression systems, it was possible to describe the impact of constitutively active receptor conformations that show ligand-independent signalling activity. Many antagonists were followingly classified as inverse agonists that bind constitutively active receptor forms and block or reduce their activity (Milligan et al., 1995; Hill, 2006; Kenakin, 2001).

It is a current research focus to identify GPCRs that exhibit a high degree of constitutive activity in endogenous systems and find selective inverse agonists to target their function (Sato et al., 2016).

The ligand-induced stabilisation of GPCR conformations can additionally trigger the selective intracellular binding of one receptor to different signal transducers and modulators depending on the ligand (Wootten et al., 2018). This characteristic is called biased agonism or functional selectivity and describes the ligand's dynamic efficacy for different signalling pathway. Biased ligands have a high clinical potential as the targeted modulation of a disease-involved GPCR signalling pathway can lead to more efficient drugs

(Wootten et al., 2018).

The multitude of GPCR activation modes that is shaped by the combination of various ligands, G-proteins, regulatory and interacting proteins as well as intrinsic capacities of the receptor itself shows the highly dynamic nature of GPCR signalling and their continuously growing potential in clinical applications.

3.1.3 Cyclic-AMP Signalling Pathways and Methods of cAMP Measurement

Cyclic AMP, first described in 1958 by Sutherland and Rall (1958), is an ubiquitinous second messenger that is integral to cellular physiology and the cells' ability to regulate functional responses to external stimuli (Sassone-Corsi, 2012). Important cellular functions, such as growth and differentiation, are influenced and governed by cAMP through its effect on gene transcription, ion currents, metabolism and other signal transducers (Sassone-Corsi, 2012). Control of intracellular cAMP levels is achieved by two enzymes, the cAMP-producing adenylyl cyclases and the cAMP-degrading phosphodiesterases (PDE) (see Figure 3.1 for an overview).
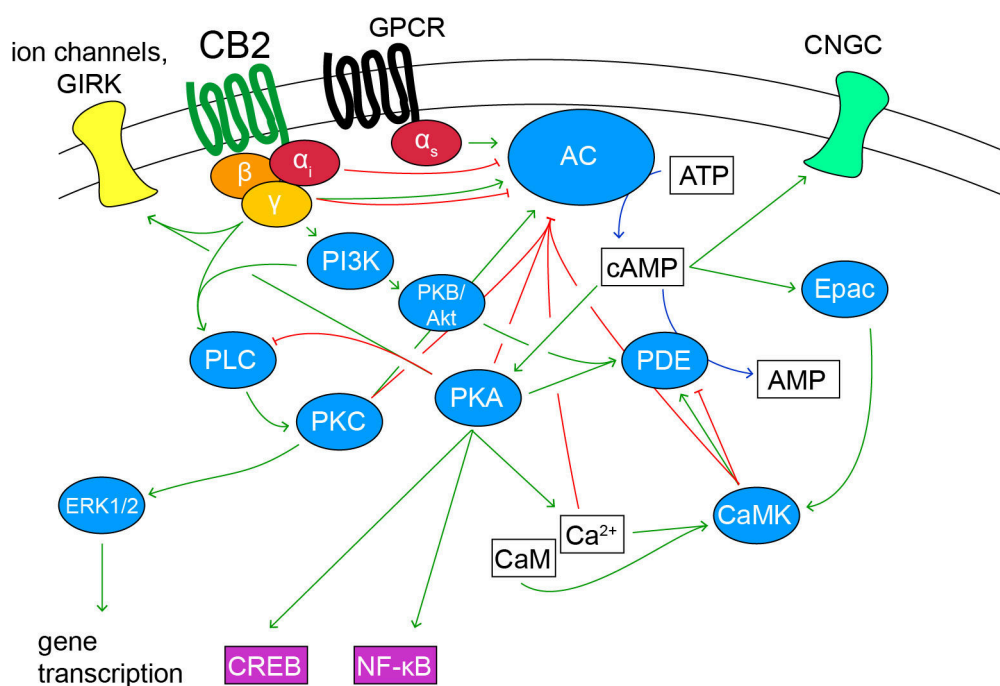
Figure 3.1. CB2-mediated signalling pathways. Depicted are a selection of signalling pathways engaged by CB2 and other GPCRs. Adapted from Sassone-Corsi (2012); Boularan and Gales (2015).

ACs catalyse the conversion of ATP to cAMP and are a main downstream target GPCR activation. In addition to the nine membrane-bound isoforms, there is a tenth, soluble isoform (AC_{10}) that is not stimulated by $G\alpha_s$ subunits (Sunahara, 2002; Sadana and Dessauer, 2009). AC activity can be modulated isoform-specific and AC isoform expression can shape tissue-specific cAMP signalling after GPCR activation. All membrane-bound isoforms are stimulated by $G\alpha_s$ subunits but only some are inhibited by members

of the $G\alpha_{i/o}$ (see Introduction section 3.1.1). Continued inhibition of ACs by $G\alpha_i$ subunits can lead to the sensitisation of ACs and followingly to a cAMP increase when receptor activation is terminated (Watts and Neve, 2005). This adaptive response is most obvious for AC_5, and AC_6, when additionally stimulated with $G\alpha_s$ (Watts and Neve, 2005).

The calmodulin (CaM)-sensitive group of ACs, AC_1, AC_3, and AC_8, is additionally stimulated by calcium-bound calmodulin and in a feedback loop AC_1 and AC_3 may be inhibited by calmodulin kinases IV and II, respectively. This group of ACs is also the only one that is inhibited by $G\beta\gamma$ subunits, which, in turn, have stimulatory effects on AC isoforms 2, 4, 5, 6, and 7 (Wettschureck and Offermanns, 2005; Sadana and Dessauer, 2009). It has been reported that $G\alpha_{12/13}$ subunits may also directly regulate AC_7 (Jiang et al., 2008, 2012), however, these effects are not well investigated and demand further specification.

The protein kinases A and C are also main regulators of AC activity with stimulatory and inhibitory effects on different AC isoforms. High intracellular Ca^{2+} concentration inhibits all ACs but AC_5 and AC_6 are sensitive towards this Ca^{2+}-mediated inhibition at much lower physiological concentrations, which highlights the link between intracellular Ca^{2+} and cAMP (Sadana and Dessauer, 2009).

The activation of ACs by the plant-derived diterpene forskolin (FSK) has been a valuable tool in the investigation of ACs and cAMP signalling as it initiates cAMP production in most cells, targeting AC_1 to AC_8. Interestingly, FSK binds to a unique site at the AC and is therefore not competitively influencing other AC regulators but may synergistically enhance their effect (e.g. $G\alpha_s$). Synergistic effects of FSK with other proteins, like $PKC\alpha$, have also been described (Insel and Ostrom, 2003; Sadana and Dessauer, 2009).

The main downstream effectors of cAMP are PKA, Epac (exchange protein directly activated by cAMP), and CNGC (cyclic-nucleotide gated ion channels). PKA, as the best described cAMP target, phosphorylates several transcription factors, such as CREB (cAMP response element-binding protein) or NF-κB (nuclear factor kappa-light-chain-enhancer of activated B cells) and therefore activates gene expression. It also interacts with different metabolic enzymes, like acetyl coenzyme A, as well as with ACs and PDEs in cAMP feedback loops (Sassone-Corsi, 2012).

The regulation of other signal transducers, like PLC, MAPK, Ras homolog gene family (Rho) or ion channels further shows the important role of cAMP-dependent PKA activation for cellular function. Through binding of AKAPs, PKA can be associated with a downstream effector to coordinate signalling spatially and temporally (Sassone-Corsi, 2012; Campbell and Smrcka, 2018).

Cyclic AMP-dependent activation of the Epac proteins (Epac1 and Epac2) leads to the activation of small GTPases from the Ras-related protein family regulating cell adhesion via integrin (Robichaux and Cheng, 2018). Through the binding of CNGC by cAMP Ca_2^+ currents are modulated, which has effects on ACs and PDEs. The activation of Na^+ or K^+ CNGC can influence membrane potentials with strong effects on, e.g. neurons.

The cAMP-degrading enzyme PDE catalyses the hydrolysis of cAMP. PDEs are encoded by eleven genes and have several different isoforms that are either cAMP-specific or cyclic guanosine monophosphate (cGMP)-specific, or act on both cyclic nucleotides. Similar to ACs, their cell specific isoform expression profile, localisation and association with other effectors makes them an important target for the regulation of cAMP levels by both endogenous signal transducers and pharmacological drugs (Keravis and Lugnier, 2012). Of special interest for drug development in cardiovascular disease, inflammation or neurodegeneration is cAMP-specific PDE4 (Fertig and Baillie, 2018; Pearse and Hughes, 2016), that is also the most diverse subfamily of PDEs with over 20 different isoforms (Keravis and Lugnier, 2012). PDE7 and PDE8 are also cAMP-specific isozymes and PDE1, 2, 3, 10, and 11 can hydrolyse cAMP as well as cGMP (Keravis and Lugnier, 2012).

PDEs are strongly regulated by PKA which leads to a negative cAMP feedback loop after cAMP-dependent activation of PKA. Furthermore, PDE activity can be inhibited by ERK1/2 and CaM kinases and stimulated by PKB/Akt and CaM (Sassone-Corsi, 2012; Agarwal et al., 2014; Froese and Nikolaev, 2015).

3.1.4 Live cAMP Measurement with FRET-based Biosensors

Over the last few years, advancements in the measurement of intracellular cAMP levels have contributed significantly to the understanding of the spatial and temporal control of cAMP-dependent signalling in cells. The use of Förster resonance energy transfer (FRET)-based cAMP biosensors allows for the live measurement of cAMP levels in the whole cell or at particular subdomains on a single cell level (Nikolaev and Lohse, 2006; Froese and Nikolaev, 2015). FRET, the emission-less energy transfer between two fluorophores via dipole-dipole coupling, is observed when the three following biophysical properties are given: (1) the distance between the fluorophores must be less than 10 nm, (2) spectral overlap of the donor's emission and the acceptor's excitation spectrum, and (3) the parallel orientation of the two fluorophores (Förster, 1948). The FRET efficiency reflects the relative amount of energy transfer to overall donor excitation and is decreasing linear to the sixth power of the distance between the fluorophores (Förster, 1965).

Green fluorescent protein (GFP) variants cyan fluorescent protein (CFP) and yellow fluorescent protein (YFP) are commonly used FRET pairs with CFP as the donor fluorophore and YFP as the acceptor. Different cAMP sensors have been designed that use cAMP binding domains of PKA, CNGC or Epac coupled to a CFP-YFP pair (Boularan and Gales, 2015). Common for FRET-based cAMP sensors is that the binding of cAMP initiates a conformational change of the sensor that leads to a change in FRET between the two sensor-coupled fluorophores.

The cAMP biosensor used in this work was developed by Nikolaev et al. (2004a) and is termed Epac1-camps (**cAMP s**ensor). It consists of the cAMP-binding domain of Epac1
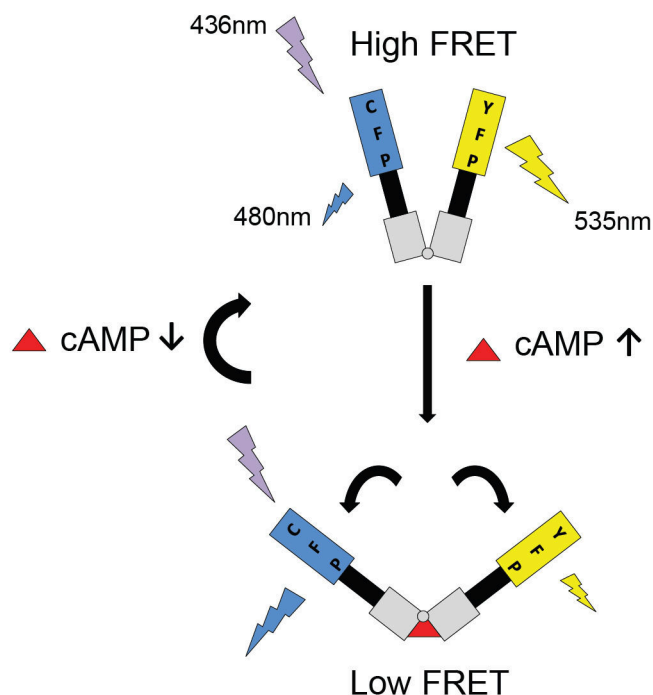
Figure 3.2. Scheme of the FRET-based cAMP biosensor Epac1-camps. When cAMP binds the cAMP-binding domain of the biosensor the distance between the fluorophores CFP and YFP increases and FRET decreases. FRET changes can be measured by detecting fluorescent emission light from CFP at 480 nm and YFP at 535 nm after excitation of CFP with 440 nm. Adapted from Calebiro et al. (2010).

and is flanked by enhanced CFP and YFP. Binding of cAMP leads to an increased distance between CFP and YFP and therefore to a reduced FRET efficiency. The change in FRET can be detected, e.g. via sensitised emission while measuring the emission intensity of CFP and YFP upon donor excitation and calculating a ratio (Börner et al., 2011; Sprenger et al., 2012) (Fig. 3.2). Due to the design of the sensor, CFP and YFP are in equimolar concentration and the single cAMP binding domain allows for a rapid activation of the sensor compared to, e.g. PKA-based sensors (Willoughby and Cooper, 2008). With an EC_{50} of 2.35 µM cAMP, Epac1-camps is suitable to sensitively detect cAMP in a physiological range of 0.1 µM to 10 µM (Nikolaev et al., 2004a; Hill, 2006).

3.2 Endocannabinoid System and Cannabinoid Receptor 2

First described in the early 1990's by Munro et al. (1993) as part of the endocannabinoid system, the cannabinoid receptor 2 has since developed into a promising target of biomedical research. For more than a decade CB2 has been termed the "peripheral" cannabinoid receptor referring to its high abundance in peripheral organs and the immune system (Bouaboula et al., 1996), which was thought to be in contrast to the "central" cannabinoid receptor 1 (CB1) predominantly found in the brain (Matsuda et al., 1990). CB1 regulates synaptic transmission and plays a role in central neurobiological processes, such as memory, anxiety, adult neurogenesis, pain transmission and food intake (Pertwee et al., 2010).

Protein expression of CB2 on immune cells, such as B cells (CD19+), T lymphocytes (CD4+ and CD8+), monocytes (CD11b+) and natural killer cells (CD335+) has been repeatedly reported (Schmöle et al., 2015; Turcotte et al., 2016) and the functional relevance of CB2 signalling in these cell types including the regulation of cell activation as well as cytokine and antibody production has been shown (Bouaboula et al., 1993; Galiègue et al., 1995; Malfitano et al., 2014). Studies in CB2-deficient mice corroborate its importance in the regulation of the immune response, specifically for B cell migration (Atwood and Mackie, 2010; Pereira et al., 2009).

Additionally, the control of autoimmunity by the endocannabinoid system has been illustrated by showing that CB1 on neurons and CB2 on T cells can suppress and control experimental autoimmune encephalitis (EAE)-associated neuroinflammation, a model for human multiple sclerosis (Maresz et al., 2005).

The spleen is the organ with the highest CB2 expression, but also thymus, bone (Ofek et al., 2006, 2011) and other tissues, such as skin (Karsak et al., 2007), fat, liver and muscles express CB2 (Pacher and Mechoulam, 2011). CB2 has been shown to regulate bone mass with effects in osteoblasts and osteoclasts (Ofek et al., 2006) and certain human CB2 variants are known to increase the risk for osteoporosis (Karsak et al., 2005).

Cannabinoid receptor ligands have been repeatedly associated with the treatment of cancer and anti-tumour activity (Sledziński et al., 2018). CB1 and CB2 expression and signalling in different cancer cell lines and in breast, liver, and prostate cancer as well as in glioblastoma and lymphoma has been shown to contribute to the important role of cannabinoids in cancer treatment (Sarfaraz et al., 2008).

The function of CB2 in the brain has been highly debated for several years, however recently, evidence for CB2 involvement in brain physiology and pathogenesis has emerged (Cassano et al., 2017; Benito et al., 2008; Prenderville et al., 2015; Molina-Holgado et al., 2007a; Quraishi and Paladini, 2016). Relatively well investigated is the presence of CB2 on microglia, especially during neuroinflammatory conditions, such as neurodegeneration or brain injury (Cassano et al., 2017; Tao et al., 2016). The CB2-mediated regulation of microglial activation during inflammation has assigned CB2 a neuroprotective role that

is continuously investigated. CB2 expression on glioblastoma (Dumitru et al., 2018) and neural stem cells (Prenderville et al., 2015; Molina-Holgado et al., 2007b) and reported functions of CB2 receptors in neurons (Stempel et al., 2016; Stumpf et al., 2018; Zhang et al., 2014) highlight the potential complexity of CB2-mediated signalling in the central nervous system which will be discussed in detail in chapter 3.3.

Debates about tissue and cell type specific CB2 expression have followed the field since the beginning (Rogers, 2015). In particular, the lack of antibodies against CB2 with sufficient specificity, a common issue in GPCR research, might have contributed to claims of CB2 expression that could not be cross-validated by other studies with different techniques (Baek et al., 2013; Marchalant et al., 2014).

As of this date, including negative CB2 knockout controls (Buckley et al., 2000; Deltagen-Inc, 2005) in antibody-based studies is necessary to unambiguously show CB2 involvement. With the use of CB2-GFP reporter mice, single cell RNA sequencing (scRNAseq) and fluorescently-labelled CB2 ligands, CB2 expression and therefore associated functions can be investigated more reliably. In addition, splicing variants of CB2 have been reported for humans, mice, and rats which most likely contributed to the conflicting results of CB2 tissue distribution in the past (Liu et al., 2009).

3.2.1 Cannabinoid Receptor 2 Signalling Pathways

As a $G\alpha_{i/o}$-coupled GPCR, the activation of CB2 leads to the inhibition of ACs via $G\alpha_i$ subunits (Munro et al., 1993; Bouaboula et al., 1999) causing a decrease in cAMP, as described in section 3.1.1 of this Introduction. In contrast to CB1, which also couples $G\alpha_o$ (Prather et al., 2000) and possibly $G\alpha_s$ (Glass and Felder, 1997) and $G\alpha_q$, (Lauckner et al., 2005), there is no evidence for the coupling of CB2 to other $G\alpha$ subunits but $G\alpha_i$.

CB2 activation PKC-dependently targets the MAPK pathways p38, ERK1/2, and c-Jun and has been linked to the regulation of cell cycle and cell proliferation by targeting the PI3K/Akt pathway that activates mTORC1 (mammalian target of rapamycin complex 1) (Sánchez et al., 2001; Palazuelos et al., 2012).

The activation of GIRK (G-protein-gated inwardly rectifying potassium) channels has been shown for CB1 (Felder et al., 1995). For CB2 however, Felder et al. (1995) did not observe this regulation. Recently, this has been challenged by Stumpf et al. (2018), who show that activation of CB2 leads to the hyperpolarisation of cortical neurons via GIRK channels.

CB2-mediated effects on intracellular Ca^{2+} levels, that are regulated through the activation of PLC and production of inositol trisphosphate (IP_3) leading to the release of Ca^{2+} from the endoplasmatic reticulum (ER) have also been reported (Zoratti et al., 2003). The enhanced production of the sphingolipid ceramide after CB2 activation has been shown to induce apoptosis in glioma and bladder cancer (Sánchez et al., 2001; Bettiga et al., 2017).

Early reports on CB2-mediated signalling from Bouaboula et al. (1999) already registered a high degree of constitutive receptor activity in cAMP measurements in heterologous expression systems that was later confirmed by describing the action of CB2 inverse agonists (Mancini et al., 2009; Bolognini et al., 2012). To this date, it is not clear if CB2 also exhibits constitutive activity *in vivo* and, if so, what the physiological role of this property might be.

3.2.2 Endogenous and Synthetic Cannabinoid Receptor Ligands

The engagement of CB2 in specific cellular signalling pathways important to physiological and pathophysiological processes can be modulated by different CB2 ligands. Although there are many studies describing functional effects of CB2 ligand treatment in animal models and *in vitro*, only recently, research has targeted the functional selectivity of known and novel CB2 ligands to shed light on the mechanisms that elicit these effects (Soethoudt et al., 2017).

The two most important and best described endogenous ligands that bind CB2, as well as CB1, are the endocannabinoids anandamide (AEA) (Devane et al., 1992) and 2-arachidonoyl glycerol (2-AG) (Stella et al., 1997).
Both endocannabinoids are lipids generated from membrane phospholipids that contain arachidonic acid (AA), and are Ca^{2+}-dependently released in response to stimuli. AEA is synthesised from NArPE (N-arachidonoyl phosphatidyl ethanolamine) predominantly through NAPE-PLD (N-acetyl phosphatidyl ethanolamine-hydrolysing phospholipase D) and degraded by the fatty acid amide hydrolase (FAAH) to AA. Synthesis of 2-AG is PLC dependent which catalyses the hydrolysis of membrane lipids to 1,2-diacylglycerol (DAG). DAG lipase (DAGL) is then converting DAG to 2-AG. Monoacylglycerol lipase (MAGL) in turn degrades 2-AG to AA (Pertwee, 2015). Although main routes of endocannabinoid synthesis, the described biosynthesis pathways are not exclusive and for AEA and 2-AG different synthesising and degrading cascades have been described (Pertwee, 2015).
In an extensive CB2 ligands study by Soethoudt et al. (2017), the authors showed that 2-AG and AEA have no selectivity towards human CB2 or CB1, bind both receptors with moderate binding affinities (see Table 3.1). For murine CB receptors, 2-AG is slightly more affine for CB2 whereas AEA is more affine for CB1. AEA and 2-AG both show a bias towards GIRK activation over cAMP signalling, whereas AEA is also biased towards the activation of MAPK ERK1/2 (Soethoudt et al., 2017).

Phytocannabinoids are natural cannabinoid receptor ligands that are produced in plants. The most prominent phytocannabinoid is *trans*-Δ^9-tetrahydrocannabinol (THC), which is predominantly responsible for the psychoactive effect of recreational cannabis use mediated by CB1 (Matsuda et al., 1990). THC is a non-selective cannabinoid receptor agonist with high binding affinity and a strong bias towards ERK1/2 signalling and against the

activation of GIRK (Soethoudt et al., 2017; Ibsen et al., 2017). Around 100 different phyto-cannabinoids have been found in plants of the genus *Cannabis*, among those cannabidiol and caryophyllenes. β-caryophyllene (BCP), an essential oil additionally but not exclusively found in hops, rosemary, and basil, has been reported to selectively bind human CB2 (Gertsch et al., 2008) and to show CB2-mediated neuroprotective effects in mouse models, such as EAE (Alberti et al., 2017). BCP acts as a CB2 agonist and activates $G\alpha_i$ signalling, leads to higher intracellular Ca^{2+} and weakly activates the MAPK ERK1/2 and p38 (Gertsch et al., 2008).

The need for selective cannabinoid receptor ligands fuelled the development of synthetic cannabinoids that bind CB2 with high affinity and selectivity. Among those JWH133, HU308 and HU910 are widely used and well established CB2 agonists that are recommended to use in studies investigating CB2 function (Soethoudt et al., 2017). When comparing GIRK, G-protein, cAMP, ERK1/2 activation and β-arrestin recruitment HU308 is a relatively well-balanced agonist at human CB2, whereas JWH133 has been shown to not activate GIRK channels. At the murine CB2, JWH133 and HU308 show a greater bias towards G-protein signalling. In general, CB2 agonists display less selectivity and potency for either cannabinoid receptor in mice compared to humans, highlighting species differences that might explain discrepancies between *in vitro* studies, which often use human cell lines, human clinical trials and *in vivo* mouse studies (Atwood and Mackie, 2010; Rogers, 2015).

Synthetic cannabinoids that act as CB2 antagonists and inverse agonists have also contributed to identify CB2 function. SR144528 and AM630 are inverse agonists that show the highest CB2 selectivity (Soethoudt et al., 2017) and have been used in various *in vitro* and *in vivo* studies. In contrast to CB2 agonists, their CB2 selectivity is higher on mouse than human receptors (Soethoudt et al., 2017) and SR144528 shows stronger CB2 selectivity than AM630. For cAMP signalling, both inverse agonists are highly potent and functionally selective over GIRK and ERK1/2 pathways, however, SR144528 also shows a strong bias towards inverse agonism for β-arrestin recruitment and G-protein signalling (Soethoudt et al., 2017; Dhopeshwarkar and Mackie, 2016).

In a study from Bolognini et al. (2012), it was also shown that AM630 acts a protean ligand at the human CB2 eliciting agonism at constitutively active receptor forms with low affinity and inverse agonism with a higher affinity at constitutively inactive CB2 forms. It must be stressed that, to this date, all CB2 ligand bias studies (Soethoudt et al., 2017; Dhopeshwarkar and Mackie, 2016) have been performed in cell models and with receptor overexpression. Additionally, ligand bias has been determined relatively to the non-selective, highly affine and potent cannabinoid receptor agonist CP55940, which in turn also shows a bias towards cAMP signalling (Soethoudt et al., 2017; Dhopeshwarkar and Mackie, 2016). It remains to be investigated to what extent ligand bias is influencing endogenous receptor signalling and how it could be used in a clinical setting.

Positive and negative allosteric modulators of GPCRs influence cellular signalling if receptor agonists bind different GPCRs with similar affinity, as it is seen for CB1 and CB2 and their endocannabinoids AEA and 2-AG. Pepcan-12 (PC12), expressed in brain, liver, and kidney (Petrucci et al., 2017) has been reported to negatively modulate the binding of synthetic CB1/CB2 agonists CP55940 and WIN55,212-2 to CB1 receptors (Bauer et al., 2012).

In 2017, it was shown by Petrucci et al. (2017) that PC12 also binds CB2 and acts as a PAM potentiating the effect of the endocannabinoid 2-AG in G-protein binding and cAMP signalling assays. The targeting of CB1 and CB2 by PC12 and its complementary effects on the receptors represents a potential endogenous regulatory mechanism of endocannabinoid signalling.

Cannabinoid ligands do not exclusively bind the cannabinoid receptors CB1 and CB2. Common off-targets for cannabinoids of different origins are G-protein coupled receptor 55 (GPR55) and transient receptor potential (TRP) channels (Pertwee et al., 2010). For the CB2 agonist JWH133 and inverse agonist AM630, significant cross-reactivity with TRPA1 at a concentration of $10\,\mu M$ has been reported (Soethoudt et al., 2017). Some compounds of the CEREP panel, a panel consisting of common off-targets, were shown to be cross-activated by AM630 and HU308, among those adenosine receptors and chloride channels (Soethoudt et al., 2017). Specifically for the inverse agonist AM630, a substance often given at higher concentrations to block agonist action, these off-target effects are of relevance when interpreting previous studies and future research.

Table 3.1. CB2 ligand binding affinities and potencies for cAMP and ERK1/2 pathways at human receptors. CB2 selectivity was determined from the ratio of the K_i at CB1 compared to the K_i value at CB2. Adapted from Soethoudt et al. (2017) and Gertsch et al. (2008). ND - not determined.

Ligand	K_i [nM]	EC_{50} cAMP [nM]	EC_{50} ERK1/2 [nM]	CB2 selectivity
AEA	123	1175	3890	1
2-AG	115	151	3890	1
THC	6.92	ND	200	0.5
CP55940	3.63	0.05	11	0.2
WIN55212,2	2.69	0.32	5	1
JWH133	66	4.17	646	153
HU308	36	2.95	138	278
HU910	60	3.89	3162	166
BCP	155	1900	ND	ND
AM630	41	28	8128	8
SR144528	13	21	1349	129

3.2.3 Cannabinoid Receptor 2 Heterodimerisation

Heterodimerisation of GPCRs represents an additional level of complexity in GPCR-mediated signalling (see Introduction section 3.1). CB2 has been found to heterodimerise with the three different GPCRs: cannabinoid receptor CB1 (Callén et al., 2012), GPR55 (Balenga et al., 2014) and the C-X-C chemokine receptor type 4 (CXCR4) (Coke et al., 2016).

The CB1-CB2 heteromer was first described by Callén et al. (2012) showing that the receptors physically interact in transfected HEK293T cells, CB2-transfected SH-SY5Y neuroblastoma cell lines and in rat brain slices. They further report a bi-directional cross-antagonism in Akt/PKB and ERK1/2 pathways as a biochemical characteristic of the CB1-CB2 heteromer. CB1 and CB2 agonists both promote neuritogenesis via the Akt pathway when applied alone, however, in the presence of both agonists negative crosstalk seems to attenuate the differentiation process via the CB1-CB2 heteromer (Callén et al., 2012). Sierra et al. (2015) also showed the existence of CB1-CB2 heteromers in basal ganglia of macaque brains with reduced expression in parkinsonian animals. Later, this negative crosstalk was corroborated by Navarro et al. (2018b) reporting it for the activation of ERK1/2 and β-arrestin recruitment in transfected HEK293T cells.

Adding to the role of cannabinoid receptors in the brain is the observation that CB1-CB2 heteromers also form in a transfected microglial cell line modulated by the cell's activation state (Navarro et al., 2018a). Lipopolysaccharides (LPS) and interferon γ (IFNγ) activated microglial cells showed cross-antagonism in the cAMP and ERK1/2 pathway, whereas resting microglia do not exhibit these characteristics, supposedly, because of lower CB2 expression showing the dynamics of heteromer formation and their specificity to the cellular state (Navarro et al., 2018a).

Two out of three criteria for a functional heteromer according to (Gomes et al., 2016) are followingly met by the proposed CB1-CB2 heteromer, the physical interaction and the biochemical footprint (Callén et al., 2012; Navarro et al., 2018b,a; Sierra et al., 2015). Different studies additionally showed CB1-CB2 functional interplay and crosstalk in T cells (Börner et al., 2009), neuropathic pain (Desroches et al., 2014), neurogenesis (Rodrigues et al., 2017), autoimmune contact dermatitis (Karsak et al., 2007) and bone loss (Sophocleous et al., 2017) underscoring the relevance of co-occurring CB1-CB2 signalling.

In 2016, Coke et al. (2016) reported heterodimerisation of CB2 and CXCR4 upon CB2 and CXCR4 agonist co-stimulation in human breast and prostate cancer cells that leads to a decrease in ERK1/2 phosphorylation and blocking of CXCR4-mediated cell migration, which is reversed by the CB2 inverse agonist AM630 (Coke et al., 2016). Additionally, signalling through Gα_{13} and Rho, member A (RhoA) was shown to be important for CXCR4-mediated cell migration (Ridley, 2015). The formation of the CB2-CXCR4 heteromer leads to a reduction of RhoA activation and therefore to a reduced migration of cancer cells (Scarlett et al., 2018). This silencing of CXCR4 signalling by CB2 association

represents the biochemical property of this heteromer and could contribute to the anti-tumour activity of cannabinoids (Sledziński et al., 2018; Gomes et al., 2016; Scarlett et al., 2018; Coke et al., 2016).

Physical interaction between CB2 and GPR55 was shown by Balenga et al. (2014) after previously reporting a functional interaction of the two receptors in the recruitment of neutrophils to inflammatory sites (Balenga et al., 2011). In transfected HEK293T, CB2-GPR55 heteromers lead to a reduced activation of transcription factors but increased activation of ERK1/2 by GPR55. Cross-antagonism of the CB2-GPR55 heteromer was also observed and the involvement of the heteromer in cancer or microglia activation was postulated (Balenga et al., 2014).

CB2 heteromer formation is a mechanism of CB2 signalling that has only been investigated for a short period of time (Callén et al., 2012) but could help to understand the diversity of cannabinoid-mediated signalling *in vivo*. However, as most of the CB2 heterodimerisation studies investigated heterologous cell models, endogenous functional heterodimerisation needs to be further characterised.

3.2.4 Crosstalk Between Endocannabinoid and β-adrenergic Signalling

The GPCR family of βAR consists of three members, β_1-adrenergic receptor (β_1AR), β_2AR, and β_3-adrenergic receptor (β_3AR). They are part of a bigger family of adrenergic receptors, α and β, that were first described by Raymond Ahlquist in 1948 and were later found to bind the hormones epinephrine and norepinephrine (also termed adrenaline and noradrenaline) (Ahlquist, 1948). Since their discovery they have been studied intensively and found to play an integral part in the regulation of cardiac function. βAR antagonists/inverse agonists, so-called β-blockers, were followingly established as treatment against different cardiac diseases, such as a hypertension, arrhythmia, heart failure, and after myocardial infarcts (Wachter and Gilbert, 2012; Waagstein et al., 1975).

βAR are predominantly $G\alpha_s$-coupled GPCRs that, upon activation, lead to a stimulation of ACs and a rise in intracellular cAMP and activation of PKA (Wachter and Gilbert, 2012). Further, the stimulation of L-type calcium channels, activation of transcription factors and parts of the contractile apparatus in cardiomyocytes are initiated and regulate, e.g. contractility (Wachter and Gilbert, 2012).
β_2AR has also been reported to couple to $G\alpha_i$ with low affinity after receptor phosphorylation by PKA (Zamah et al., 2002). The switch to $G\alpha_i$ was reported to mediate ERK1/2 activation that was shown to be pertussis toxin sensitive, an indication of $G\alpha_i$ involvement (Daaka et al., 1997). The existence of a $G\alpha_s$ to $G\alpha_i$ switch at β_2AR is supported by studies linking it to the localised activation of L-type calcium channels (Chen-Izu et al., 2000) and showing that the $G\alpha$ subunit switch can be modulated by the involvement of

PDE4D and β-arrestin (Baillie et al., 2003; Bruss et al., 2008). However, regarding β_2AR-mediated ERK1/2 activation, a substantial $G\alpha_i$ involvement was challenged by Friedman et al. (2002) who postulated that activation of the tyrosine kinase Src is the main requirement for the activation of MAPK ERK1/2.

Functional interaction between cannabinoid and β-adrenergic receptor signalling has been reported previously. Effects of THC, endocannabinoids and synthetic cannabinoids on heart rate and blood pressure are well described (Ho and Kelly, 2017). Additionally, activation of CB1 via 2-AG on sympathetic nerve terminals in the bone can inhibit norepinephrine release that is capable to elicit bone formation (Tam et al., 2008). A similar mechanism for pre-synaptic CB1-mediated inhibition of norepinephrine release has also been shown in the hippocampus (Schlicker et al., 1997) and other parts of the sympathetic nervous system (Pakdeechote et al., 2007).
Moreover, CB1 and CB2 inverse agonists AM521 and AM630 have been reported to modulate the cardiostimulatory effects of βAR agonist isoprenaline that was either increased or reduced depending on the concentration of the inverse cannabinoid receptor agonists (Weresa et al., 2019).
Interestingly, the authors postulate that a possible interaction of CB1 and CB2 with β_1AR might be responsible for these effects (Weresa et al., 2019). In 2010, Hudson et al. (2010) showed that CB1 and β_2AR are physically interacting in transfected HEK293 cells and report the positive influence of β_2AR presence on CB1 surface expression (Hudson et al., 2010). They additionally show a reduction of CB1 constitutive activity with β_2AR expression, an increase in CB1-mediated ERK1/2 activation in co-expressing cells as well as the cross-antagonism of CB1 inverse agonist AM251 on β_2AR-mediated phosphorylation of ERK1/2 (Hudson et al., 2010).

In addition to the role of βAR in cardiac health and disease, their involvement in other physiological processes, such as smooth muscle relaxation (Tanaka et al., 2005), bone homeostasis (Bonnet et al., 2008), and brain-immune system crosstalk (Gyoneva and Traynelis, 2013) shows the universality of (nor)epinephrine mediated signalling. The functional crosstalk of the endocannabinoid and β-adrenergic signalling systems has already proven relevant and further investigation in tissues that express receptors from both systems should provide a better mechanistic understanding.

3.3 Cannabinoid Receptor 2 in the Central Nervous System

The role of CB2 in the brain has become increasingly important in the context of neuronal injury and neuroinflammatory processes, such as neurodegeneration (Cabral et al., 2008; Cassano et al., 2017; Ashton and Glass, 2007). It has been known since the discovery of cannabinoid receptors that they can mediate neuroprotection via neuronal CB1 and CB2 on microglia, the tissue-resident macrophages of the brain (Cabral et al., 2008).

In addition to that, cannabinoids have been linked to the regulation of adult neurogenesis in the brain, a process in the hippocampus, the subventricular zone and possibly other regions of the post-developmental brain, where new neurons are generated throughout life.

In recent years, it has also been shown that not only CB1 is expressed on neurons but that also CB2 has a functional relevance in at least a subpopulation of cortical neurons (Stumpf et al., 2018), the hippocampus (Stempel et al., 2016), the midbrain (Zhang et al., 2014) and brainstem (Van Sickle et al., 2005). The cannabinoid influence on tumour growth, cell invasion, and glioma stem-like cells of glioblastoma has been reported and reflects another area of possible CB2 action in the brain (Dumitru et al., 2018).

For this work, the role of CB2 in adult neurogenesis and neuroinflammation are most important and are discussed in more detail in the following subchapters.

3.3.1 Adult Hippocampal Neurogenesis

Adult neurogenesis (AN) is a process in the mammalian brain that takes place in stem cell niches in the adult brain and is responsible for the continued generation of new neurons (Altman and Das, 1965). AN is best described in rodents, mainly mice, and in two areas of the brain that show the largest rate of neurogenesis, the subgranular zone (SGZ) of the dentate gyrus (DG) in the hippocampus and the subventricular zone (SVZ).

In the DG, AN contributes to learning and memory (Gonçalves et al., 2016) and in the SVZ new-born neurons migrate to the olfactory bulb (Doze and Perez, 2012). In the hippocampus, new granule neurons are generated from stem cells called radial glia-like type 1 cells (RGC) that are located in the SGZ between hilus and granular cell layer (GCL) and have a bipolar/unipolar shape (Garcia et al., 2004). These cells express the marker proteins Sox2 (sex determining region Y-box 2), GFAP (glial fibrillary acidic protein), and nestin, and show a low rate of proliferation detectable with markers, such as the endogenous antigen KI-67 (Ki67) or via BrdU (5-bromo-2'-deoxyuridine) incorporation (Nicola et al., 2015; Aimone et al., 2014) and have the capability to differentiate into neurons, astrocytes, and oligodendrocytes (Noctor et al., 2001) (see Figure 3.3).

Type 2a non-radial intermediate progenitor cells are characterised by their round shape, loss of GFAP and gain of Tbr2 (T-box brain protein 2) expression and a high proliferation rate. They further develop into type 2b intermediate proliferating progenitors that are committed to the neuronal fate and, in addition to nestin, Sox2 and Tbr2, express dou-
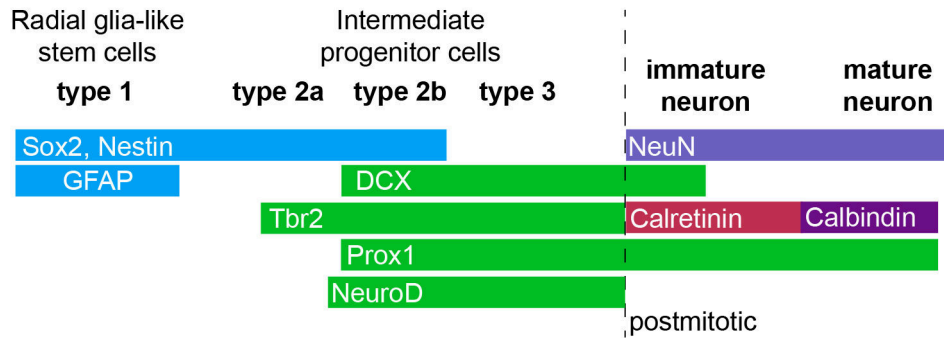
Figure 3.3. Marker expression of neuronal progenitor cells in the subgranular zone of the dentate gyrus. Adapted from Nicola et al. (2015).

blecortin (DCX), NeuroD1 (neurogenic differentiation 1) and Prox1 (prospero homeobox protein 1) (Nicola et al., 2015) (Fig. 3.3).

Type 3 neuroblast-like cells lose nestin and Sox2 expression, proliferate less than type 2 progenitors and migrate into the granule cell layer where they receive glutamatergic inputs (Nicola et al., 2015; Gonçalves et al., 2016). They stop proliferating, form axons and dendrites, and express neuronal markers such as NeuN and calretinin (CR) (Nicola et al., 2015; Kempermann et al., 2004). They then further maturate into calbindin-positive granule neurons that are integrated into the hippocampal network (Gonçalves et al., 2016) (Fig. 3.3).

AN is hierarchically regulated by a variety of extrinsic and intrinsic factors that range from environmental stimuli and perception to glia cell function, cytokines, neurotransmitters and intracellular signalling pathways (Kempermann, 2011). These factors are integrated leading to the regulation of gene transcription that can be further altered by epigenetics or post-translational modifications (Kempermann, 2011).

Physical activity, enriched environment and caloric restriction have all been shown to increase the proliferation of neural progenitor cells (NPC), whereas stress or neuroinflammation have been reported to attenuate neurogenesis (Aimone et al., 2014). A decline in neurogenesis with age has also been reported, although this decrease is most significant in the early postnatal period (until four months of age in mice) and relatively stable low levels of AN are seen for the remaining lifetime (Kempermann, 2011; Knoth et al., 2010; Nada et al., 2010).

Even in mice where AN has been extensively investigated on a molecular and cellular level, linking these observations to brain function and behaviour has been challenging (Kempermann, 2011; Aimone et al., 2014). The most significant function of AN is still a highly debated topic (Kempermann, 2011; Becker, 2016). There is considerable evidence that AN might play a role in the reduction of interference between similar memories (Becker, 2016). In mice with low levels of neurogenesis the discrimination between memory events is impaired, which may lead to a generalisation of fear and associated stress

responses via a yet unclear mechanism (Besnard and Sahay, 2015; Becker, 2016).

How AN is manifested in humans has been causing controversy in the research field (Lee and Thuret, 2018; Dey et al., 2019) with a report by Sorrells et al. (2018) showing no evidence for AN in the adult human brain contradicting previous and following research (Eriksson et al., 1998; Boldrini et al., 2018; Moreno-Jiménez et al., 2019). Further research must aim to find reliable methods to investigate AN in post-mortem human brain tissues to answer open questions about the existence and function of human hippocampal neurogenesis (Lee and Thuret, 2018; Dey et al., 2019).

The involvement of the endocannabinoid system in AN processes such as proliferation, differentiation, survival, and migration of NPCs has been reported (Prenderville et al., 2015; Downer, 2014). In 2006, Palazuelos et al. (2006) showed that CB2 is expressed on nestin-positive NPCs *in vitro* and *in vivo* and that stimulation with HU308 leads to an increased NPC proliferation and neurosphere formation which is abrogated in CB2-deficiency (Palazuelos et al., 2006).
The proliferative effect of CB2 agonists on NPCs was also found for CB1 agonists (Molina-Holgado et al., 2007a) and is mediated by the engagement of PI3K/Akt/mTORC1 and ERK1/2 signalling, which was shown in NPC cell lines, primary embryonic NPCs and cortical slice cultures, as well as in hippocampi of eight week old adult mice after CB2 activation (Molina-Holgado et al., 2007a; Palazuelos et al., 2006, 2012; Prenderville et al., 2015). The treatment of wildtype and CB2-deficient mice with CB2 agonist HU308 shows an increase in cell proliferation measured with BrdU in the SGZ of the DG that is absent in knockout animals. The excitotoxicity-induced increase in neurogenesis via kainic acid treatment is also reduced in CB2-deficient animals (Palazuelos et al., 2006, 2012). In Palazuelos et al. (2006) the authors report reduced basal levels of cell proliferation in the SGZ in CB2 knockout mice at ages embryonic day 17.5 and eight weeks postnatal. However, in a subsequent study by the same group using only eight week old animals, the observation of reduced basal levels of AN in CB2-deficiency was not made (Palazuelos et al., 2012).

The interaction between CB1 and CB2 in the modulation of AN has been investigated in a study by Rodrigues et al. (2017) using hippocampal slice cultures from early postnatal rats. Here, they showed that only the co-stimulation of CB1 and CB2 leads to an increase in cell proliferation in the SGZ, but that neuronal differentiation and maturation are increased by single- or co-stimulation of both cannabinoid receptors (Rodrigues et al., 2017). The observation of cross-antagonism additionally suggests the involvement of CB1-CB2 heteromers (Rodrigues et al., 2017). In two different disease models, CB2 has also been shown to impact neurogenesis positively (Downer, 2014). In a mouse model for human immunodeficiency virus 1 (HIV-1) infection where mice express the HIV-1 glycoprotein gp120 and exhibit decreased AN in the hippocampus, treatment with a CB2 agonist rescued the phenotype (Avraham et al., 2013). After cortical stroke the activation

of CB2 promotes neuroblast migration to and differentiation at the infarct site (Bravo-Ferrer et al., 2016).

Cannabinoids as regulators for AN are an emerging topic in neurogenesis research. The role of CB2 in NPC proliferation could act in synergy with other neuroprotective effects associated with CB2 in the context of neurodegeneration, where impairment of AN is a common hallmark (Prenderville et al., 2015; Downer, 2014; Rom and Persidsky, 2013; Horgusluoglu et al., 2016).

3.3.2 Neuroinflammation

Neuroinflammatory processes in the central nervous system (CNS) are detrimental to neuronal health and physiological brain function. A main player in the regulation of neuroinflammation are the brain-resident immune cells of myeloid origin, microglia, that were first discovered by Río Hortega (1918) and represent 5 to 12 % of all brain cells (Lawson et al., 1990). Over the last two decades the function of microglia in the brain has been intensively studied and revealed their importance for brain homeostasis, defence against pathogens, ageing and during neurodegenerative diseases (Hickman et al., 2018; Joseph and Venero, 2013; Izquierdo et al., 2019; Neher and Cunningham, 2019).
Ribonucleic acid (RNA) sequencing studies have further advanced the field by identifying microglial heterogeneity in the healthy and diseased brain (Li et al., 2019a). To perform their tasks, microglia are particularly dependent on the sensing of external stimuli and possess a large repertoire of ion channels, GPCRs and other cell surface receptors (Izquierdo et al., 2019).

In the normal brain, homeostatic microglia with ramified processes form a network that constantly surveils the CNS environment (Lawson et al., 1990; Nimmerjahn et al., 2005). They interact with neurons and astrocytes to support synaptic remodelling and neuronal health mainly via the complement system, transforming growth factor β (TGFβ) and the C-X3-C chemokine receptor 1 (CX3CR1) (Butovsky et al., 2013; Vasek et al., 2016; Harrison et al., 1998). TREM2 (triggering receptor expressed on myeloid cells 2)-dependent phagocytosis of apoptotic neurons and an intact progranulin pathway that supports neuronal survival are other crucial microglial functions that maintain brain homeostasis (Krasemann et al., 2017; Minami et al., 2014). Microglia keep their surveilling and ramified phenotype through the regulation of potassium currents that lead to a negative membrane potential and through low cAMP levels mediated by Gα_i-coupled receptors, such as CX3CR1 or purinergic P2Y receptors (Izquierdo et al., 2019). The activation of P2Y receptor 12 (P2YR$_{12}$) by ATP also mediates the chemotactic process extension towards an injury site possibly via the ERK1/2 pathway (Haynes et al., 2006; Lee et al., 2012; Gyoneva and Traynelis, 2013).

In response to pathological stimuli, such as pathogens, protein aggregates, oxidative stress, injury or CNS tumours, microglia change their state and adapt a less ramified

morphology (Hickman et al., 2018; Izquierdo et al., 2019). Through the engagement of Toll-like receptors via, e.g. bacterial lipopolysaccharides or purinergic receptors via free ATP and ADP the NLP3 inflammasome and NF-κB are activated leading to the production of pro-inflammatory cytokines, such as interleukin 1β (IL-1β) and tumour necrosis factor α (TNFα) (Katsnelson et al., 2015; Izquierdo et al., 2019; Hickman et al., 2018). Low levels of intracellular cAMP levels facilitate the activation of NF-κB and may be promoted through a IL-1β- and TNFα-mediated increase in PDE4B activity (Ghosh et al., 2012, 2015). A rise of intracellular cAMP levels, however, has been associated with process retraction and diminished surveillance function (Kalla et al., 2003). The upregulation of adenosine activated Gα_s-coupled adenosine A$_{2A}$ receptors and downregulation of homeostatic P2YR$_{12}$ during microglia activation is proposed to lead to a cAMP/PKA-mediated process retraction (Orr et al., 2009). A similar mechanism that leads to reduced microglia motility has been reported for norepinephrine signalling. β_2AR on homeostatic microglia is downregulated after cell activation which is accompanied by the upregulation of the predominantly Gα_i-coupled α_{2A}-adrenergic receptor (α_{2A}AR) promoting process retraction (Gyoneva and Traynelis, 2013). Interestingly, for both GPCRs, coupling to Gα_s and Gα_i has been reported (see Introduction section 3.2.4 and Eason et al. (1992)) and it remains to be investigated how the adrenergic influence on microglia motility in associated with cAMP levels.

Protein aggregates such as amyloid β plaques, a hallmark of Alzheimer's disease (AD), can be cleared through their detection by microglial scavenger receptors and the production of reactive oxygen species (El Khoury et al., 1996). Further release of proteases, glutamate and induced nitric oxide synthase (iNOS) and the reduced production of neuron survival promoting factors by activated microglia give them the means to cause neuronal death (Brown and Vilalta, 2015).

The most important immunological checkpoints to prevent a microglial overreaction to pathological stimuli are CX3CR1 and TREM2 signalling, in addition to progranulin and scavenger receptor pathways (Hickman et al., 2018). A dysfunction of these pathways in microglia leads to the continued death of neurons in neurodegenerative diseases like AD and Parkinson's or during CNS infection by, e.g. HIV-1 (Hickman et al., 2018; Duan et al., 2014). Finding targets that restore homeostatic microglia function in conditions of chronic CNS inflammation could ameliorate disease progression. A possible candidate that acts neuroprotectively is CB2.

Carlisle et al. (2002) first reported the expression of CB2 on rat microglia stimulated with the pro-inflammatory cytokine IFNγ. Weak expression of CB2 in homeostatic microglia was proposed by Schmöle et al. (2015) using a CB2 reporter mouse. On the other hand, López et al. (2018), using a different reporter mouse, only reported CB2 expression in microglia associated with amyloid β plaques and not during homeostasis. This upregulated expression of CB2 in neuroinflammatory conditions, such as AD, Parkinson's

disease, multiple sclerosis or activated microglial cell models has been shown repeatedly by different groups (Cassano et al., 2017; Benito et al., 2008; Navarro et al., 2018a). The main functions associated with CB2 activation in microglia are the inhibition of cell activation and the reduction of pro-inflammatory factor release, such as IL-1β, TNFα, and iNOS from activated cells (Ehrhart et al., 2005; Klegeris et al., 2003; Ramírez et al., 2005). For this, Eljaschewitsch et al. (2006) propose a mechanism via the MAPK phosphatase-1 that silences MAPK signalling activated by microglial scavenger receptors.

In different disease models, activation of CB2 has been shown to directly affect functional outcome. CB2 activation via JWH133 or non-selective cannabinoid agonist WIN55, 212-2 leads to improved cognitive and memory function and less amyloid β plaques in an AD mouse model (Martín-Moreno et al., 2012; Fakhfouri et al., 2012). Treatment of mice with induced Parkinson's using the CB2 agonist HU308 shows a reduction of microglia activation and cytokine production with improved levels and activity of surviving dopaminergic neurons (García-Arencibia et al., 2007; Gómez-Gálvez et al., 2016).

As a majority of studies show that both cannabinoid receptors are beneficial in the context of neuroinflammation (Cassano et al., 2017; Ashton and Glass, 2007) and CB1-CB2 heteromers might be relevant to microglia function (Navarro et al., 2018a), it highlights the role of the complete endocannabinoid system as a neuroprotective factor. However, because of the non-psychoactive effects, CB2 is a more suitable target for drug development. Research on CB2 as a positive modulator of neuroinflammatory pathologies must focus on cellular and molecular mechanisms behind CB2 function in microglia and their translation from animal models to humans.

4 Aim of this Work

The endocannabinoid system with its two GPCRs cannabinoid receptor 1 and 2 is known to have important functions in the central nervous system. This work aims to further characterise CB2 function and CB2-mediated signal transduction in a neurobiological context.

In the first part of this thesis, the role of CB2 in the regulation of adult hippocampal neurogenesis is investigated. Activation of CB2 shows proliferative effects on NPCs and has been implicated in increasing cell proliferation in the subgranular zone of adult mice (Palazuelos et al., 2006, 2012; Molina-Holgado et al., 2007a). However, there is some inconsistency in previous reports about the reduction of SGZ cell proliferation of CB2-deficient mice (Palazuelos et al., 2006, 2012) and therefore the question about the contribution of CB2 function towards basal neurogenesis in adult mice remains open.
Accordingly, the aim is to decipher the influence of CB2 on the size of the DCX+ NPC population, the abundance of postmitotic immature neurons (DCX+/CR+) and the overall cell proliferation (Ki67+) in the SGZ of the DG at a basal state. For this purpose, hippocampal brain sections of adult, untreated, CB2-deficient and wildtype mice were stained for Ki67 and co-stained for DCX and CR and positive cells per sample volume were quantified and compared between the genotypes.

The second, more extensive part of this thesis, targets CB2-mediated signal transduction with a focus on cAMP dynamics and receptor crosstalk with the β-adrenergic system in a cell model and in primary mouse microglia. The involvement of microglial CB2 in regulating neuroinflammatory processes by reducing cell activation and pro-inflammatory cytokine release is well established (Ehrhart et al., 2005; Klegeris et al., 2003; Ramírez et al., 2005) and cAMP/PKA and MAPK pathways have been associated with this function (Tao et al., 2016; Eljaschewitsch et al., 2006).
Reports about crosstalk between endocannabinoid and β-adrenergic signalling (Hudson et al., 2010) and the presence of both systems in microglia (Gyoneva and Traynelis, 2013; Cassano et al., 2017) suggest the possibility of an involvement of CB2 receptor interactions in microglia signalling.
To investigate CB2-mediated cAMP dynamics, a heterologous HEK293 cell model with CB2 expression was generated that allows for the live imaging of intracellular cAMP levels using the FRET-based cAMP biosensor Epac1-camps (Nikolaev et al., 2004a). βAR-CB2 cAMP and ERK1/2 signalling crosstalk was investigated in this cell model and β_2AR-CB2 heterodimerisation was analysed using immunoprecipitation and co-localisation

studies. In addition, CB2- and βAR-mediated cAMP signalling was investigated in primary microglia from wildtype and CB2-deficient mice expressing Epac1-camps ubiquitously in order to identify receptor-specific and crosstalk effects on microglial cAMP levels.

The frequent involvement of cannabinoid receptor 2 in disease-associated conditions and its reported protective role in these pathologies (Pacher and Mechoulam, 2011) puts CB2 in the focus of biomedical research and drug development (Dhopeshwarkar and Mackie, 2014). The aim of this work is to further characterise CB2 focussing on the above-mentioned aspects of receptor function.

5 Results - Part I: Influence of Cannabinoid Receptor 2 Presence on Adult Hippocampal Neurogenesis

5.1 Quantification of Adult Hippocampal Neurogenesis in Wildtype and CB2-deficient mice

No alteration of neuronal progenitor populations and cell proliferation in dentate gyrus of adult CB2-deficient mice

The involvement of CB2 in neuronal progenitor cell proliferation and adult hippocampal neurogenesis in mice has been reported previously (Palazuelos et al., 2006, 2012; Prenderville et al., 2015). However, an estimation of the baseline size of neuronal progenitor populations, immature neurons as well as the quantification of cell proliferation without animal treatment in CB2-deficient mice is needed to determine the contribution of CB2 towards basal levels of neurogenesis in the SGZ of the DG.

For the quantification of type 2b and 3 neuronal progenitors (DCX+/CR-) and postmitotic immature neurons (DCX+/CR+) 40 µm brain sections were co-stained for the neuronal progenitor marker doublecortin (DCX) and calretinin (CR), which is expressed by immature neurons together with DCX as well as inhibitory neurons (Nicola et al., 2015) (Fig.5.1C). Immunostaining of brain sections with the proliferation marker Ki67 was used to quantify the number of dividing cells without prior animal treatment, that is necessary when using, e.g. BrdU (Fig.5.1B).

Positive cells were counted in the SGZ of the DG and normalised to the sample volumes in mm^3 of the infra- (ventral) and suprapyramidal (dorsal) blades of the GCL and SGZ (Fig.5.1A). Figure 5.1B and C show representative stainings for Ki67 (Fig.5.1B) and DCX/CR (Fig.5.1C) from brain sections of CB2-deficient mice and wildtype littermates. In both genotypes the cellular distribution of the fluorescent signals was identical. Ki67 was detected in the nucleus (Fig.5.1B), whereas DCX signal was seen in the cytosol (Fig.5.1C). Positive cells were distributed along the full length of the SGZ and in both DG blades. In DCX and CR double positive cells (Fig.5.1C, white arrows), CR staining was predominantly seen in the nucleus. CR positive inhibitory neurons were significantly larger than neuronal progenitors and located mainly in the deep hilus (Fig.5.1C).
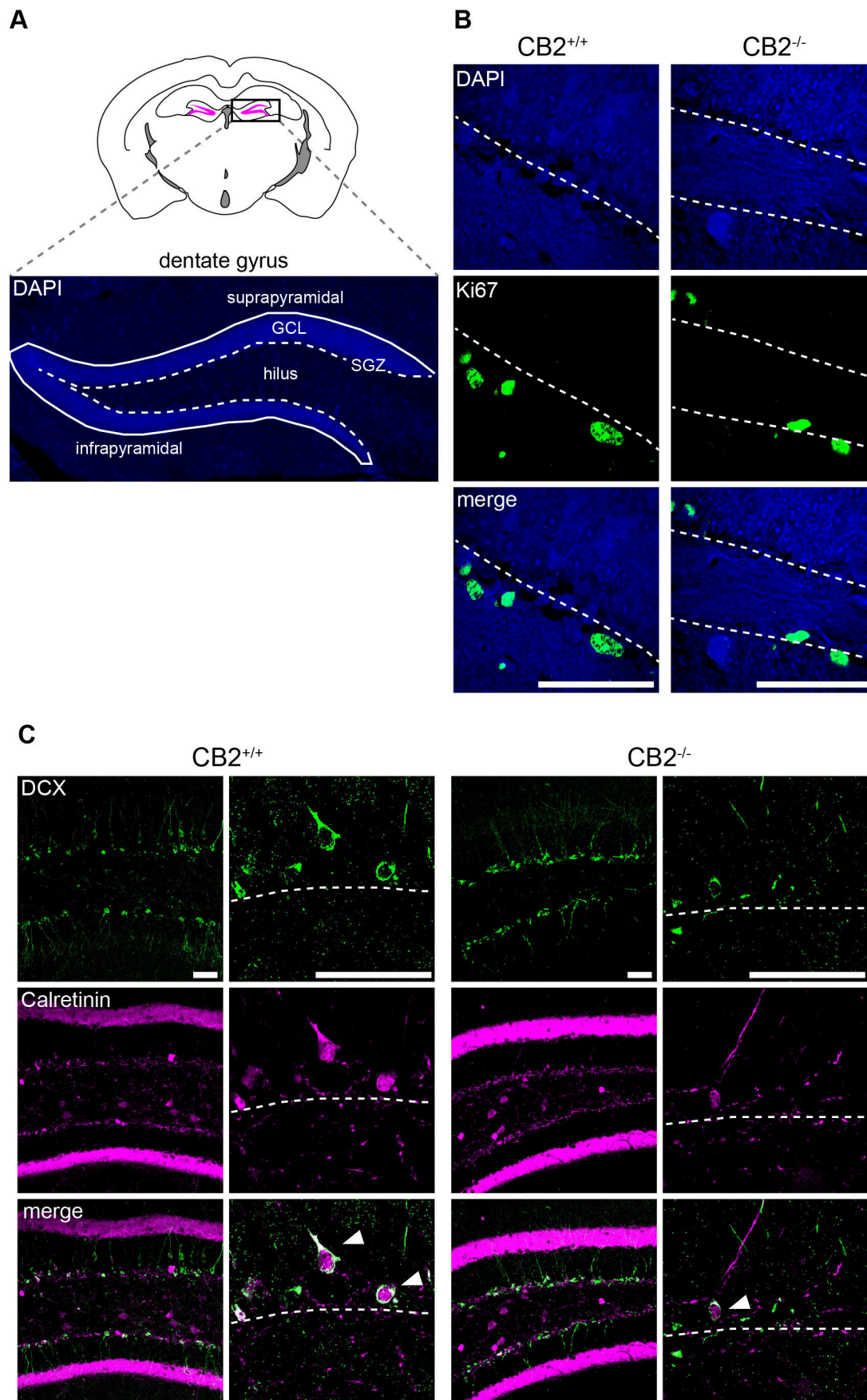
A

B

C

Figure 5.1. Representative confocal microscopy images of immunohistochemistry detection of Ki67, DCX and CR in CB2 wildtype and knockout brain sections. See next page for figure description.

Figure 5.1. Representative confocal microscopy images of immunohistochemistry detection of Ki67, DCX and calretinin in CB2 wildtype and knockout brain sections. (A) Overview of the mouse dentate gyrus (magenta in black rectangle) in the hippocampus and identification of relevant structures in an representative microscopy image of a brain section with DAPI-staining. **(B)** First column of images shows sections from WT mice and the second column shows fluorescent images from CB2-deficient mice. DAPI-staining (blue) is seen in the first row, Ki67-staining in the second (green) and a merge of the two channels in the third row. The dotted line represents the SGZ. **(C)** Fluorescent images of SGZ from both genotypes in lower (left) and higher (right) magnification with staining for DCX (first row, green) and CR (second row, magenta). Merged images are seen in the third row of images with white arrowheads indicating the location of DCX+/CR+ cells. The dotted line represents the SGZ. Scale bar = 100 μm. Scheme in **(A)** modified from (Bakker et al., 2015; Badhwar et al., 2013).

Morphological investigation of the brain sections showed no difference in the distribution or location of DCX, CR or Ki67 positive cells in the DG between the genotypes. These observations corroborate the results of the cell population quantification (Fig.5.2A). Overall cell proliferation per GCL and SGZ volume (Fig.5.2A) did not differ between the blades of the DG or between genotypes. Neither did the amount of DCX+ type 2b and 3 NPC (Fig.5.2B), that was four times larger than the number of Ki67+ proliferating cells per GCL-SGZ volume (see Table 5.1).

Around three quarters of all DCX positive cells were postmitotic immature neurons (DCX+CR+) (Fig.5.2C, DCX+CR+/DCX+). In the infrapyramidal blade (M = 72.70, 95% CI = 67.81, 77.59, n = 8) there was an overall lower percentage of double positive cells compared to the suprapyramidal blade (M = 78.84, 95% CI = 75.63, 82.05, n = 8) of the DG (F (1, 6) = 16.44, p = 0.0067). However, no difference in the ratio of DCX+CR+ to DCX+ cells was seen between genotypes. This result of a higher density in CR-expressing immature granule cells in the dorsal DG is in agreement with previously published research (Plümpe et al., 2006; Jinno, 2011).

However, in contrast to the previously reported involvement of CB2 in adult neuroge-
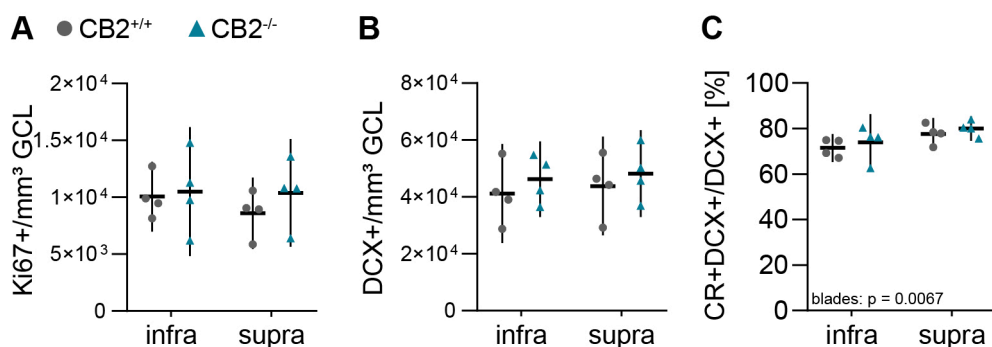
Figure 5.2. Quantification of neural progenitor cell populations and proliferation in the dentate gyrus of wildtype and CB2-deficient mice. Amount of cells positive for Ki67 **(A)** and DCX **(B)** per sample volume (GCL and SGZ) in the infra- and suprapyramidal blade of the dentate gyrus in CB2 WT (grey) and KO (blue). **(C)** Percentage of post-mitotic DCX+/CR+ immature neurons from total amount of DCX+ cells in the infra- and suprapyramidal blade of the dentate gyrus in both genotypes. Each *n* represents one animal. Values from infra- and suprapyramidal blades are paired and were analysed using Two-Way ANOVA with repeated measures and Sidak-adjusted p-values. CB2 WT n = 4, CB2 KO n = 4. Mean±95%CI.

nesis (Palazuelos et al., 2006, 2012), the quantification of type 2b and 3 neuronal progenitor cells as well as cell proliferation in this study did not show a difference between adult CB2-deficient and wildtype mice. In 16 to 17 week-old mice that show low rates of neuronal progenitor cell proliferation in the hippocampus (Nicola et al., 2015; Kempermann, 2011) either CB2 may not play a significant role in the regulation of basal levels of adult neurogenesis or its function is compensated by a different mechanism in CB2-deficient mice.

Table 5.1. Mean [95% CI] values of Ki67+ and DCX+ cells per mm^3 of the granular cell layer and percentage of immature neurons (CR+DCX+) from all DCX+ positive cells in wildtype and CB2-deficient mice and in both blades of the dentate gyrus. inf. - infrapyramidal, sup. - suprapyramidal.

	Ki67+			DCX+			CR+DCX+/DCX+		
	inf.	sup.	both	inf.	sup.	both	inf.	sup.	both
CB2$^{+/+}$	10060	8604	9174	41188	46220	42739	71.49	77.68	75.25
	[7004,	[5467,	[6410,	[23830,	[32928,	[25563,	[65.34,	[70.68,	[69.37,
	13116]	11741]	11939]	58545]	59512]	59914]	77.63]	84.67]	81.12]
CB2$^{-/-}$	10504	10388	10443	43837	48191	47390	73.92	80.00	77.63
	[4834,	[5659,	[5364,	[26465,	[32915,	[33025,	[61.50,	[74.63,	[69.68,
	16175]	15118]	15523]	61209]	63467]	61755]	86.33]	85.37]	85.58]

6 Results - Part II: Cannabinoid Receptor 2-mediated Cyclic AMP Dynamics and Receptor Crosstalk

6.1 Generation of a Cell Model to Investigate CB2-mediated Cyclic AMP dynamics with Live Cell FRET Imaging

6.1.1 Stable expression of FLAG-hCB2 in Epac1-HEK cells

To generate a HEK293 cell model that allows for the live recording of CB2-mediated changes in intracellular cAMP levels, cells were transfected with a plasmid encoding for a FLAG-tagged human CB2 (Q-H variant) protein. Epac1-camps-HEK293 (short Epac1-HEK) that were transfected for this purpose were kindly donated by Prof. Viacheslav Nikolaev (Experimental Cardiology, University Medical Center Hamburg-Eppendorf). These cells stably express the FRET-based cAMP-biosensor Epac1-camps (see Introduction section 3.1.4) with a selection resistance to hygromycin-B.

After the 14-day-treatment of FLAG-hCB2- and pcDNA 3.1(+)- transfected Epac1-HEK cells with the selection antibiotic G-418, surviving clones were propagated and cell lysates were analysed for CB2 expression via immunoblotting (Fig.6.1A). In Figure 6.1A the detection of CB2 at around 38 kDa using a polyclonal rabbit antibody against CB2 is seen in lysates from different G-418-surviving colonies.
Seven out of twelve Epac1-HEK colonies transfected with FLAG-hCB2 show CB2 expression after the selection period, whereas colonies from pcDNA 3.1(+)-transfected Epac1-HEK cells were negative for CB2. CB2 expressing colonies 2 and 8 were propagated further and compared to Epac1-HEK cells for CB2 expression via immunoblotting, which showed no CB2 expression (Fig.6.1B). As the strongest expression for CB2 was seen in colony 8, these stable clones were used for further studies and are from here on called Epac1-camps FLAG-hCB2 HEK293, or short Epac1-CB2-HEK cells.

Figure 6.1C shows CB2 protein levels of Epac1-HEK and Epac1-CB2-HEK cells under culturing conditions that confirmed the stable expression of CB2 in Epac1-CB2-HEK cells. Immunocytochemistry of Epac1-CB2-HEK cells revealed the cytosolic expression of Epac1-camps and the membrane localisation of FLAG-hCB2 (Fig. 6.1D) using an antibody
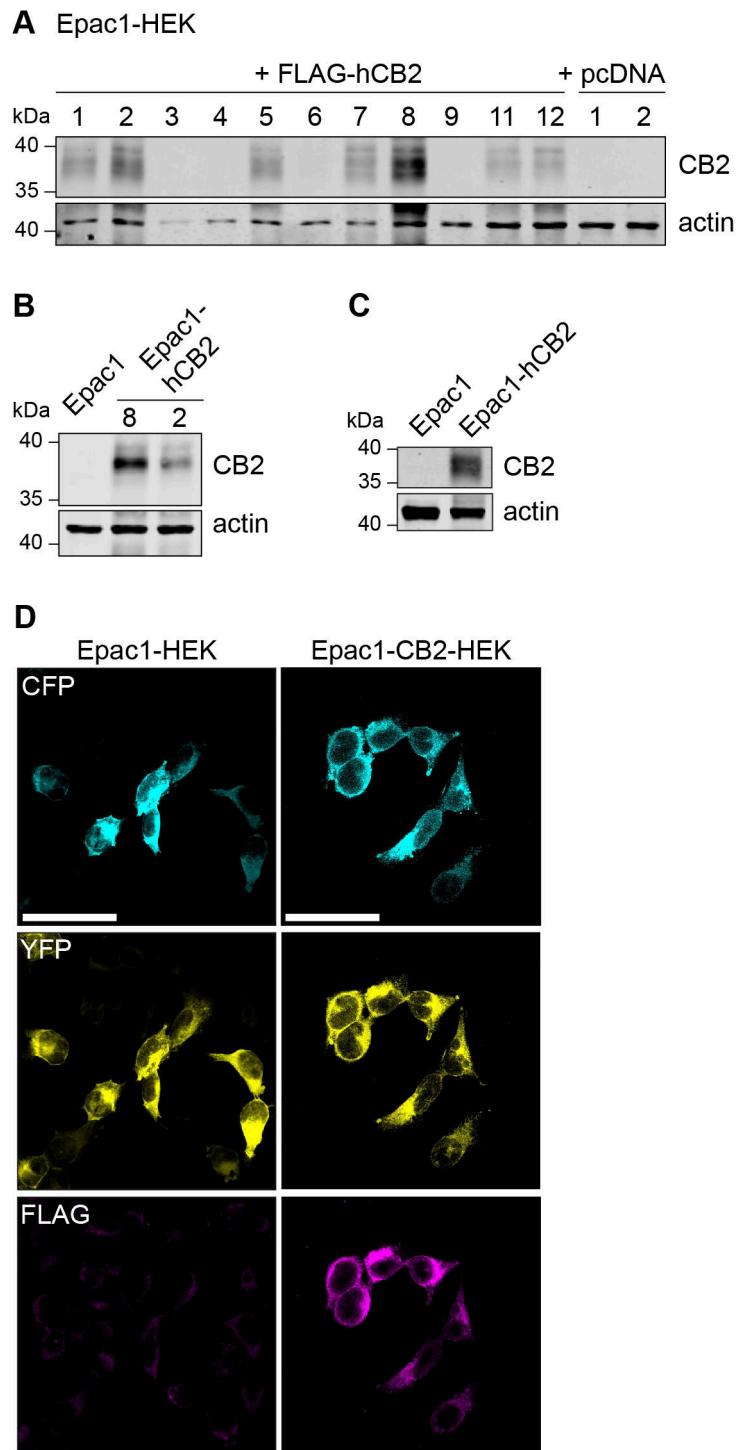
Figure 6.1. Expression of FLAG-CB2 and Epac1-camps in Epac1- and Epac1-CB2-HEK cells. (A) Western Blot of FLAG-CB2- and mock-transfected Epac1-HEK cells after selection process, **(B)** propagated selected Epac1-CB2-HEK colonies 8 and 2 and Epac1-HEK cells, as well as **(C)** Epac1-HEK and Epac1-CB2-HEK cells used in all further experiments with detection for CB2 and actin as loading control. **(D)** Representative confocal microscopy images of immunofluorescent detection of Epac1-camps and FLAG-CB2. First column of images shows Epac1-HEK and the second column shows Epac1-CB2-HEK cells. CFP (cyan) and YFP (yellow) fluorescent signals are seen in the first two rows respectively. FLAG-staining for FLAG-CB2 is seen in the third row of images (magenta). Scale bar = 50 μm. Complete blots are found in the Appendix 10.4.

against the FLAG-tag. In Epac1-HEK cells, no fluorescence for FLAG-hCB2 was detected and homogenous cytosolic expression of Epac1-camps comparable to Epac1-CB2-HEK cells was seen. However, in Epac1-CB2-HEK cells not all cells show membranous FLAG-hCB2 expression or equal levels of fluorescent signals from FLAG. For cAMP-FRET imaging in Epac1-CB2-HEK, this could result in variation regarding the magnitude and response rates after CB2 stimulation. With the stable and homogenous expression of Epac1-camps, on the other hand, FRET imaging was expected to be feasible in Epac1-CB2-HEK cells.

6.1.2 Evaluation of live cell FRET imaging and cAMP measurement in Epac1-HEK cells

To evaluate CB2-mediated cAMP signalling in Epac1-CB2-HEK cells a reliable FRET imaging and stimulation protocol had to be established. For the detection of $G\alpha_i$-mediated inhibition of AC activity and cAMP production in model systems, it is often necessary to pre-activate the AC before applying a potentially inhibitory stimulus to elevate low cellular cAMP levels (Insel and Ostrom, 2003; Storch et al., 2017). In a majority of cAMP studies the direct AC activator FSK is used for this purpose (Insel and Ostrom, 2003) and a comparable stimulation protocol has been applied in this work.

A suitable FSK concentration was determined using Epac1-HEK cells aiming at a sufficient signal amplitude while rapidly reaching the post-FSK baseline to minimise recording time. Epac1-HEK cells were also used to exclude any off-target effects on cAMP signalling from CB2 ligands. An overview of the FRET imaging method and analysis pipeline with analysed response parameters is seen in Fig. 6.2.

Figure 6.3 shows time-dependent FRET ratio (R) images from a representative recording of Epac1-HEK cells stimulated with 1 µM FSK, then 1 µM CB2 agonist JWH133 and finally 1 µM CB2 inverse agonist AM630. The corresponding ΔR_t line plots from selected ROIs (1, 2, and 5) show stimulation time points and the increase of ΔR after FSK stimulation in all ROIs (Fig. 6.3B). No FRET change was observed after application of CB2 ligands in Epac1-HEK cells. The average ΔR_t time traces of Epac1-HEK cells stimulated with 1 µM, 3 µM and 10 µM FSK show the step-wise concentration-dependent increase in cAMP production within the first 480 s after FSK stimulation (Fig. 6.3C). Maximal ΔR amplitudes, time to half maximum t1/2 and the maximal slope of the FSK responses (in positive direction) corroborate this observation.

Comparing the data from 1 µM, 3 µM and 10 µM FSK recordings, larger ΔR amplitudes, shorter half-times as well as steeper max. slopes of the signals were seen with increasing FSK concentration (Fig. 6.3D, E, F). This was most evident regarding the 10-fold concentration increase from 1 µM to 10 µM FSK. The max. slope of the FRET response showed significant differences between all concentration steps (Fig. 6.3F), leading to the possible conclusion that this parameter most accurately represents the changes in cAMP
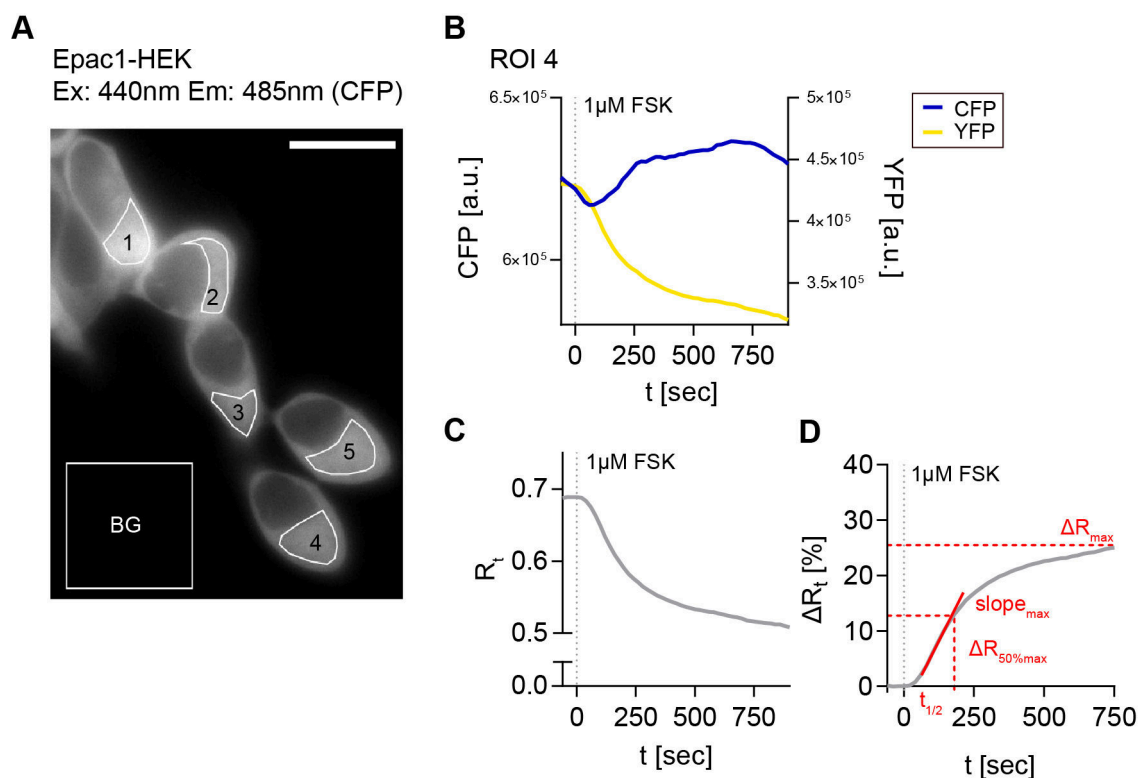
Figure 6.2. cAMP-FRET imaging of Epac1-HEK cells and FRET data analysis. (A) Representative fluorescent CFP image of Epac1-HEK cells excited with 440 nm light, measured ROIs and background ROI. **(B)** Individual bleedthrough-corrected time-dependent fluorescence intensity traces (blue - CFP, yellow - YFP) from ROI 4 in (A) after stimulation with 1 μM FSK. **(C)** Time-dependent FRET ratio R_t (grey) calculated from fluorescence intensities in (B). **(D)** Normalised, time-dependent FRET ratio changes ΔR_t calculated from (C) and analysed FRET response parameters (red). Scale bar = 20 μm.

accumulation caused by FSK (1 μM FSK vs. 3 μM FSK max. slope: M = -0.0465, 95% CI = -0.0813, -0.0117, p = 0.0073; 1 μM FSK vs. 10 μM FSK max. slope: M = -0.0708, 95% CI = -0.1048, -0.0369, p <0.0001).

FRET recordings from FSK-stimulated Epac1-HEK cells showed the feasibility of detecting live cell FRET signals with the image acquisition and analysis pipeline implemented within the scope of this work. For investigation of CB2 signalling in Epac1-CB2-HEK cells, a concentration of 1 μM FSK was chosen as the initial pre-stimulation of adenylyl cyclases. Stimulation of Epac1-HEK cells with 1 μM FSK showed that response parameters are suitable for a subsequent stimulation with CB2 agonists (ΔR_{max}: M = 22.49, 95% CI = 20.00, 24.99; t1/2: M = 352.1, 95% CI = 247.5, 456.8; slope: M = 0.0615, 95% CI = 0.0469, 0.0761; n = 13) and the response was not significantly slower than the FRET response to 3 μM FSK. Although FRET responses to 10 μM FSK were on average faster and larger (ΔR_{max}: M= 29.72, 95% CI = 25.37, 34.06; t1/2: M = 174.3, 95% CI = 137.8, 210.9; slope: M = 0.1324, 95% CI = 0.1097, 0.1552; n = 9), choosing 1 μM FSK minimises the risk of masking the anticipated $G\alpha_i$-mediated inhibition of cAMP production after CB2 activation.
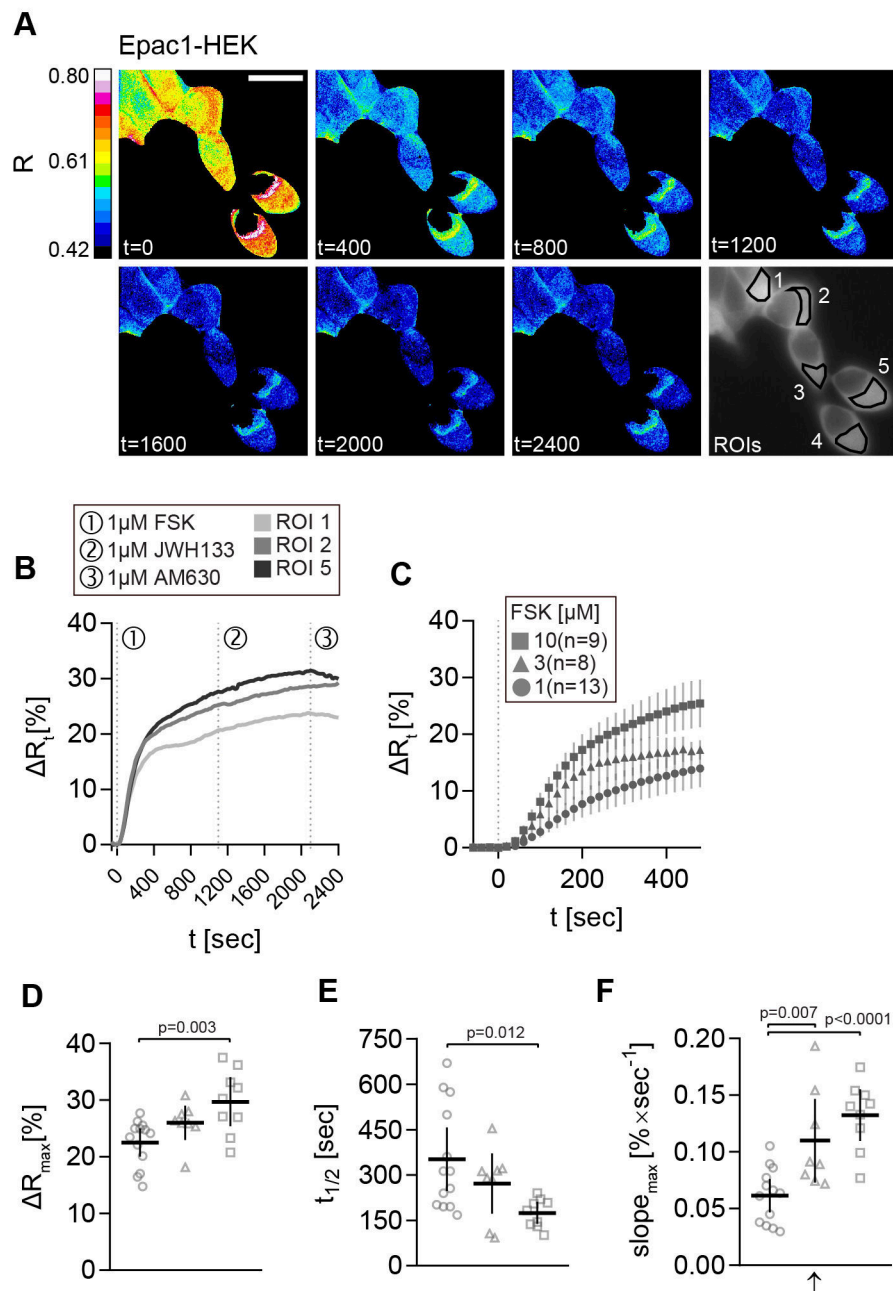
Figure 6.3. cAMP-FRET imaging of Epac1-HEK cells after stimulation with different concentrations of FSK. (A) Representative FRET ratio (R) images at different time points (t in seconds) and corresponding single cell FRET ratio (ΔR_t) **(B)** traces from indicated Epac1-HEK cells stimulated with 1 µM FSK (1), 1 µM CB2 agonist HU308 (2) and 1 µM AM630 (3). **(C)** Mean±95%CI ΔR_t FRET ratio traces showing the first 480 s after stimulation of Epac1-HEK cells with 1 µM, 3 µM and 10 µM FSK. **(D)** Maximum peak ΔR, **(E)** t1/2 and **(F)** max. slope values (arrow represents slope direction) of FRET responses to varying concentrations of FSK in Epac1-HEK cells. Data were analysed using Nested One-Way ANOVA with Tukey-adjusted p-values. Each independent data point *n* represents the average of all cells in one recording/coverslip. 1 µM FSK n = 13, 3 µM FSK n = 8, 10 µM FSK n = 9. Mean±95%CI. Scale bar = 20 µm.

6.2 Live Measurement of CB2-mediated cAMP Dynamics in Epac1-CB2-HEK Cells

6.2.1 Different CB2-mediated cAMP response patterns in Epac1-CB2-HEK cells

To investigate CB2-mediated cAMP signalling in living cells, a stimulation protocol in the generated stably transfected Epac1-CB2-HEK cells was established. First, cells were stimulated with 1 µM FSK to sub-maximally activate ACs and elicit cAMP production. After a baseline was reached, cells were stimulated with different CB2 agonists in supra-maximal concentrations to activate CB2 and inhibit cAMP production via $G\alpha_i$ subunits. Epac1-CB2-HEK cells were then stimulated with 1 µM AM630, a CB2-selective inverse agonist, to block recorded responses to CB2 agonists and show their CB2 specificity.

The data acquired from this stimulation scheme revealed the heterogeneity of the generated Epac1-CB2-HEK cell model in the response to CB2 stimulation. Three response types were distinguished, that all showed a clear relative increase of ΔR and therefore intracellular cAMP levels after stimulation with FSK: (1) Type R (responder), a "classical" cellular response with a detectable inhibition of FSK-mediated cAMP production after CB2 agonist stimulation, that was blocked by AM630; (2) Type CA (constitutive activity), no response of the cell to a CB2 agonist but a detectable increase in cAMP following stimulation with AM630 comparable to reported effects when a GPCR shows a high degree of constitutive activity (Bolognini et al., 2012); (3) Type N (non-responder), no response to either CB2 ligand.

In Fig. 6.4A processed FRET ratio (R) images from a representative recording of a group of Epac1-CB2-HEK cells are seen. These cells showed differences in their cAMP response to the stimulation protocol. Stimulation time points and individual cellular responses are seen in the corresponding ΔR line plots of three chosen cells (ROI 1, 5 and 7) (Fig. 6.4B). These cells representatively show the three different response types of Epac1-CB2-HEK cells to CB2 stimulation with ROI 1 as type R, ROI 7 as type CA and ROI 5 as type N. To further investigate the observed response patterns and to characterise them, first, the FRET responses to FSK were analysed.

Taking together FSK-response parameters from all recordings of Epac1-CB2-HEK cells with the different CB2 agonists and analysing them according to response type, small differences in the FRET response were seen (Fig. 6.4C,D,E,F). Within the first 480 s after FSK application, cells with response type N show the largest FRET change, which is depicted in Fig. 6.4C in averaged ΔR line plots. Maximal ΔR (M = 26.58, 95% CI = 24, 29.15) as well as max. slope values (M = 0.1106, 95% CI = 0.0855, 0.1356) (n = 6) were also increased in type N responders compared to R or CA types.

On average, type R responses were only marginally larger (M = 20.94, 95%CI = 19.21,
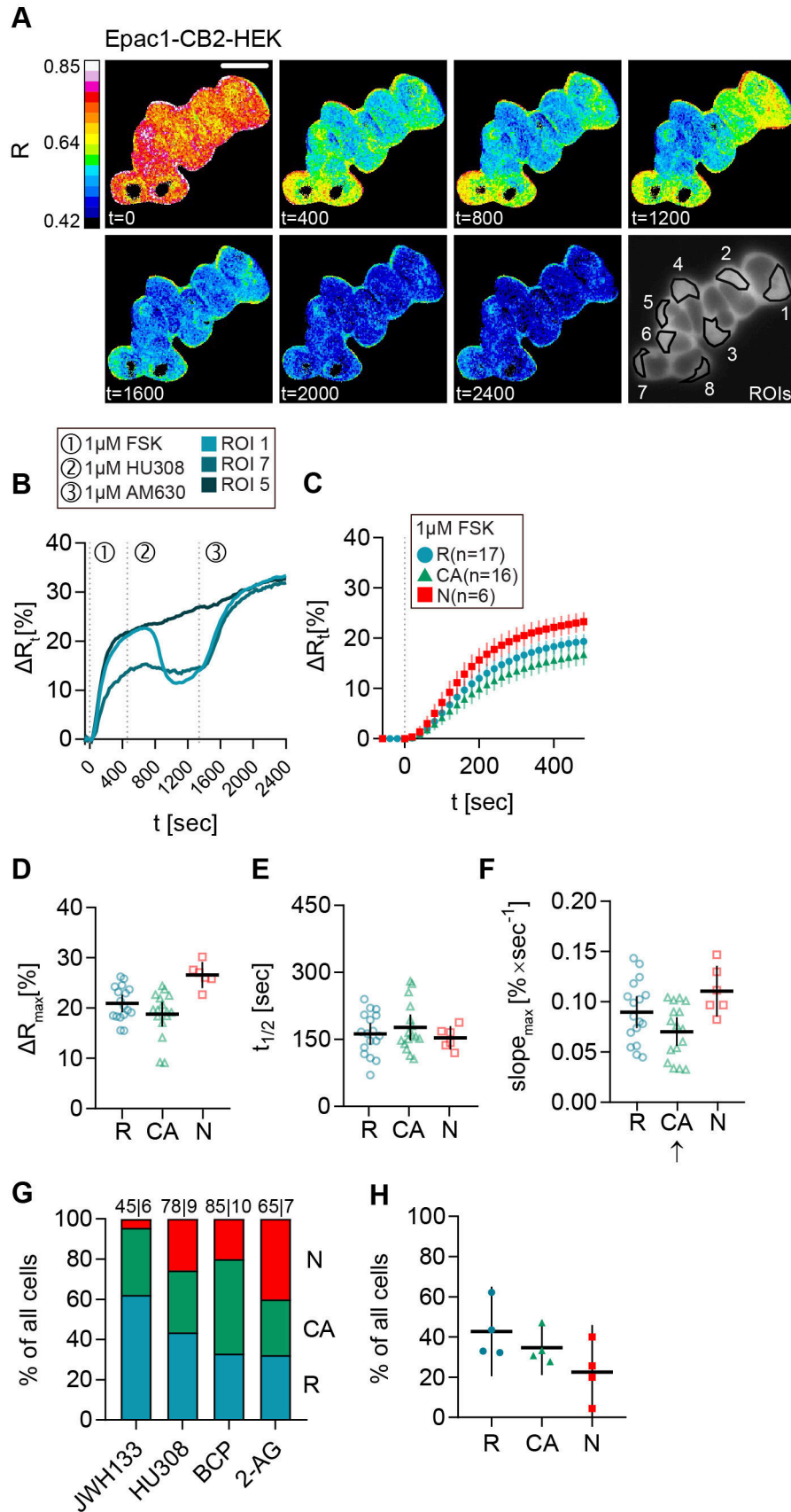
Figure 6.4. FSK response of different CB2 response types in Epac1-CB2-HEK cells. See next page for figure description.

Figure 6.4. FSK response of different CB2 response types in Epac1-CB2-HEK cells. (A) Representative FRET ratio (R) images at different time points (t in seconds) and corresponding single cell FRET ratio (ΔR_t) **(B)** traces from indicated cells stimulated with 1 µM FSK (1), 1 µM CB2 agonist HU308 (2) and 1 µM AM630 (3) showing the three response types R (ROI 1), CA (ROI 7), and N (ROI 5). **(C)** Mean±95%CI ΔR_t FRET ratio traces showing the first 480 sec after FSK stimulation of the different Epac1-CB2-HEK response types. **(D)** Maximum peak ΔR, **(E)** t1/2 and **(F)** max. slope values of FRET responses to FSK (arrow represents slope direction) of the different Epac1-CB2-HEK response types. **(G)** Relative frequencies of Epac1-CB2-HEK response types in recordings with different CB2 agonists. Numbers on top of bars represent the number of single cells/ROIs in total number of recordings. **(H)** Overall mean±95%CI percentage of each response type in Epac1-CB2-HEK cells. Each data point n in D, E, and, F represents the average of all cells in one recording/coverslip with at least three cells of a response type. Type R n = 17, Type CA n = 16, Type N n = 6. Mean±95%CI. Scale bar = 20 µm.

22.68) and steeper (M = 0.0898, 95% CI = 0.074, 0.1056) (n = 17) than responses from type CA cells (Fig. 6.4C,D,F). As sometimes three or more ROIs of two different response types were seen in one recording, the data are partially paired and further statistical test were not applied. Average half time values from the different response types that were around 150 s did not differ (Fig. 6.4E).

In Figure 6.4G the relative frequency of a cell's response type from Epac1-CB2-HEK cell recordings with different CB2-agonist stimulation protocols is seen. In these recordings the most abundant response type was R (M = 42.77, 95%CI = 20.54, 64.99) followed by CA (M = 34.71, 95%CI = 21.11, 48.31) and N (M = 22.52, 95%CI = -0.87, 45.91) (n = 4) (Fig. 6.4H).

In Figure 6.5A the mean±95%CI ΔR_t FRET ratio traces of type R, CA, and N Epac1-CB2-HEK cells are depicted together with Epac1-HEK cells after 1 µM FSK stimulation. Figure 6.5B, C, and D shows the mean±95%CI differences betwenn response parameters from type R, CA, and N cells to the results of the Epac1-HEK cell stimulation with 1 µM FSK (see Results subsection 6.1.2). Max. ΔR values of type R cells stimulated with 1 µM FSK differed the least compared to control cells (M = -1.55, 95%CI = -5.04, 1.94) but showed lower max. ΔR on average. Type CA showed max. ΔR responses smaller than control cells with a larger difference than type R (M = -3.72, 95%CI = -7.25, -0.19). A higher FSK-elicited max. ΔR compared to Epac1-HEK cells was seen for Epac-CB2 type N cells (M = 4.08, 95%CI = -0.59, 8.75) (Fig. 6.5B). FRET responses from Epac1-CB2-HEK cells to FSK had faster half-time values compared to control cells in all response types (R: M = -190, 95%CI = -276, -104; CA: M = -175, 95%CI = -263, -88; N: M = -198, 95%CI = -314, -83) (Fig. 6.5C). Max. slopes of FRET responses from type CA showed the smallest difference to control cells (M = 0.0089, 95%CI = -0.0159, 0.034), whereas type R and N max. slopes were steeper by a higher margin (R: M = 0.0283, 95%CI = 0.0039, 0.0528; N: M = 0.0491, 95%CI = 0.0164, 0.0819) (Fig. 6.5D).

The analysis of FSK-elicited FRET responses in Epac1-CB2-HEK cells showed that through functional CB2 receptors, either possibly constitutively active (type CA) or not (type R), the cAMP production upon direct AC activation via FSK might already be affected in magnitude and speed. The presence of different GPCR conformations and their abun-

Difference to Epac1-HEK 1µM FSK
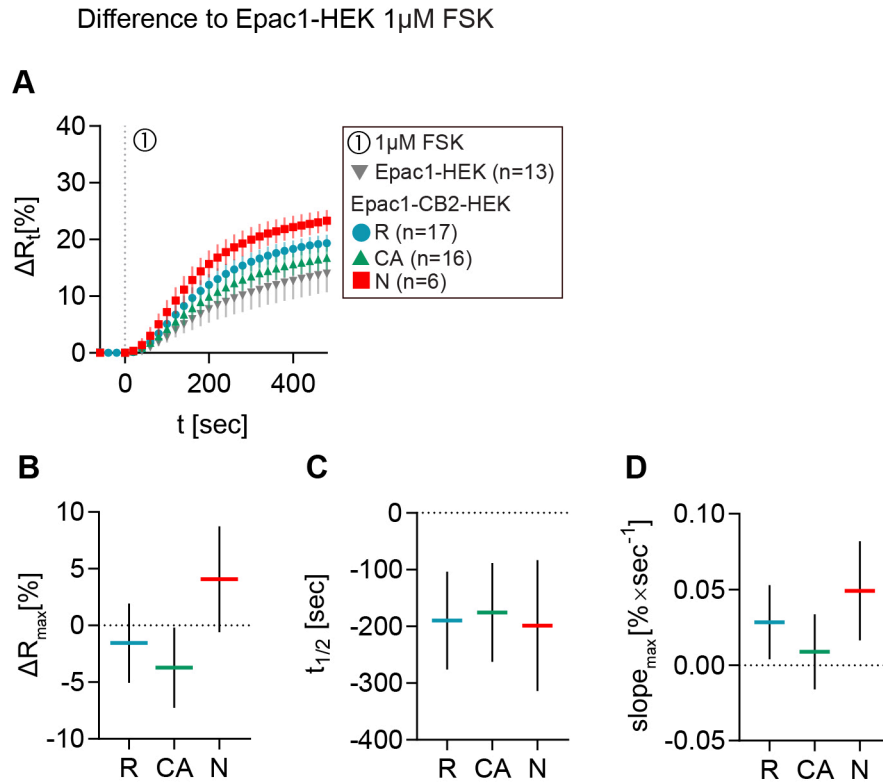
Figure 6.5. Differences in FRET response parameters after FSK stimulation between Epac1-CB2-HEK response types and Epac1-HEK cells. (A) Mean±95%CI ΔR_t FRET ratio traces showing the first 480 s after FSK stimulation of the different Epac1-CB2-HEK response types compared to Epac1-HEK cells (taken from 6.3C and 6.4C). **(B)** ΔR, **(C)** t1/2, and **(D)** max. slope mean±95%CI differences between Epac1-CB2-HEK type R, CA, and N responders to Epac1-HEK cells stimulated with 1 µM FSK. Mean±95%CI.

dance at the membrane has been shown to influence availability of $G\alpha_i$ and $G\beta\gamma$ subunits as well as AC activation via FSK or $G\alpha_s$ subunits specifically in heterologous expression systems (Mancini et al., 2009; Bolognini et al., 2012).

6.2.2 Reduction of cAMP levels after CB2 activation with different agonists in Epac1-CB2-HEK cells

To evaluate the generated cell model regarding its functionality and reliability of characterising CB2-mediated cAMP signalling and CB2 ligands, the stimulation protocol explained in Results subsection 6.2.1 was applied. A variety of CB2 agonists was used to investigate the universality of observed cellular responses to CB2 activation. Agonists used in these experiments are the synthetic selective CB2 agonists JWH133 and HU308, the phytocannabinoid β-caryophyllene as well as the endocannabinoid and CB1/CB2 agonist 2-AG. All CB2-agonists were applied in supra-maximal concentrations to elicit maximal CB2 activation.

Following agonist stimulation, cells were stimulated with $1\,\mu M$ of the selective CB2 inverse agonist/antagonist AM630 to specifically block the agonist response. FRET data summarised in Figure 6.6 originates from all Epac1-CB2-HEK cell recordings with at least three individual type R cells/ROIs.

Figure 6.6A shows ΔR_t line plots from different representative ROIs stimulated with FSK (1), JWH133, HU308, BCP or 2-AG (2) and AM630 (3). The cells showed a ΔR increase by about 20% after stimulation with $1\,\mu M$ FSK and following stimulation with CB2 agonist a ΔR decrease between 5 and 10% was seen. This ΔR decrease represents the direct inhibition of FSK-elicited cAMP production via CB2 activation in living Epac1-CB2-HEK cells. Subsequent stimulation with $1\,\mu M$ AM630 resulted in a ΔR increase of about 15%. The blockage of CB2-mediated cAMP inhibition via AM630 shows the specificity of the agonist response and the reversibility of receptor activation.

Summarised ΔR extreme values after each stimulation time point (within one recording) show the similarity between type R recordings from different CB2-agonist stimulation protocols (Fig. 6.6B). Corresponding analysis of ΔR differences between each baseline after substance stimulation revealed similar mean values between recordings from different CB2-agonists that ranged between a decrease of 5 to 7% (JWH133: M = -5.77, 95%CI = -8.3, -3.24; HU308: M = -6.92, 95%CI = -9.17, -4.66; BCP: M = -5.98, 95%CI = -8.49, -3.47; 2-AG: M = -5.78, 95%CI = -9.53, -2.03) (Fig. 6.6E). This was also reflected by the small variation of overall cAMP inhibition caused by the different CB2 agonists (JWH133: M = 31.85, 95%CI = 21.70, 41.99; HU308: M = 33.95, 95%CI = 26.41, 41.49; BCP: M = 25.50, 95%CI = 19.85, 31.15; 2-AG: M = 25.20, 95%CI = 7.02, 43.38) (Fig. 6.6C). On average, agonist-elicited response parameters max. slope and time to half-maximum did not show significant differences between recordings (Fig. 6.6D, G).

FRET responses of Epac1-CB2-HEK cells to $1\,\mu M$ of CB2 inverse agonist AM630 showed more variability depending on precedent CB2 agonist stimulation (Fig. 6.6D, G, F). Mean differences in ΔR between CB2 agonist and AM630 baseline ranged between 10 and 17% (JWH133: M = 13.00, 95%CI = 10.10, 15.91; HU308: M = 16.42, 95%CI = 13.80, 19.04;

BCP: M = 11.94, 95%CI = 4.81, 19.07; 2-AG: M = 12.27, 95%CI = 9.63, 14.90) (Fig. 6.6F). AM630 responses in JWH133 stimulated cells showed on average a larger half-time (M = 379, 95%CI = 297, 461) and lower max. slope values (M = 0.0261, 95%CI = 0.0198, 0.0323) compared to the other agonist stimulation protocols (Fig. 6.6D, G). The difference in AM630 response half-time between JWH133 and BCP stimulated cells was most prominent (JWH133 vs. BCP: M = 133, 95%CI = 28, 239, p = 0.0125) (Fig. 6.6D).

The comparison of the maximal FRET response ΔR_{max} in Epac1-HEK cells after stimulation with 1 µM FSK and the end-point ΔR values of Epac1-CB2-HEK cells after completion of the stimulation protocol revealed that after stimulation with AM630, Epac1-CB2-HEK cells had higher cAMP levels than control cells stimulated with FSK (Fig. 6.6H). This difference in ΔR was most evident in Epac1-CB2-HEK cells from the HU308 (Epac1-HEK FSK vs. HU308: M = -5.96, 95%CI = -10.96, -0.96, p = 0.0153) and 2-AG (Epac1-HEK FSK vs. 2-AG: M = -6.02, 95%CI = -11.64, -0.41, p = 0.0323) stimulation protocol (Fig. 6.6H). This observation was also made when comparing ΔR values after FSK stimulation to ΔR values after AM630 stimulation within the same recording from Epac1-CB2-HEK cells (Fig. 6.6B) and additionally hints towards the presence of constitutive CB2 activity in Epac1-CB2-HEK cells that show a type R response.

Acquired FRET data from Epac1-CB2-HEK cells stimulated with different CB2 agonists showed that detecting the inhibition of cAMP production in live cells via activation of the $G\alpha_i$-coupled receptor CB2 was possible with the implemented imaging pipeline. The cellular cAMP-FRET response to all supra-maximally applied CB2 agonist showed high similarity in all analysed response parameters and overall cAMP inhibition. Remarkably, none of the CB2 agonists completely inhibited all FSK-elicited cAMP production in live cells in these assays. Although there was some variation and a higher variety in cellular responses towards the CB2 inverse agonist AM630, that was applied after CB2 agonists, a clear blockage of CB2-mediated cAMP inhibition was seen in all analysed recordings. Part of the AM630 response variation may be explained by its competition with an agonist for CB2 binding as well as the single-cell-dependent composition of different receptor conformations. The ligands have different affinities towards CB2 (see Introduction section 3.2.2) and its varying conformational states that could account for stronger or weaker blocking of the agonist effects. It was evident from the AM630 elicited cAMP response that Epac1-CB2-HEK type R responders may also exhibit some degree of constitutive activity.

This Epac1-CB2-HEK cell model may therefore be used to detect intracellular cAMP changes in living cells upon CB2 activation or blockage. However, in terms of precisely characterising the efficacy of CB2 agonists to engage cAMP pathways in living cells, the obtained maximal FRET changes and accuracy in the detection of FRET responses might not be sufficient.
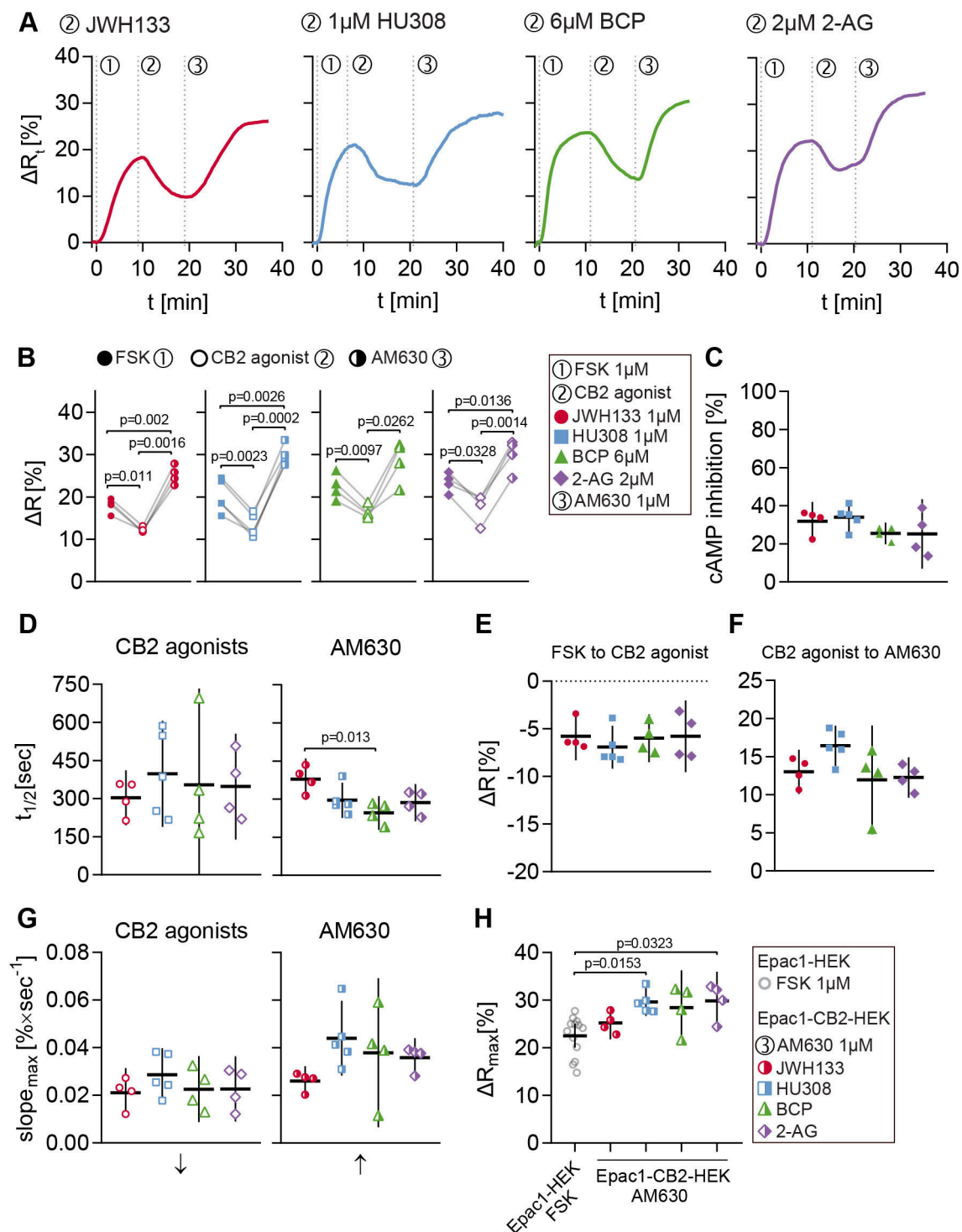
Figure 6.6. FRET responses to CB2 agonists and AM630 in Epac1-CB2-HEK type R cells. (A) Representative single cell FRET ratio (ΔR_t) traces of Epac1-CB2-HEK cells stimulated with 1 μM FSK (1), 1 μM then JWH133 (n=4), HU308 (n=5), BCP (n=4) or 2-AG (n=4) (2) and 1 μM AM630 (3). **(B)** Baseline FRET (ΔR) values after FSK (full icon), CB2 agonists (hollow icon; JWH133: red circles; HU308: blue squares; BCP: green triangles; 2-AG: violet diamonds) and AM630 (half-full icon). Data were analysed using Two-Way ANOVA with repeated measures and Sidak-adjusted p-values. **(C)** Inhibition of FSK-elicited cAMP production by different CB2 agonists. **(D)** t1/2 and **(G)** max. slope values (arrows indicate direction of slope) of FRET responses until CB2 agonist (left) and AM630 (right) baselines from stimulations with different CB2 agonists. **(E)** ΔR differences from FSK to CB2 agonist and CB2 agonist to AM630 **(F)** baselines from stimulations with different CB2 agonists. **(H)** Comparison between max. ΔR responses from Epac1-HEK cells stimulated with 1 μM FSK (n=13) and Epac1-CB2-HEK cells after the AM630 response. Data were analysed using Nested One-Way ANOVA with Tukey- (C, D, E, F, G) or Dunnett- (H) adjusted p-values. Each data point *n* represents the average of all cells in one recording with at least three responding cells. Mean±95%CI.

6.3 CB2 Effects on β-adrenergic Receptor Signalling in Epac1-CB2-HEK Cells

6.3.1 Stimulation of β-adrenergic receptors in Epac1-CB2-HEK cells leads to a negative cAMP feedback

In order to further characterise CB2-mediated cAMP signalling and to investigate receptor crosstalk with the β-adrenergic system, a CB2/βAR stimulation protocol was applied. As previously reviewed (see Introduction section 3.2.4), βAR are predominantly Gα_s-coupled receptors that activate ACs causing an increase in intracellular cAMP levels. Specifically β_1AR and β_2AR are highly expressed in mammals and in HEK293 cells β_2AR is the most abundant βAR (Atwood et al., 2011). Signalling from βAR is well investigated because of their important physiological role in various tissues.

To characterise the cAMP response of Epac1-CB2-HEK cells to the activation of βAR and to investigate a possible modulation by CB2, cells were stimulated with 100 nM of the βAR-agonist isoprenaline (ISO) either solely or together with 1 µM JWH133. Last, 1 µM AM630 were applied to block CB2 effects and obtained results were compared to FRET responses of Epac1-HEK cells treated with the same stimulation protocol.

In Figure 6.7A, ΔR_t line plots from three representative Epac1-HEK or Epac1-CB2-HEK ROIs stimulated with ISO or ISO and JWH133 followed by AM630 are seen. Epac1-HEK cells (grey) responded to βAR activation via ISO with a strong, persistent increase in ΔR (ISO$_{max}$) representing the production of cAMP via Gα_s subunits (M = 27.57, 95%CI = 20.89, 34.24, n = 4) (Fig. 6.7B). With a mean half time of 76 s (M = 76, 95%CI = -3, 156) and max. slope of 0.2454 ΔR per second (M = 0.2454, 95%CI = 0.1394, 0.3515) the ISO$_{max}$ baseline was reached rapidly (Fig. 6.7C,D). Epac1-HEK cells were non-responsive towards AM630 in this stimulation protocol confirming the results from 6.1.2 (Fig. 6.7A).

In Epac1-CB2-HEK cells the cAMP response to ISO stimulation showed differences compared to Epac1-HEK cells as a negative cAMP feedback response was observed (6.7A, blue). After reaching a transient ISO$_{max}$, the ΔR signal decreased to a lower baseline (ISO$_{fb}$). This βAR response to ISO was seen in Epac1-CB2-HEK cells with (6.7A, red) and without CB2 co-activation (6.7A, blue). Comparing mean response parameters of ISO$_{max}$ between cell types and conditions, Epac1-CB2-HEK cells showed a slightly smaller mean ΔR amplitude (M = 17.46, 95%CI = 10.02, 24.89) without than with CB2 co-activation (M = 20.23, 95%CI = 14.51, 25.94).

However, both Epac1-CB2-HEK conditions showed a mean reduction of ISO$_{max}$ ΔR compared to Epac1-HEK cells (6.7B). Mean t1/2 and max. slope values of the ISO$_{max}$ responses showed a higher similarity between cell types and conditions. CB2 activation modulated the ISO$_{max}$ response towards shorter t1/2 and larger max. slope values compared to no CB2 activation (Epac1-CB2 vs. Epac1-CB2 + JWH133; t1/2: M = 29, 95%CI = -32, 90; slope: M = -0.0474, 95%CI = -0.1318, 0.037) (Fig. 6.7C,D).
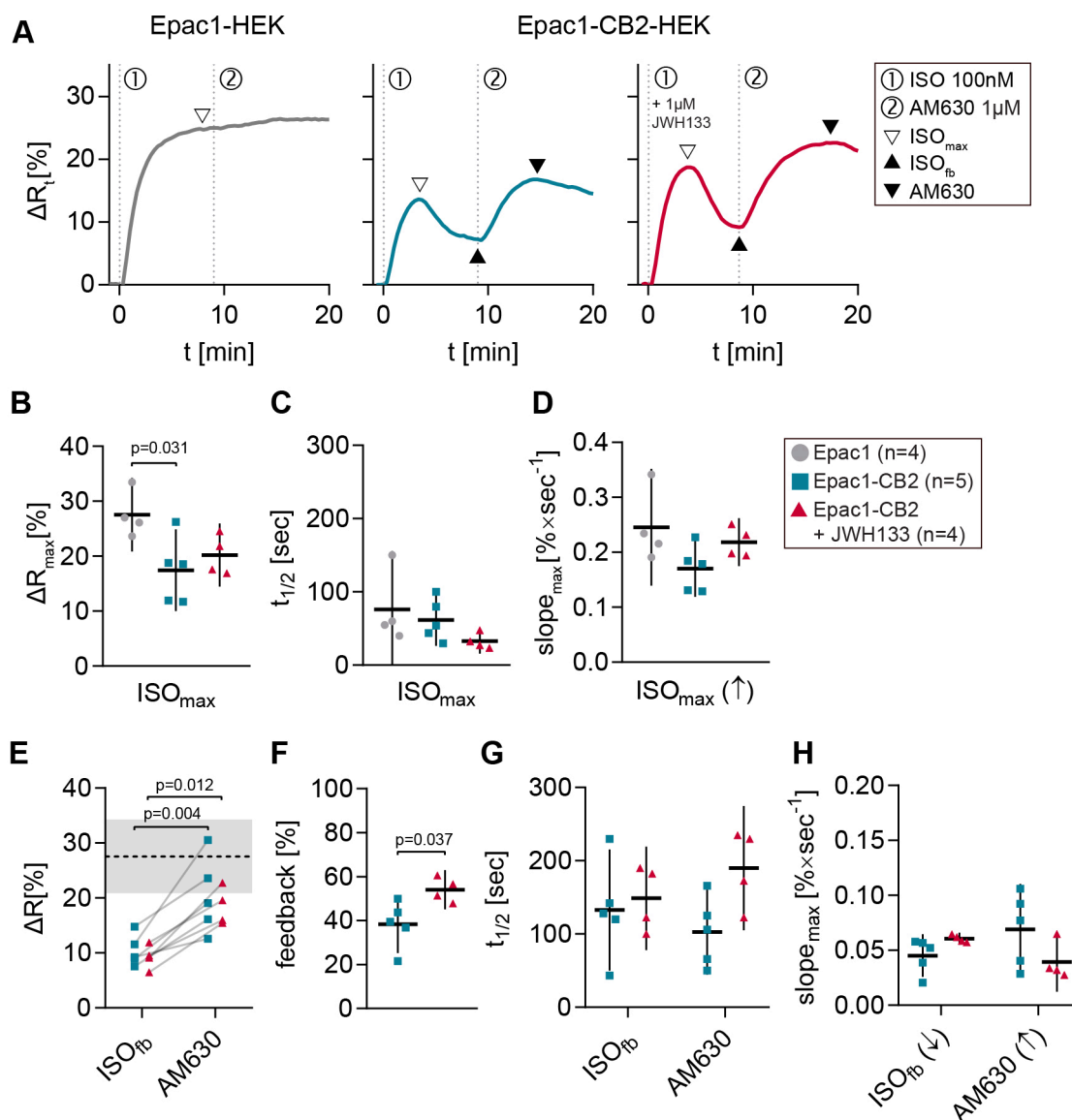
Figure 6.7. FRET responses to βAR activation and co-stimulation of CB2 in Epac1- and Epac1-CB2-HEK cells. (A) Representative single cell FRET ratio (ΔR_t) traces of Epac1-HEK (left, grey) and Epac1-CB2-HEK (middle, blue) cells stimulated with 100 nM βAR-agonist ISO (1) and 1 μM AM630 (2) as well as Epac1-CB2-HEK cells co-stimulated with 100 nM ISO and 1 μM JWH133 (1, right, red) and AM630 (2). **(B)** Maximum peak ΔR, **(C)** t1/2 and **(D)** max. slope values (arrow indicates direction of slope) of the FRET response until the max. ISO peak (ISO$_{max}$) are shown for all cell types and conditions. Data were analysed by using Nested One-Way ANOVA with Tukey-adjusted p-values. **(E)** Baseline FRET (ΔR) values after negative ISO feedback (ISO$_{fb}$) and AM630 response. The dotted black line represents the mean and the grey area shows the 95%CI of ISO$_{max}$ ΔR from Epac1-HEK cells. Data were analysed using Two-Way ANOVA with repeated measures and Sidak-adjusted p-values. **(F)** Negative cAMP feedback in percent in Epac1-CB2-HEK cells ($\pm$ JWH133). Analysed with Nested unpaired t-test. **(G)** t1/2 and **(H)** max. slope (arrows indicate direction of slope) of the indicated responses in Epac1-CB2-HEK cells ($\pm$ JWH133). Data were analysed using Two-Way ANOVA with Sidak-adjusted p-values. Each independent data point *n* represents the average of all cells in one recording/coverslip with at least three responding cells. Epac1-HEK n = 4, Epac1-CB2-HEK n = 5, Epac1-CB2-HEK + JWH133 n = 4. Mean$\pm$95%CI.

Investigation of the negative cAMP feedback response to ISO ($\pm$ JWH133), ISO_{fb}, in Epac1-CB2-HEK cells in relation to ISO_{max} showed that it was larger with CB2 activation than without (Epac1-CB2 vs. Epac1-CB2 + JWH133: M = -15.29, 95%CI = -29.35, -1.23, p = 0.0369) (Fig. 6.7F). Application of AM630 in Epac1-CB2-HEK cells further revealed that the feedback was partially blocked by AM630 as it did not reach Epac1-HEK ISO_{max} ΔR values (mean, dotted black line) ($\pm$ 95%CI, grey area), but still led to an increase in ΔR of about 10% in both conditions (Fig. 6.7E). FRET response parameters t1/2 and max. slope of ISO_{fb} supported the similarity of the cAMP feedback dynamics between Epac1-CB2-HEK cells with and without additional CB2 activation (Fig. 6.7G, H). Cellular responses towards AM630, however, were slower (Epac1-CB2 vs. Epac1-CB2 + JWH133; M = -87, 95%CI = -178, 3, p = 0.0591) and had flatter slopes (M = 0.0295, 95%CI = -0.0062, 0.0651, p = 0.1114) in Epac1-CB2-HEK cells co-stimulated with ISO and JWH133 than cells stimulated with ISO alone (Fig. 6.7G, H).

The results showed that $G\alpha_s$-mediated cAMP signalling via βAR is potentially affected by the presence of CB2 in Epac1-CB2-HEK cells. The negative cAMP feedback upon βAR-activation in these cells, that is absent in Epac1-HEK cells, seems to be independent of direct CB2 activation. However, the significant difference seen in the feedback relative to ISO_{max} between βAR and βAR-CB2 stimulated cells may be attributed to the increased ISO_{max} ΔR in co-stimulated Epac1-CB2-HEK cells.

Small differences in mean t1/2 and max. slope values of ISO_{max} in co-stimulated cells support the interpretation that CB2 activation may modulate βAR mediated cAMP signalling in addition to affecting cells by its presence. Addition of JWH133 also led to the deceleration of the cAMP increase after stimulation with AM630 in Epac1-CB2-HEK cells, but not to its general reduction.

Overall, intracellular cAMP levels after βAR activation in Epac1-CB2-HEK cells were lower compared to Epac1-HEK cells irrespective of CB2 activation, which may hint towards a potential cross-activation of CB2 upon βAR activation and/or the possible influence of constitutively active CB2 receptors and their effect on ACs.

6.3.2 β_2AR and CB2 form a complex and co-localise at the membrane of co-transfected HEK293 cells

The data from FRET studies with single- and co-stimulation of βAR and CB2 receptors in Epac1-CB2-HEK cells offered different interpretations of the obtained results, among those the co-activation of CB2 upon stimulation with βAR-agonist isoprenaline. Cross- or co-activation of GPCRs may happen if the two receptors in question form a heteromer (see Introduction section 3.1) and because β_2AR is the most abundant βAR in HEK293 cells, the possibility of heterodimerisation between β_2AR and CB2 was investigated.

To test whether CB2 and β_2AR form a complex when co-expressed, constructs coding for FLAG-hCB2 and HA-hβ_2AR were transfected into HEK293 cells. Each receptor was immunoprecipitated and imunoprecipitation (IP) samples were analysed using SDS-PAGE (sodium dodecyl sulfate polyacrylamide gel electrophoresis).
Figure 6.8A shows the detection of HA-β_2AR at 55kDa in FLAG-CB2 IP probes (Fig. 6.8A, FLAG-IP, second row, first lane from the left) and FLAG-CB2 at 35kDa in the HA-β_2AR-IP (Fig. 6.8B, HA-IP, first row, first lane from the left) from co-transfected HEK293 cell lysates. The detection of each bait receptor for each IP in co-transfected HEK293 was detected for both receptors (Fig. 6.8A, FLAG-IP, first row, first lane; Fig. 6.8B, HA-IP, second row, first lane). Control IPs from single-transfections did not show the co-precipitation of either HA-β_2AR in FLAG-IP (Fig. 6.8A, FLAG-IP, both rows, second lane) or FLAG-CB2 in HA-IP (Fig. 6.8B, HA-IP, both rows, third lane). In input samples, HA-β_2AR and FLAG-CB2 were detected in all lysates from cells that were transfected with the constructs (Fig. 6.8A,B, Input, all rows, lanes 1-3). Mock-transfected cells were negative for HA and FLAG expression in input and IP samples (Fig. 6.8A,B, all rows, fourth lane).

To further investigate the localisation of potential HA-β_2AR-FLAG-CB2 complexes in co-transfected HEK293 cells, receptor expression was detected using ICC. Mouse anti-HA and rabbit anti-CB2 antibodies (and rabbit anti-β_2AR and mouse anti-FLAG) were used to specifically bind the receptors. Representative confocal microscopy images (Fig. 6.9) of stained transfected HEK cells revealed abundant receptor expression and specific fluorescent signals for HA (green), CB2 (magenta) and DAPI (nuclei, blue). Strong fluorescent signals from both HA and CB2 were seen at the plasma membrane of co-transfected HEK cells (Fig. 6.9, first column).
Object-based co-localisation analysis of confocal z-stacks further showed that 24.23 % of all detected pixels (HA and CB2 signal) were co-localised in the presented samples (repetitions see Table 6.1) and mainly localised at the membrane (Fig. 6.9, first column: coloc (red) and merge (white arrows)). Single-transfected control cells showed robust fluorescent signal for each transfected construct and none to weak unspecific signals (Fig. 6.9, second and third column: HA, CB2, DAPI).
Co-localisation analysis showed 3.61 % co-localised pixels in HA-β_2AR single transfected and 1.29 % in FLAG-CB2 transfected cells (Fig. 6.9, second and third column, coloc).
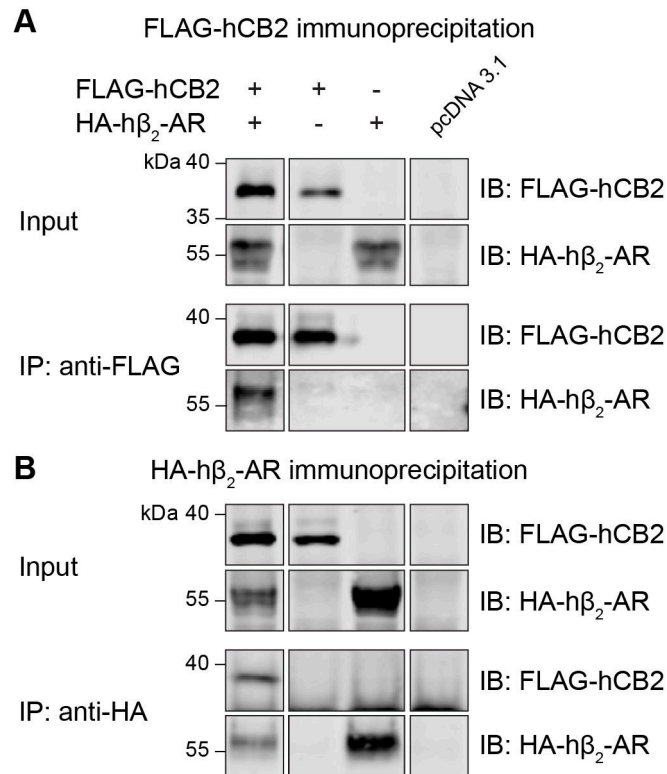
Figure 6.8. Co-immunoprecipitation of HA-β_2AR and FLAG-CB2 in transfected HEK293. Representative Western Blots of **(A)** FLAG-CB2 and **(B)** HA-β_2AR Co-IP experiments from single-, co- and mock-transfected HEK293. Bands are cropped and complete blots are found in Appendix 10.4.

The combination of co-immunoprecipitation and ICC showed that HA-β_2AR and FLAG-CB2 may form protein-complexes that localise at the cell membrane of co-transfected HEK293 cells. Judging from present results, a possible formation of functional β_2AR-CB2 heterodimers at the plasma membrane may be possible and may play a role in the observed receptor cAMP crosstalk (see Results subsection 6.3.1).

Table 6.1. Object-based co-localisation analysis of confocal image z-stacks from HA-β_2AR and FLAG-CB2 co-transfected HEK293

Coverslip	HA-β_2AR stain	FLAG-CB2 stain	% co-localised pixel from total pixel
1	anti-HA	anti-CB2	24.23
2	anti-HA	anti-CB2	19.23
			15.60
			17.50
			22.00
3	anti-β_2AR	anti-FLAG	19.12
			27.38
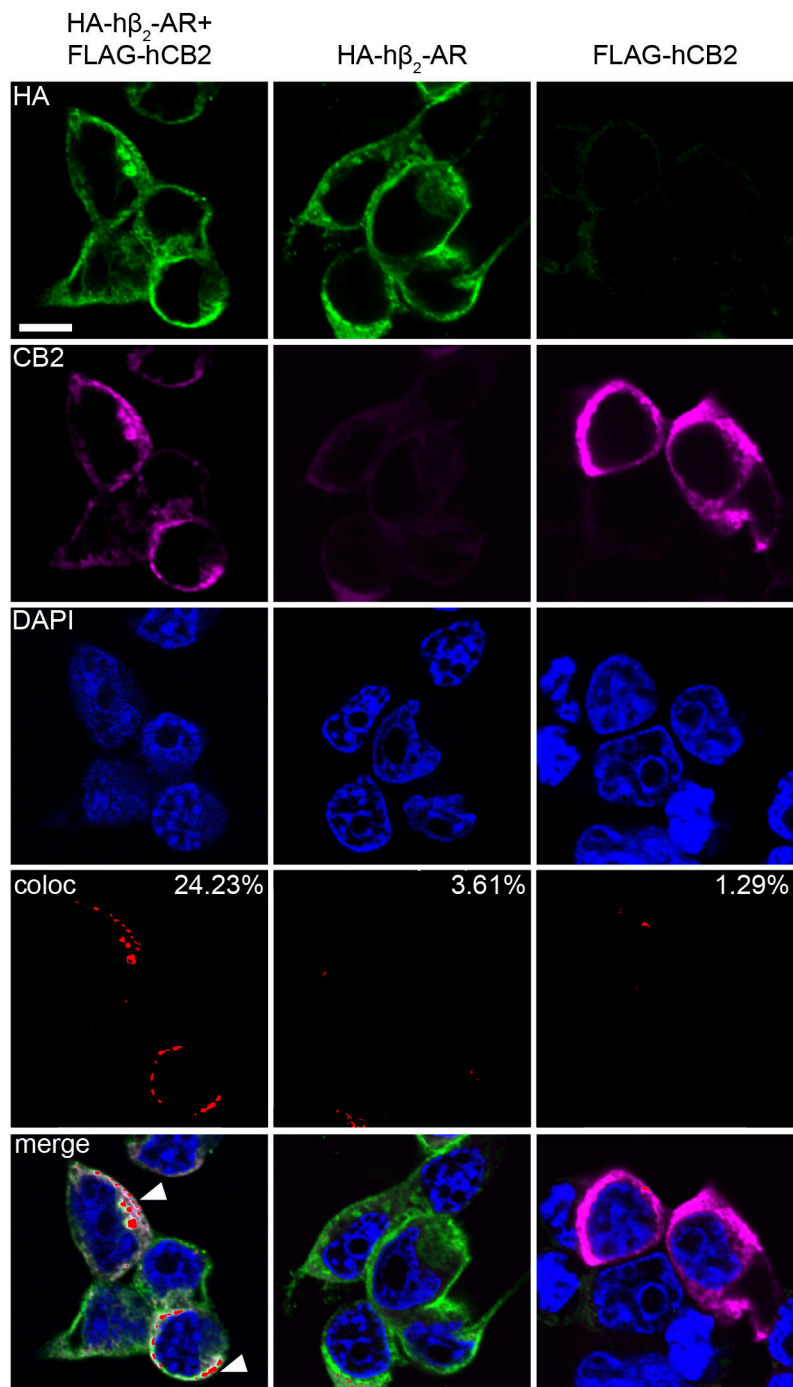
Figure 6.9. Representative confocal microscopy images of ICC detection of HA and CB2 and co-localisation analysis in single- and co-transfected HEK293. First column of images shows co-transfected HEK with human HA-β_2AR and FLAG-CB2. Second and third column show single-transfections with HA-β_2AR and FLAG-CB2, respectively. HA-staining of cells is seen in the first row of images (green), CB2-staining in the second (magenta) and DAPI-staining in the third row (blue). Red objects in the coloc images (fourth row) depict regions of fluorescence signal co-localisation and in the right corner of the images the percentage of co-localised pixels for the complete image stack is given. White arrowheads in the merged images (fifth row) also show areas of co-localisation from HA and CB2 fluorescent signals. Scale bar = 10 µm.

6.3.3 Co-stimulation of βAR and CB2 receptors enhances ERK1/2 activation in Epac1-CB2-HEK cells

CB2 as well as βAR receptors activate the ERK1/2 signalling pathway upon activation with an agonist. To investigate effects of a possible β_2AR-CB2-heterodimer and/or receptor crosstalk on ERK1/2 signalling, Epac1- and Epac1-CB2-HEK cells were stimulated with combinations of JWH133, ISO and AM630 and protein levels of activated (phosphorylated) ERK1/2 were analysed using SDS-PAGE and immunoblotting.

Figure 6.10A shows representative immunoblots of phosphorylated ERK (pERK) and total ERK (ERK) protein expression from four hours serum-starved Epac1- and Epac1-CB2-HEK cells stimulated with the indicated substances for 5 minutes. These blots showed stronger pERK band intensities in both cell types for conditions with ISO (Fig. 6.10A, lanes 2, 3, 4, 6 from the left) compared to vehicle control (Fig. 6.10A, DMSO). Epac1-CB2-HEK cells additionally showed a stronger pERK signal in JWH133 stimulated cells (Fig. 6.10A, lane 1 from the left) and the absence of this observation in the JWH133 + AM630 condition (Fig. 6.10A, lane 5 from the left).

Quantification of all blots and analysis of the mean log_2 fold change of the pERK to ERK ratio normalised to DMSO (vehicle control) corroborated this by showing that ISO stimulated cells have a 2 to 4-fold increase in pERK/ERK compared to control cells in both cell types (Fig. 6.10B). In single CB2-stimulated conditions, Epac1-CB2-HEK cells showed a two-fold increase in relative pERK levels upon JWH133 stimulation (M = 0.90, 95%CI = 0.58, 1.23, n = 9) compared to JWH133-stimulated Epac1-HEK cells (Epac1 vs. Epac1-CB2: M = -1.15, 95%CI = -1.94, -0.35, p = 0.001) (Fig. 6.10B). This increase in ERK1/2 phosphorylation was blocked by using AM630 in Epac1-CB2-HEK cells (M = -0.05, 95%CI = -0.46, 0.37, n = 9) (Fig. 6.10B). Stimulation with AM630 alone did not elicit a change in pERK/ERK compared to control cells from both cell types (Epac1: M = -0.08, 95%CI = -0.32, 0.15, n = 8; Epac1-CB2: M = -0.35, 95%CI = -0.81, 0.1, n = 9) (Fig. 6.10B).

βAR/CB2 co-stimulated Epac1-CB2-HEK cells (JWH133 + ISO) showed pERK levels twice as high as Epac1-HEK cells (Epac1 vs. Epac1-CB2: M = -1.04, 95%CI = -1.84, -0.25, p = 0.0034) reflecting a stronger activation of ERK1/2 upon stimulation of both βAR and CB2 (Fig. 6.10B). The enhanced ERK1/2 response to βAR-CB2 co-stimulation in Epac1-CB2-HEK cells was again reduced to Epac1-HEK levels with AM630 present to block CB2 activation (ISO + JWH133 + AM630; Epac1 vs. Epac1-CB2: M = 0.34, 95%CI = -0.45, 1.13, p = 0.86) (Fig. 6.10B). Stimulation with ISO + AM630 did not elicit different responses in Epac1- and Epac1-CB2-HEK cells (Epac1 vs. Epac1-CB2: M = 0.47, 95%CI = -0.34, 1.29, p = 0.57) and showed a two-fold increase in pERK/ERK for both cell types compared to DMSO control (Epac1: M = 1.41, 95%CI = 0.87, 1.95, n = 9; Epac1-CB2: M = 0.94, 95%CI = 0.38, 1.49, n = 9) (Fig. 6.10B).
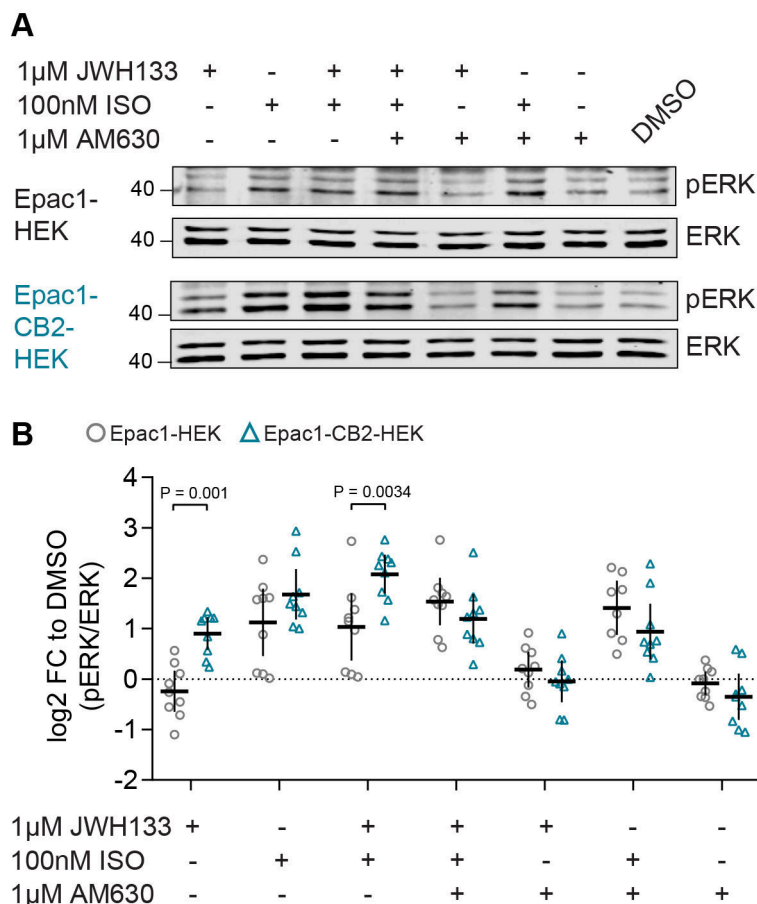
Figure 6.10. Analysis of MAPK ERK1/2 signalling pathway activation after βAR and CB2 activation Epac1- and Epac1-CB2-HEK cells. (A) Representative Western Blots of pERK and ERK detection in 4-hrs-serum-starved Epac1- and Epac1-CB2-HEK cells stimulated for 5 min with JWH133, ISO, AM630 and solvent control (DMSO) as indicated. **(B)** Quantification of ERK1/2 activation is represented by the log_2 fold change (FC) of the pERK/ERK band intensity ratio of each condition relative to the solvent control on the same blot. Each independent data point n represents the quantification of one blot (Epac1-HEK: grey circle; Epac1-CB2-HEK: blue triangle). Data were analysed by using Two-Way ANOVA with Sidak-adjusted p-values. Mean$\pm$95%CI. Complete blots are found in the Appendix 10.4.

The results from the analysis of ERK1/2 activation in Epac1- and Epac1-CB2-HEK cells showed that 5-minute ISO-stimulation robustly phosphorylated ERK1/2 in both cell types and that differences in Epac1-CB2-HEK cells were seen in conditions where CB2 was (co-)activated. In Epac1-CB2-HEK cells, JWH133 increased ERK1/2 activation which was blocked by AM630 and, in addition to ISO, JWH133 enhanced pERK/ERK levels. AM630 blocked this enhancement in Epac1-CB2-HEK cells. Although stimulation with ISO alone and together with AM630 shows small mean pERK/ERK differences between Epac1-CB2-HEK and Epac1-HEK cells, these changes were not statistically significant or large enough to conclude that CB2 is co-activated by βAR-stimulation or that βAR-mediated ERK1/2 activation may be blocked by an CB2 antagonist (cross-antagonism). However, the observed enhancement of ERK1/2 activation after co-stimulation of βAR and CB2 in Epac1-CB2-HEK cells may hint towards synergistic effects and/or positive crosstalk between the receptors.

6.4 cAMP Measurement in Adult Mouse Microglia Primary Cell Cultures and Effects of CB2 and βAR activation

6.4.1 Meta-analysis of GPCR-related RNAseq expression data from mouse microglia

RNA sequencing (RNAseq) studies have provided valuable insights in the expression profiles of tissues and cell types and helped to understand their plasticity and function. As a majority of microglia RNAseq studies did not focus on GPCR biology, coherent data on the GPCR composition of these cells is not easily accessible although the data is publicly available. To gather knowledge on microglial GPCR expression, especially CB2 and βAR, and proteins relevant in cAMP signalling, such as adenylyl cyclases and phosphodiesterases, publicly available RNAseq data repositories were searched for expression data from adult mouse microglia and summarised with the same analysis pipeline.

Studies were chosen that provide microglia RNAseq data from untreated wildtype or $Cx3cr1^{GFP/+}$ mice that had different genetic backgrounds, ages, sexes and cell isolation methods. The aim was to identify genes from relevant proteins that are robustly and highly expressed in mouse microglia and may serve as a summary of previously published messenger RNA (mRNA) expression data and may facilitate the interpretation of cAMP-FRET experiments in the scope of this work. Data from selected studies were analysed with the same pipeline for RNAseq raw data (GREIN) and gene counts (R packages: *EdgeR*) and were ranked according to their median $\log_2$-transformed counts per million (cpm).

Among the top 20 expressed class A GPCRs in mouse microglia common to all analysed studies were *Cx3cr1* and *P2yr12*, two well established markers for microglia (Fig. 6.11A). Several studies used $Cx3cr1^{GFP/+}$ or $Cx3cr1^{GFP/+}/Ccr2^{RFP/+}$ transgenic mice and sorted the cells for GFP+ or RFP+ GFP+, therefore *Cx3cr1* and *Ccr2* (rank 22) expression may be overestimated in this summary.
Common to all studies was also the high expression of mRNA from purinergic receptors *P2yr13* and *P2yr6* as well as chemokine receptor *Ccr5* and complement C3a receptor 1 (*C3ar1*). Sphingolipid receptor *S1pr1*, platelet receptor *Ptafr*, cysteinyl leukotriene receptor *Cysltr1*, and the adenosine receptor *Adora3* were also common robustly expressed genes in the analysed studies (Fig. 6.11A).

Different GPCRs with just recently found endogenous ligands, such as *Gpr34*, *Gpr35*, *Gpr183*, *Cmklr1*, *Gpr84* and *Ccrl2* were also present in the most robustly expressed GPCRs (Fig. 6.11A). The importance of purinergic and chemokine signalling for microglia physiology has been intensively studied *in vitro* and *in vivo* (see section 3.3.2). However, a variety of these just recently de-orphaned GPCRs that were found to be expressed by mouse microglia have not been characterised very well and their function remains elu-

sive in most parts. Messenger RNA from orphan GPCRs *Gpr146* and *Gpr160* (Fig. 6.11A) was also detected in all analysed studies but these receptors have not been the target of any published scientific study to this date.

Finally, the expression of *Cnr2* (CB2) in mouse microglia was found in all studies additional to *Adrb2* (β_2AR), the two receptors of most interest for this work (Fig. 6.11C). Considering the median (MED) log$_2$(cpm) and interquartile range (IQR) of cannabinoid receptor 1 (*Cnr1*) (MED = 1.764, IQR = 5.694) and *Gpr55* (MED = 0.3033, IQR = 4.963) (Fig. 6.11C), the other cannabinoid-stimulated GPCRs, these receptors were not as homogenously expressed as *Cnr2* (MED = 4.343, IQR = 1.281) (Fig. 6.11C) in the analysed studies. Although *Adrb1* (β_1AR) was abundant in all studies (MED = 3.95, IQR = 2.116), *Adrb2* was among the most highly and robustly expressed GPCRs in all selected microglia studies (MED = 7.882, IQR = 1,781). Interestingly, a majority of highly-ranked GPCRs are known to be predominantly $G\alpha_{i/o}$ coupled which could hint towards a tight restriction of microglial cAMP concentration regulated by a variety of extracellular stimuli (Izquierdo et al., 2019) (Fig. 6.11A).

Some Cannabinoid receptor ligands have been found to bind TRP cation channels in high concentrations (Soethoudt et al., 2017). *Trpv2* was robustly found in all studies and *Trpv4* was expressed in some of the selected microglia studies (Fig. 6.11E). For experiments using CB2 ligands, the potential presence and activation of TRP channels may have effects on cAMP signalling that need to be considered.

The most prominent $G\alpha$ subunits found in samples from all microglia studies were the AC-stimulatory *Gnas*. *Gnai2* was the only inhibitory isoform consistently expressed and robust expression was also seen for *Gna12* and *Gna13* of the $G\alpha_{12/13}$-family, as well as *Gna15* and *Gnaq* of the $G\alpha_q$-family (Fig. 6.11B). $G\beta$-isoforms *Gnb1*, *Gnb2*, and *Gnb4* were common to all selected microglia studies and the composition of $G\gamma$-isoforms consisted of *Gng10*, *Gng2*, *Gngt2*, *Gng12*, *Gng5*, and *Gng7* in this sample group (Fig. 6.11B).

Isoform 7 of the adenylyl cyclase *Adcy7* was most robustly expressed in microglia (Fig. 6.11D), which corroborates previous reports of important functions of AC$_7$ in the closely related macrophages (Jiang et al., 2008, 2012). *Adcy9* and the abundantly expressed *Adcy6* isoform were also consistently found in the selected studies (Fig. 6.11D). Top commonly expressed phosphodiesterases were *Pde3b*,*Pde1b*, *Pde4b* and *Pde12* (Fig. 6.11F). Specifically PDE4B has been previously implicated in the regulation of microglia cell activation (Pearse and Hughes, 2016).

This summary of RNAseq data from mouse microglia studies is in agreement with a large body of functional GPCR data already published on the matter (Hickman et al., 2018; Izquierdo et al., 2019). High expression ranking of GPCRs that are commonly used as microglia marker (*Cx3cr1*, *P2yr12*, *Gpr34*) was expected and seen in this meta-analysis
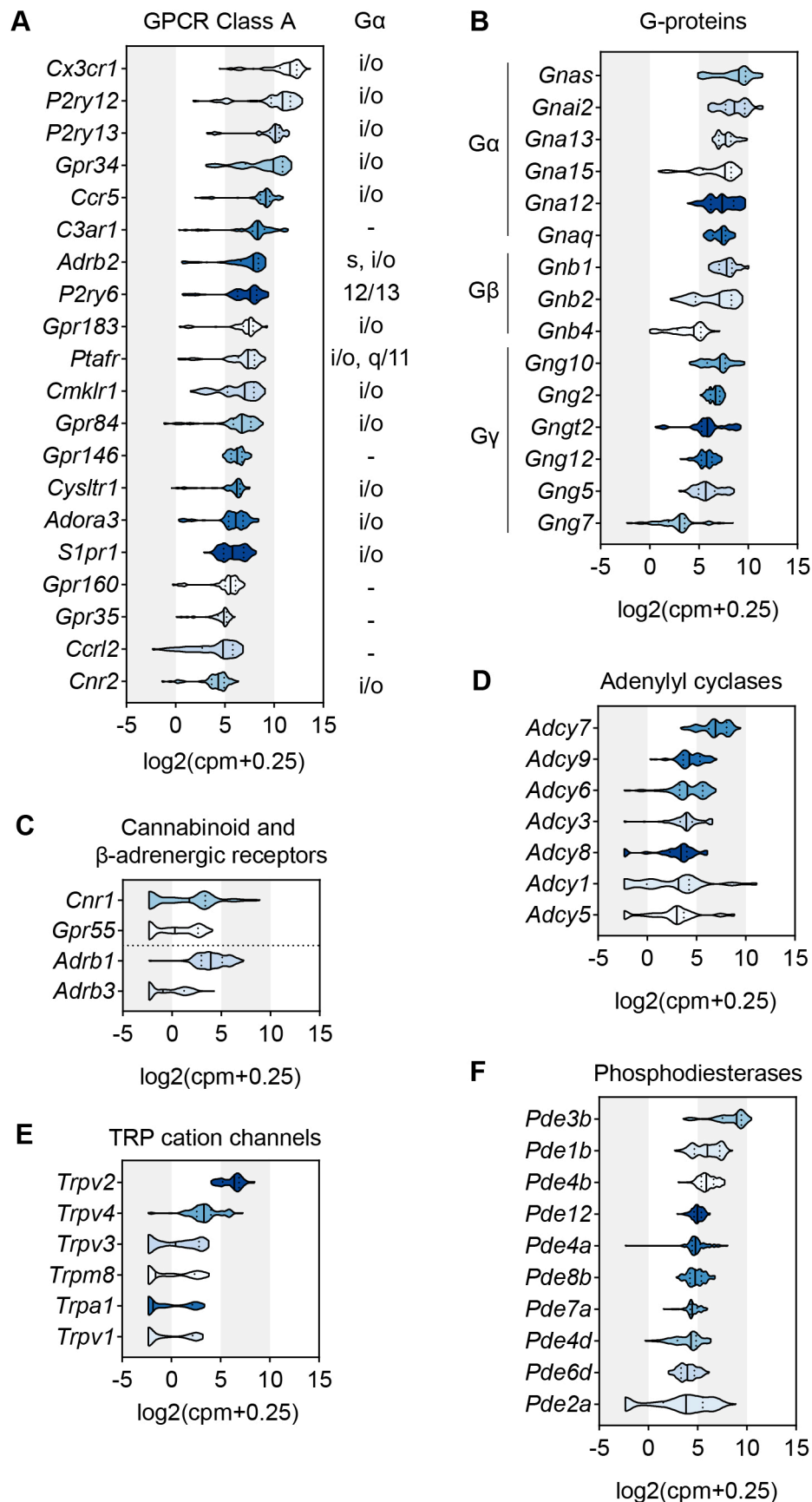
Figure 6.11. Meta-analysis of GPCR-related expression data from adult mouse microglia. (A) Top 20 ranked class A GPCRs and coupled Gα subunit. **(B)** Isoforms of the three G-protein subunits Gα, Gβ, and Gγ. Summarised expression data from **(C)** cannabinoid and βAR receptors, **(E)** TRP channels, **(D)** ACs and **(F)** PDEs. n = 132 from 18 different studies (see Appendix 10.5). Information on G-protein coupling retrieved from Harding et al. (2017).

across the selected studies. As GPCR signalling proteins are too abundant to be used as markers of any form, their cell specific composition is often not well investigated and reference literature is sparse.

With this meta-analysis, a framework was built that may stress previous findings from unrelated functional microglia studies and that may also serve as a theoretical reference point in the scope of this thesis.

6.4.2 Cell culture of primary adult mouse microglia

To investigate CB2-mediated cAMP signalling in an endogenous system, where CB2 has been reported to play an important role, microglia were isolated from adult mice and cultured in order to record CB2-mediated live cell cAMP dynamics with the cAMP-FRET-biosensor Epac1-camps. To ensure the microglial identity of isolated cells from adult mouse brains according to the described protocol, cultures were prepared from brain tissue of transgenic $Cx3cr1^{YFP/+}$ mice (kindly donated by Dr. Laura Laprell, Institute for Synaptic Physiology, ZMNH, University Medical Center Hamburg-Eppendorf).

As CX3CR1 is highly expressed in microglia, cultured cells from these animals were expected to show a positive YFP-signal (immunostaining with mouse anti-GFP antibody, that also recognises YFP (see Methods section 9.2.11)). Ionized calcium-binding adapter molecule 1 (Iba-1), another widely used microglia and activation marker, served as a second control for microglia identity.

Figure 6.12 shows four representative cultured microglia at 14 days *in vitro*. Although different in shape, all cells were positive for CX3CR1-YFP in the nucleus and in the cytosol. Minor variations in the CX3CR1-YFP signal were seen (Fig. 6.12, first column, green, row two and three vs. row 4), which might reflect the heterogeneity of isolated and cultured cells as expression of CX3CR1 can be regulated dynamically.

Fluorescent signal for Iba-1 was strong in all cells and localised throughout the whole cytosol (Fig. 6.12, second column). This might indicate that microglia cells were strongly activated because Iba-1 is upregulated in activated microglia (Mori et al., 2000; Ito et al., 2001; Imai and Kohsaka, 2002). Overall, with this isolation method, cell yields were very low. For FRET imaging experiments this may be negligible, however, for cell survival and function this could be a potential source of variation. This was also reflected by the low grade of ramification seen in these cultures, which corroborates the strong Iba-1 staining and may hint towards a high activation status.

Immunostaining of cultured adult mouse microglia revealed that the cells showed characteristic expression of two widely used microglia markers, CX3CR1 and Iba-1. Using the same isolation and culture method for the conduction of cAMP-FRET imaging from CB2 WT and KO mice with Epac1-camps expression should yield similar results and cells with microglia identity. However, as the cultured cells were morphologically prominent and possibly highly activated, they may not resemble homeostatic microglia.
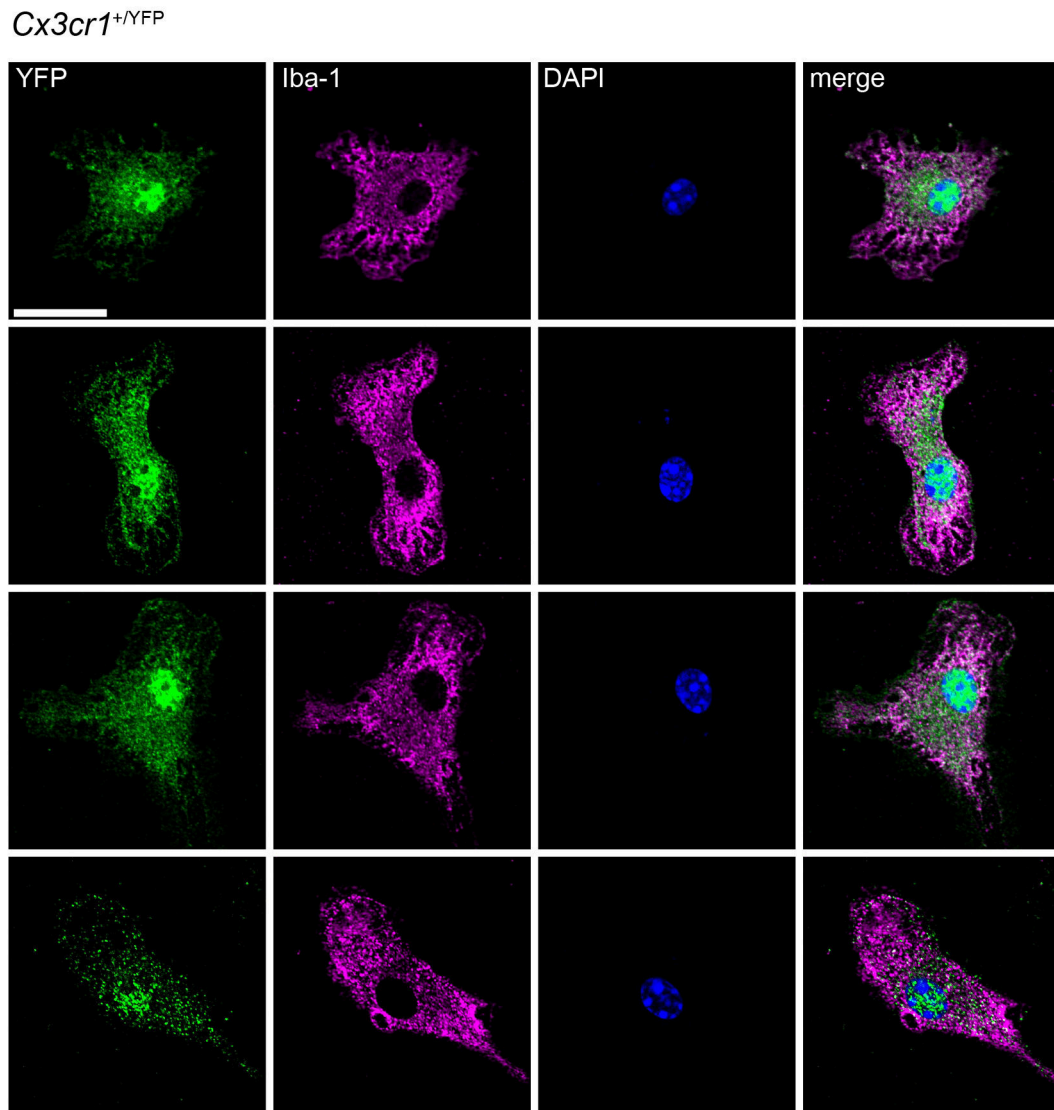
Cx3cr1^{+/YFP}

Figure 6.12. Immunocytochemistry of isolated adult microglia from *Cx3cr1*^{*YFP/+*} mice. Representative confocal images of single adult microglial cells that were positive for YFP (green) and microglia marker Iba-1 (magenta). Scale bar = 20 µm.

6.4.3 CB2-βAR-mediated cAMP signalling in primary mouse microglia

To analyse the effects of CB2 activation and CB2-βAR crosstalk on cAMP levels in primary adult microglia, mice that express the Epac1-camps FRET-biosensor ubiquitinously *CAG-Epac1-camps$^{T/+}$* transgenic ((Calebiro et al., 2009); kindly donated by Prof. Dr. Viacheslav Nikolaev, Experimental Cardiac Research, University Medical Center Hamburg-Eppendorf) were crossed with *Cnr2^{tm1Dgen}* to generate CB2 WT and KO mice with Epac1-camps expression in all cells.

Adult microglia were isolated from 8-10 week-old mice and cultivated for 14 days. Cells were directly stimulated with 1 µM CB2 agonist JWH133 to investigate the effect of CB2 activation on intracellular cAMP levels because it was not possible to detect reliable FRET responses using the stimulation protocol applied in Results subsection 6.2.2.
For the investigation of CB2-βAR crosstalk that was observed in Epac1-CB2-HEK cells, single isolated CB2 WT and KO adult microglia were stimulated with 100 nM βAR agonist isoprenaline with or without CB2 agonist JWH133 or CB2 inverse agonist AM630 (both at 1 µM). As FRET experiments in Epac1- and Epac1-CB2-HEK cells showed differences in the βAR-mediated cAMP response depending on the presence of CB2, it was investigated if CB2 KO microglia show altered cAMP responses to βAR stimulation compared to CB2 WT cells.
FRET imaging of primary microglia cells from CB2 WT and KO animals showed a lower fluorescence intensity of the Epac1-camps biosensor compared to the generated HEK293 cell model Epac1-CB2-HEK (Fig. 6.13A), therefore extended excitation times had to be used to reach an acceptable signal-to-noise ratio for the detection of FRET changes. For this reason, the recording time was kept to a minimum by stimulating the cells simultaneously with CB2 ligand and/or βAR agonist.

Mean ($\pm$95%CI) ΔR_t line plots from CB2 WT and KO microglia stimulated with 1 µM CB2 agonist JWH133 showed that there were no short-term effects of direct CB2 activation on cAMP signalling in wildtype cells (Fig. 6.13B). Also CB2 KO microglia did not show changes in intracellular cAMP levels after stimulation with JWH133, which showed that there were no off-target effects of this CB2 agonist in the applied concentration.
Figure 6.13C shows representative ΔR_t line plots from three different CB2 WT and KO microglia stimulated with 100 nM ISO. For both genotypes three different response types to ISO alone (Fig. 6.13C) and co-stimulated with JWH133 or AM630 (individual plots not shown) were observed. Feedback responders, showing a transient maximum (ISO$_{max}$) and then a negative cAMP feedback after stimulation (ISO$_{fb}$), similar to Epac1-CB2-HEK cells, were the most common response type for all conditions and genotypes (6.13D) (feedback, M = 63.27, 95%CI = 56.1, 70.43, n= 6) .
Primary microglia that showed persistent cAMP production (up, M = 20.19, 95%CI = 11.46, 28.91, n= 6) or reduction (down, M = 13.43, 95%CI = 5.61, 21.24, n= 6) to stimulation were overall less frequent. Non-responders were very rare (Fig. 6.13C, D). As the

feedback responders showed similarity to Epac1-CB2-HEK cells after CB2-βAR stimulation, a possible modulation of this response by CB2 was further explored.

FRET ratio changes (ΔR) after ISO stimulation with and without CB2 ligands in CB2 WT and KO microglia are seen in Figure 6.14A, B, and C. For both genotypes and all conditions ΔR values for ISO_{max} and ISO_{fb} were within a range 5 to 8% and 2 to 5%, respectively and no statistically significant differences were found between the genotypes or ISO_{max} and ISO_{fb} values of the different stimulation conditions. The negative feedback percentage relative to the transient maximum was around 50% for all conditions in CB2 WT cells. In CB2 KO microglia stimulated with ISO alone, mean feedback relative to ISO_{max} was larger compared to all other conditions but also more variable (M = 75.27, 95%CI = 31.06, 119.5, n = 16) (Fig. 6.14A and D (black circle)).
For both genotypes and independent of CB2 stimulation, overall cAMP levels after stimulation remained above initial baseline cAMP on average (Fig. 6.14D). Maximum slope values of ISO_{max} (Fig. 6.14E) and ISO_{fb} (Fig. 6.14F) responses also did not reflect large differences between conditions and genotypes.

In the present set of experiments on cAMP signalling in primary mouse microglia, no evidence for a potential involvement of CB2 in the short-term regulation of the intracellular cAMP concentration was seen. In the majority of recorded microglia, βAR activation led to a transient increase in cAMP, that was restricted by a negative feedback response. Net cAMP levels, however, remained above the initial cAMP baseline level. CB2 activation or blockage had no modulating effect on the FRET response seen after βAR activation in wildtype microglia.
Although the direct stimulation of CB2 showed no detectable effect on cAMP signalling in adult primary microglia, βAR-elicited FRET responses were variable but robustly detectable, showing the feasibility of FRET imaging on these cells. With optimised culturing conditions and phenotype monitoring, the variability of FRET responses might be reduced and/or identification of suitable, healthy cells might be improved.
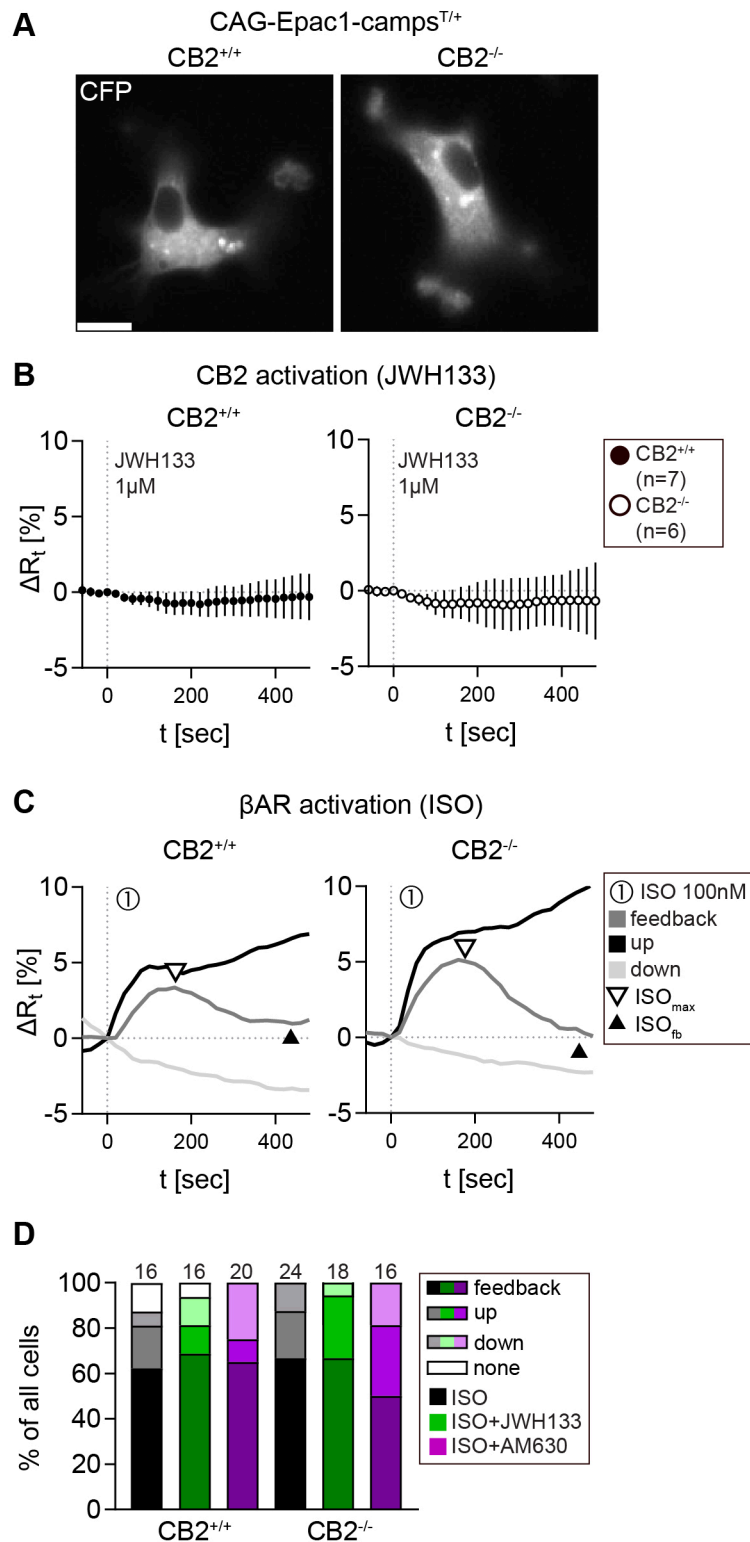
Figure 6.13. FRET imaging of CB2-βAR-mediated cAMP signalling in microglia from CAG-Epac1-camps wildtype and CB2-deficient transgenic mice. **(A)** Representative epi-fluorescent images (YFP emission channel) of single adult microglial cells expressing cAMP-FRET sensor Epac1-camps. Scale bar = 20 μm. **(B)** Representative single cell FRET ratio (ΔR_t) traces of different cellular responses (feedback (grey), up (black), and down (light grey)) to 100 nM βAR-agonist ISO (1) in CB2 WT and KO primary microglia. **(C)** Relative frequencies of response schemes of CB2 WT and KO microglia stimulated with ISO, ISO and 1 μM JWH133, or ISO and 1 μM AM630. Numbers on top of bars represent the number of single cells measured. ISO: WT n = 10, KO n = 16. ISO + JWH133: WT n = 11, KO n = 12. ISO + AM630: WT n = 13, KO n = 8.

Figure 6.14. FRET imaging of CB2-βAR-mediated cAMP signalling in microglia feedback responders. Max. ISO peak (ISO_{max}) and negative cAMP feedback (ISO_{fb}) of feedback responders in CB2 WT and KO microglia stimulated with **(A)** ISO, **(B)** ISO+JWH133 and **(C)** ISO+AM630. **(D)** Negative cAMP feedback from microglia of both genotypes and all conditions in percent. Max. slope values of **(E)** ISO_{max} and **(F)** ISO_{fb} FRET responses from microglia of both genotypes and all conditions (arrows represent slope direction). Data were analysed using Two-Way ANOVA with Sidak-adjusted p-values. Mean±95%CI, each *n* represents one ROI/cell.

7 Discussion

7.1 Adult Hippocampal Neurogenesis in Wildtype and CB2-deficient Mice

The quantification of adult hippocampal neurogenesis in the SGZ of CB2-deficient and wildtype mice in this work revealed that CB2-deficiency did not seem to influence the size of the DCX+ neural progenitor cell population, the relative frequency of postmitotic immature neurons (DCX+/CR+) or overall cell proliferation. This observation contradicts previously published research to some degree. Palazuelos et al. (2006) investigated 8-week-old CB2 wildtype and knockout mice from the *Cnr2^{tm1Zim}* strain (Buckley et al., 2000) and found a reduction in cell proliferation after treatment of animals with a CB2 agonist, which was abolished in the knockout animals. They also showed that already basal levels of cell proliferation in the SGZ are reduced in prenatal and 8-week-old CB2 deficient mice. In a later study, however, they observed that SGZ proliferation rates of 8-week-old animals do not differ between wildtype and CB2 knockout animals (Palazuelos et al., 2012).

As highlighted by Nada et al. (2010), between two and three months of age the decline in cell proliferation in the mouse SGZ is still highly dynamic, and only from an age of four months onwards, stable proliferation rates are reached. That is why, in this work, the animals were investigated after they reached the four-month-timepoint at 16 or 17 weeks of age. The use of BrdU was also avoided in this study, which stands in contrast to previous research on DG neurogenesis in CB2-deficient mice and reduces the comparability to this work because mice might have been subject to additional stress due to daily BrdU injections over the defined treatment period (Palazuelos et al., 2006, 2012).

Labelling cell proliferation with Ki67 in mice that reached a stable low rate of cell proliferation in the SGZ and avoiding handling stress for the animals that might influence neurogenesis (Lipp and Bonfanti, 2016) should reduce variability to a minimum. However, using Ki67 or BrdU as proliferation markers does not provide the information about the cell type that proliferates. This can only be determined by an additional staining for one or more of NPC markers. In this and previous studies, marker positive cells were only counted in the SGZ of the DG and it was assumed that a large proportion of the cells were NPCs.

BrdU is incorporated into the cell's DNA during the S-phase of the cell cycle, whereas Ki67 is expressed during the complete interphase and mitosis. Depending on the BrdU-treatment length, positive cells can be very scarce, which can potentially lead to higher variation during quantification. Using Ki67 instead of BrdU should yield a higher amount of positive cells and a reduction of variation in the quantification results. After quantifying cell proliferation with Ki67 in wildtype and CB2-deficient mice at the mentioned age, no differences in the amount of proliferating cells in the SGZ were detected between genotypes. This reflects that the presence and basal signalling of CB2 *in vivo* might not influence cell proliferation rates in the SGZ.

The DCX+ neural progenitor cell population (type 2b and 3 NPC) is a representative measure for the structural plasticity in the SGZ (Bonfanti and Nacher, 2012). In combination with calretinin it allows for the determination of the amount of postmitotic immature neurons that undergo further maturation within the hippocampus (Brandt et al., 2003). Plümpe et al. (2006) quantified the relative frequency of immature neurons from DCX+ with 75-80% which is in good agreement with the data obtained from the present quantification. In both genotypes there was a minor increase in the proportion of CR+ positive cells in the total DCX+ population in the suprapyramidal compared to the infrapyramidal blade of the DG. It has been reported previously that the suprapyramidal blade of the DG shows higher experience-dependent activity than the infrapyramidal blade (Snyder et al., 2011) and that this could increase the survival of immature neurons (Snyder et al., 2012). Present results indicate that CB2 basal activity is most likely not integral to this mechanism.

In this work, the quantification of positive cells was done blinded to avoid counting bias. Because sections were not obtained from standardised positions, a relative measure of positive cells per cubic metre examined SGZ and GCL volume was calculated. The GCL volume was included here because the SGZ alone was too narrow to reliably measure, however, only positive cells within the SGZ were counted. Overall the quantification method seems reliable reflected by the agreement with previously published data stating that in the mouse SGZ there are around four times more DCX+ than Ki67+ cells (Nada et al., 2010) and by the quantified proportion of immature neurons ($\sim 70\,\%$ to $80\,\%$ of DCX+ cells) (Plümpe et al., 2006).

As recommended by Sisay et al. (2013) and Lipp and Bonfanti (2016) and in contrast to previous research, in this study, 16- to 17-week-old animals from the $Cnr2^{tm1Dgen}$ (DeltagenInc, 2005) strain were investigated instead of 8-week-old animals from the $Cnr2^{tm1Zim}$ strain (Buckley et al., 2000; Palazuelos et al., 2006, 2012). $Cnr2^{tm1Dgen}$ have a deletion in the N-terminal region of the gene coding for CB2, whereas $Cnr2^{tm1Zim}$ have an insertion of a neomycin cassette into the C-terminal region of the gene, that most likely leads to the presence of truncated CB2 protein and differences in the pharmacological response compared to $Cnr2^{tm1Dgen}$ that might interfere with signalling of other receptors (Sisay

et al., 2013). Given that the interaction of CB1 and CB2 is relevant for the proliferative effect of endocannabinoids in the SGZ (Rodrigues et al., 2017), it is a concern that the use of *Cnr2^{tm1Zim}* knockout animals might have led to unspecific effects possibly rendering adult neurogenesis and therefore caused the observed differences (Palazuelos et al., 2006).

Although no effect of basal CB2-mediated signalling on adult neurogenesis was seen in this study, it cannot be concluded that CB2 is irrelevant for the regulation of AN. The afore-mentioned interaction of CB1 and CB2 in promoting neurogenesis (Rodrigues et al., 2017) might be of high importance here. To a certain degree, CB1 signalling might compensate for the lack of CB2, so basal levels of neurogenesis might not be affected. CB1-deficiency alone has been implicated in reduced baseline neurogenesis (Wolf et al., 2010; Aguado et al., 2006) and could be a more relevant factor in basal adult neurogenesis than CB2. However, simultaneous stimulation of CB2 by endocannabinoids might still be of importance during the negative modulation of adult neurogenesis (Palazuelos et al., 2012).

Additionally, CB2 activation has been shown to promote NPC proliferation in the DG in an inflammatory model of viral infection (Avraham et al., 2013) and blocking CB2 decreases the migration and differentiation of NPCs at the injury site in a murine stroke model (Bravo-Ferrer et al., 2016). These results suggest that the role of CB2 in neurogenesis might be more important in neuroinflammatory conditions and in response to pathophysiological stimuli than during the maintenance of basal AN levels.

It remains to be determined if and how CB2 expression on neural progenitors is regulated to influence neurogenesis and if CB2-mediated effects on other cells, such as microglia, might play a role in the observed effects of CB2 stimulation in *in vivo* studies (Sellner et al., 2016; Morrens et al., 2012; Bravo-Ferrer et al., 2016).

7.2 Measurement of CB2-mediated cAMP Dynamics with Epac1-CB2-HEK cells

7.2.1 Live Cell FRET imaging

The method used in this work to analyse the relative changes of intracellular cAMP concentration upon GPCR stimulation is the imaging of living cells that express the FRET-based cAMP biosensor Epac1-camps. In this work, a FRET imaging and analysis pipeline for live cell cAMP measurement in the generated cell model Epac-CB2-HEK and control Epac1-HEK cells as well as in adult primary microglia from mice ubiquitinously expressing Epac1-camps was implemented.

Through the simultaneous epi-fluorescent detection of CFP and YFP emission after excitation of CFP and their signal quantification using image analysis tools with corrections for spectral bleedthrough, background fluorescence and noise, a FRET ratio was calculated that reflects the relative changes of the intracellular cAMP concentration (Börner et al., 2011; Kraft and Nikolaev, 2017).

The advantage of this method is the possibility to track live cAMP changes after cellular stimulation with different reagents (Nikolaev et al., 2004b) using a cost-effective set-up (Sprenger et al., 2012) and the analysis of the response on a single cell level (Nikolaev and Lohse, 2006).

In this work, the baseline of the maximal FRET change after stimulation, the time to the half-maximum and the maximum slope of the FRET ratio increase or decrease were determined using computational scripts that analyse the FRET ratio traces over time. All three measures give a good description of the response and can reflect specific differences between stimulation conditions (e.g. max. slope differences in responses to different FSK-concentrations from Epac1-HEK cells).

This parameter analysis was done in a semi-automated way that facilitated the baseline detection but also allowed the fast retrieval of the other signal response parameters. It was still required to manually oversee the parameter analysis and bias could be reduced by implementing an unsupervised analysis of time-dependent FRET traces.

Storch et al. (2017) showed that Epac-based cAMP sensors are not only dynamic enough to detect $G\alpha_s$-mediated effects (Nikolaev et al., 2004a) but that they also allow for the detection of $G\alpha_i$-mediated decreases in cAMP, which was confirmed in this work. The detection of CB1-mediated reduction of cAMP levels was shown by Ladarre et al. (2014) in primary neurons using the FRET-sensor $^T\text{Epac}^{VV}$ (Klarenbeek et al., 2011). However, most cAMP FRET-sensors including Epac1-camps are not sensitive enough to reliably detect cAMP decreases without FSK pre-stimulation, especially in cells with low basal cAMP (Storch et al., 2017; Klarenbeek et al., 2015). Present data adds to this, as no reliable signal after direct CB2 activation in Epac1-CB2-HEK cells was detected (see Appendix

Fig. 10.1). On the other hand, there is the possibility that the variability of CB2 expression also plays a role in this (see Discussion section 7.2.2).

Live cell FRET imaging approaches naturally display limitations associated with fluorescence live cell imaging such as photobleaching, phototoxicity, poor signal-to-noise and cell movement (Ettinger and Wittmann, 2014; Woehler et al., 2010). For Epac1-camps the spectral bleedthrough of the two fluorophores CFP and YFP has to be considered and determined for each imaging setup (Börner et al., 2011). The most significant influence on FRET imaging with CFP and YFP has the bleedthrough from CFP emission light into the YFP emission channel, that can vary between 50 and 90% (Börner et al., 2011) and was measured to be around 50% in this setup. Because the imaging system used in this work is only equipped with an excitation source for CFP, bleedthrough correction for YFP emission into the CFP emission channel, that is estimated at 5 to 10%, or cross-excitation were not determined. This is also the reason for the lack of YFP photobleaching correction that also requires the direct excitation of YFP. The image acquisition with this setup can be significantly improved with an excitation source for YFP to correct for bleedthrough and bleaching and to specifically improve the reliability of FRET imaging from primary cells that also display signal-to-noise issues.

Noise propagation during ratiometric analysis of images with poor signal-to-noise ratios can further diminish FRET data quality (Woehler et al., 2010). During imaging, different excitation times were tested to determine the best possible signal-to-noise ratio without significant bleaching. Countermeasures like background subtraction and the image correction using a Kalman filter were applied post-imaging to address this limitation (Spiering et al., 2013). Further image registration of the CFP and YFP channel and the analysis of the image time-stacks to determine regions of the cell with minimal movement throughout the imaging period were used avoid cell movement artefacts.
The usage of an incubator that keeps the cells at a constant temperature during live cell imaging would further minimise unspecific effects on cellular signalling. The cell-specific sensitivity towards factors like temperature or pH needs to be considered. In this approach, the FRET imaging buffer was supplied with 10 mM HEPES to control the pH, however, without bicarbonate in the imaging medium bicarbonate transporters on the cell surface cannot control the intracellular pH (Ettinger and Wittmann, 2014), which might have unspecific effects on cAMP signalling or the fluorescent signals itself (Betolngar et al., 2015).

With the present image acquisition setup reliable live measurements of CFP and YFP fluorescence intensity were possible and could be analysed with the implemented FRET analysis routine. However, especially the imaging of cells with low Epac1-camps expression resulting in poor signal-to-noise ratios would benefit from additionally FRET corrections and a controlled environment to improve data quality and replicability.

7.2.2 Epac1-CB2-HEK Cell Model

In the scope of this work, a HEK293 cell model with expression of human CB2 and the FRET-based cAMP biosensor Epac1-camps was generated to dynamically monitor CB2-mediated cAMP signalling via live cell FRET imaging on a single cell level. With this cell model, it was possible to detect the inhibitory effect of CB2-mediated $G\alpha_i$ activation on FSK-elicited cAMP production using different CB2 agonists (JWH133, HU308, BCP, and 2-AG). With the inverse agonist AM630, the CB2-specificity of the agonist response was confirmed and the inhibitory effect on cAMP was blocked.

The measurement of cAMP levels on a single cell level revealed the heterogeneity of the generated cell model. Three different types of cellular responses to the CB2 stimulation protocol were observed that possibly reflect different receptor expression levels and conformations. From the observation of an inhibitory effect of cAMP production elicited by CB2 agonists, it can be deduced that type R responder cells have CB2 receptors in an equilibrium state that allows the agonists to shift it towards more receptor activity visible in the $G\alpha_i$-mediated inhibition of ACs.

Cells that only responded to the CB2 inverse agonist AM630 (type CA) supposedly have a different composition of receptor conformations with a high degree of constitutively active receptors. AM630 as a CB2 protean ligand binds and stabilises inactive receptor conformations with high affinity (Bolognini et al., 2012) and therefore shifts the activity equilibrium towards inactivity. In a system with high basal activity, corroborated by the inability of CB2 agonists to elicit additional activity, this will lead to pronounced inverse agonism as seen in type CA cells (Sato et al., 2016).

In type R cells, it was also detected that AM630 stimulation after application of FSK and CB2 agonist led to higher intracellular cAMP levels compared to control cells without CB2 after stimulation with 1 µM FSK. This also suggests the presence of constitutively active receptor forms in type R responders. In CB2 cell models with heterologous expression, a high degree of constitutive activity has been observed before (Bolognini et al., 2012; Bouaboula et al., 1999; Mancini et al., 2009) and therefore might be a characteristic of the receptor.

The faster response to 1 µM FSK in all Epac1-CB2-HEK cell response types compared to Epac1-HEK cells might indicate that heterologous CB2 expression alters the available G-protein pool. It has been reported that free $G\alpha_i$ subunits can cause effects at ACs that are independent of receptor activation (Melsom et al., 2014). Through the presence of, e.g. spontaneously inactive CB2 that couple $G\alpha_i$ subunits (Tubio et al., 2010) but do not elicit a signalling response, the pool of free $G\alpha_i$ might be reduced leading to a faster cAMP production after direct AC activation with FSK in Epac1-CB2-HEK cells. This, however, would also mean that type N responders, that do not show a response to either CB2 agonist or AM630, express CB2 because the faster cAMP production after FSK compared to Epac1-HEK cells was also seen in these response types. A possible explanation for

this observation could be the sensitivity of Epac1-camps that might be too low to detect small changes in cAMP produced by a small amount of active CB2 receptors. A more sensitive Epac-based FRET-sensor like, e.g. mTq2-Epac-^{cp}mV^{cp}mV (H187) (Storch et al., 2017; Klarenbeek et al., 2015), could elucidate if there is in fact a very small CB2-agonist induced inhibition of cAMP or not. Other than that, the FSK responses did not seem to differ significantly between Epac1-CB2-HEK cell response types and Epac1-HEK cells.

Although CB2 protein expression levels in Epac1-CB2-HEK cells were overall moderate when analysed in bulk, judging from the functional FRET data it is likely that CB2 expression varies on a single cell level. Epigenetic silencing of integrated DNA, or the disintegration of DNA during the selection process or culturing of cells might have led to the growth of cells with low or no functional receptor expression (type N). Using viral delivery of CB2 or site-directed integration of the target gene via, e.g CRISPR/Cas9 a more stable and homogenous expression of CB2 could be achieved. Another possibility to avoid the FRET imaging of clones with low or without CB2 expression is the simultaneous expression of cAMP biosensor Epac1-camps and CB2 using an IRES- (internal ribosome entry site) containing bicistronic vector. With this, fluorescence intensity of Epac1-camps can be correlated to receptor expression and therefore appropriate single cells can be chosen during live cell imaging. This can additionally be combined with a fluorescent tag on CB2 that does not interfere with the detection of the FRET fluorophores or receptor signalling itself which would allow live detection of CB2 receptors at the plasma membrane.

The ambiguity concerning CB2 expression at a single cell level is the main limitation of this cell model. The determination of CB2 presence relies strongly on the inverse agonism of AM630 and using a post-hoc two-point identification (CB2 agonist and AM630 response) to distinguish response types is prone to bias. An unsupervised analysis method of single cell FRET traces could reduce bias in the determination of response differences and show different clusters within one cell population. However, this cell model would greatly benefit from the possibility to detect CB2 expression during live cell imaging in order to more efficiently record relevant FRET responses to CB2 stimulation.

7.2.3   cAMP Dynamics upon CB2 Stimulation with Different CB2 Agonists

The analysis of FRET data from type R Epac1-CB2-HEK cells stimulated with FSK, different CB2 agonists and AM630 showed similar functional effects of CB2 activation on intracellular cAMP levels. All CB2 agonists applied at supra-maximal concentration that should elicit maximal possible efficacy for cAMP signalling (Dhopeshwarkar and Mackie, 2016; Soethoudt et al., 2017; Gertsch et al., 2008) caused an inhibition of around 30% of cAMP produced by 1 µM FSK. This response was further blocked by CB2 inverse agonist/antagonist AM630 indicating the CB2 specificity of the observed cAMP inhibition. The similar maximum effect of all agonists, including the synthetic cannabinoids JWH133 and HU308 that are recommended to use as CB2 selective reference agonists (Soethoudt et al., 2017), suggests that the observed response is the maximum of CB2-mediated $G\alpha_i$ inhibition of ACs in Epac1-CB2-HEK cells. In this study, BCP was confirmed as a functional CB2 agonist (Gertsch et al., 2008; Alberti et al., 2017) that elicited the same effect on intracellular cAMP levels in live Epac1-CB2-HEK cells like the endogenous CB2 ligand 2-AG.

Previous studies of CB2-mediated cAMP signalling have exclusively used multi-cell approaches that allow for the precise endpoint measurements of cAMP concentration to determine the inhibition of cAMP production after CB2 activation (Soethoudt et al., 2017; Börner et al., 2009; Dhopeshwarkar and Mackie, 2016). Similar to this study, FSK and often also the PDE inhibitor IBMX (3-isobutyl-1-methylxanthine) are added to the stimulation with the receptor ligands to increase basal cAMP levels. A study that also uses 1 µM FSK as pre-stimulant and additionally IBMX was published by Dhopeshwarkar and Mackie (2016). They showed around 60% inhibition of FSK-elicited cAMP production after five minutes stimulation time by JWH133 (61±1.1 %, mean±SEM) and HU308 (60±3.4 %) as well as 39±0.7 % and 5±1.1 % for 2-AG and BCP, respectively.
Different CB2 agonists might have varying dynamics and signalling bias dependent on CB2 phosphorylation that could originate from PKA activation downstream of cAMP production by FSK (Storch et al., 2017; Insel and Ostrom, 2003; Shen et al., 2018). Because the highly potent and cAMP biased CB1/CB2 agonist CP55940 is regularly used as a reference ligand to establish experimental protocols (Soethoudt et al., 2017; Dhopeshwarkar and Mackie, 2016), with regard to this, previously reported agonist differences have to be interpreted accordingly.

With endpoint measurements, it is unclear if the cAMP concentration at a given time-point has already reached a stable baseline or a transient extreme. Through the live imaging of cAMP levels in this present work it was possible to stimulate the cells once they reached a new baseline after FSK or CB2 agonist application and therefore detect effects on net intracellular cAMP concentration that are attributable to the stimulants. Dhopeshwarkar and Mackie (2016) conducted their analysis with the murine CB2 stably transfected into cells of human origin (HEK293) which could also result in the observed

discrepancy of overall cAMP inhibition by BCP and the other CB2 agonists in this work, through the, e.g. different binding of intracellular signal transducers or general receptor surface expression.

Although monitoring the live dynamics of cAMP allows for the improved dissection of CB2 responses to stimulants, effects of the FSK stimulation can still overlap and influence the interpretation of FRET responses to CB2 agonists. The reported low levels of intracellular cAMP in HEK293 cells (Börner et al., 2011; Mukherjee et al., 2016) and sensitivity of the Epac1-camps FRET sensor (Nikolaev et al., 2004a; Storch et al., 2017) required the use of FSK to elevate basal cAMP levels in order to detect its inhibition. Through this, the imaging time period had to be increased for measurements on Epac1-CB2-HEK cells which possibly led to further variability due to the above-mentioned pitfalls of live cell imaging (see Discusion section 7.2.1). In an almost identical stimulation setup to investigate the inhibitory effect on cAMP by $G\alpha_i$-coupled receptors, Storch et al. (2017) report that pre-stimulation with 1 µM FSK reduces the potency of the μ-receptor agonist DAMGO and that using a FRET-sensor with high cAMP affinity and omitting FSK pre-stimulation a more accurate determination of the EC_{50} value for DAMGO was possible. Interestingly, the detectable $G\alpha_i$-mediated inhibition of FSK-elicited cAMP accumulation by activation of $\alpha_{2A}AR$ and μ-opioid receptors did not show a complete reversal to pre-stimulation basal cAMP levels (Storch et al., 2017). For CB2, Dhopeshwarkar and Mackie (2016) report a maximum inhibition of 1 µM FSK-mediated cAMP accumulation for JWH133 with 61±1.1 % corroborating the observations by others (Storch et al., 2017) and in this study.

The observed incomplete inhibition of FSK-stimulated cAMP production by CB2 agonists might also have a physiological basis. As the activation or inhibition of AC isoforms can also be regulated by $G\beta\gamma$ subunits, their effect on cAMP signalling after CB2 activation might overlay the anticipated $G\alpha_i$-mediated inhibition of cAMP production. HEK293 cells, that have been used in this study, have been shown to express AC isoforms 1, 3, 5, 6, 7 and 9 (Atwood et al., 2011).
All of them except AC_9 are activated by FSK but only AC_1, AC_5, and AC_6 can be inhibited by $G\alpha_i$. Taking $G\beta\gamma$ subunits into consideration, that have stimulatory effects on AC_5, AC_6, and AC_7 and are known to act inhibitory on AC_1 and AC_3 (Sadana and Dessauer, 2009), it illustrates that the integration of these and other factors that regulate AC activity shape the observed net cAMP response to CB2 activation in live Epac1-CB2-HEK cells in this study.
The unknown quantitative expression of AC isoforms and bias of signalling from either $G\alpha_i$ or $G\beta\gamma$ subunits hampers the interpretation of the observed CB2-mediated effect on cAMP levels. However, to rule out sensitivity issues of Epac1-camps an AC inhibitor like SQ22,536 (Emery et al., 2012) could be applied after a CB2 agonist response to detect the minimum of the dynamic range of Epac1-camps in relation to the decrease of cAMP after

CB2 stimulation.

With the present setup, it was feasible to detect CB2-mediated cAMP dynamics in a time period of 30 to 45 minutes. Long-term effects over days of CB2 activation, however, might have a more significant contribution to physiological CB2 signalling and relevance for CB2 as a potential therapeutic target (Martín-Moreno et al., 2012; Atwood et al., 2012). Börner et al. (2009) showed that prolonged activation of CB1 and CB2 led to an increase in cAMP in a T cell line, an observation that might be linked to the heterologous sensitisation of ACs by the continued inhibition with $G\alpha_i$ and/or to additionally signalling from $G\beta\gamma$ (Rhee et al., 2000; Brust et al., 2015; Duan et al., 2010). To monitor long-term CB2 agonist and inverse agonist effects on cAMP signalling with this cell model, an incubation setup with focus correction as well as an appropriate cell medium to ensure cell viability over time would be required. This could show how CB2 stimulation with different ligands impacts intracellular cAMP levels in the long-term and would allow to detect short-term signalling effects.

Overall, type R responders of Epac1-CB2-HEK cells showed the short-term CB2-mediated inhibition of FSK-elicited cAMP production and all tested CB2 agonists had similar effects on the intracellular cAMP concentration. The effect of CB2 agonists was robustly blocked by the selective CB2 inverse agonist AM630 and confirmed the CB2 specificity. With this model, it is possible to determine whether a potential CB2 ligand mediates a functional CB2 effect on cAMP signalling or not. However, the precise evaluation of CB2 ligands cannot be addressed reliably because this would require a more sensitive cAMP detection that would also allow the omittance of FSK pre-stimulation and its unspecific effects.

7.3 Crosstalk between Endocannabinoid and β-adrenergic Signalling and CB2-β_2AR Heterodimerisation in HEK cell models

In this work, evidence for a cAMP and ERK1/2 signalling crosstalk between CB2 and the predominantly $G\alpha_s$-coupled βAR has been gathered and physical interaction between CB2 and β_2AR was detected.
The response to βAR agonist isoprenaline in Epac1-CB2-HEK cells showed a transient increase in cAMP mediated by endogenous βAR that was followed by a negative feedback which was absent in Epac1-HEK control cells, where isoprenaline caused a persistent increase in cAMP. In Epac1-CB2-HEK cells, the application of AM630 was able to counteract the cAMP feedback decrease, net cAMP levels, however, remained below Epac1-HEK cell levels. Co-activation of CB2 via JWH133 modulated the feedback response by causing a slightly stronger initial increase in cAMP that led to a larger relative negative feedback. The blockage of the feedback by AM630 resulted in similar increased cAMP levels, but

with CB2 agonist JWH133 present, the FRET response to AM630 tended to be slower and with a smaller maximal increase per second. Both CB2 and βAR activate MAPK pathways by causing the phosphorylation of ERK1/2. In Epac1-CB2-HEK cells, the co-stimulation of CB2 and βAR led to a two-fold stronger activation of ERK1/2 compared to cells without CB2.

Rapid negative cAMP feedback responses after βAR stimulation have been described previously for, e.g. cardiomyocytes, neurons, or embryonic fibroblasts (Nikolaev et al., 2006; Calebiro et al., 2009). In cardiomyocytes, these are linked to a PKA and Epac/CaM kinase dependent activation of PDE4D (Mika et al., 2015). The PDE control of βAR signalling is subtype-specific and stronger for β_1AR and PDE4 than for β_2AR and PDE3 and 4 (Nikolaev et al., 2006). Possibly depending on βAR subtype or PDE expression in a given cell type, the observation of the cAMP feedback could differ (Calebiro et al., 2009). In this study and in Börner et al. (2011), HEK293 cells have not shown a pronounced negative cAMP feedback to isoprenaline stimulation. According to Atwood et al. (2011), βAR expression is very low in HEK293 cells with β_2AR as the most abundant βAR. This might hint at a β_2AR dominant cAMP response to βAR agonist isoprenaline in the analysed cell models Epac1- and Epac1-CB2-HEK.

The observed cAMP feedback in Epac1-CB2-HEK cells can be caused by a variety of factors. The heterologous expression of CB2 could change the gene expression of components of the cAMP signalling machinery including PDEs or diminish the pool of available G proteins that might cause the attenuation of signalling from other GPCRs (Tubio et al., 2010). The possible high degree of constitutive CB2 activity could additionally contribute to the silencing of $G\alpha_s$ signalling by βAR through constitutive $G\alpha_i$ activation although it is not clear if the observed cAMP feedback is more pronounced in Epac1-CB2-HEK type R or CA response types.
PDE activity, specifically PDE3, is also stimulated by the PKB/Akt pathway (Han et al., 2006) that is targeted by CB2 activation (Sánchez et al., 2001; Palazuelos et al., 2012). In a system with high basal CB2 activity, constant activation of PKB/Akt could lead to an increased basal PDE3 activity that might control β_2AR cAMP signalling (Nikolaev et al., 2006). As PDE4 activity is high and PDE3 activity comparably lower in HEK293 (Xin et al., 2015), an increase in PDE3 activity could potentially alter β_2AR-mediated cAMP levels.

An alteration of the proposed $G\alpha_s$ to $G\alpha_i$ switch at β_2AR that might have led to a stronger ERK1/2 activation (Daaka et al., 1997) in ISO-stimulated Epac1-CB2-HEK compared to Epac1-HEK cells was not observed in this study. Only co-stimulation of CB2 led to a two-fold higher activation of ERK1/2 in Epac1-CB2-HEK compared to control cells. The assessment of ERK1/2 activation was conducted in starved cells which aimed to reduce constitutive receptor activity and facilitating the detection of CB2-mediated ERK1/2 activation via insensitive Western Blot quantification (Degasperi et al., 2014). Using fixed

point normalisation (here to DMSO control) is more prone to false-negative than false-positive results therefore possible CB2-βAR effects on ERK1/2 might have been too small to detect (Degasperi et al., 2014) with this method. Stimulation with JWH133 and AM630 that showed an increase in ERK1/2 activation and no further reduction of basal activation in Epac1-CB2-HEK cells, respectively, hints towards the successful reduction of basal receptor activity, which on the other hand might have altered the functional crosstalk between CB2 and βAR.

There is also the possibility that CB2 directly interacts with a βAR and that the observed functional crosstalk originates from and/or is supported by the heterodimerisation of CB2 with a βAR and following co-activation of CB2 upon βAR stimulation. CB1 has been shown to physically interact with β_2AR (Hudson et al., 2010), the most abundant βAR in HEK293 cells, and in this work the interaction between CB2 and β_2AR has been shown via membrane co-localisation and co-immunoprecipitation in co-transfected HEK293, that represents one requirement for functional heterodimerisation (Gomes et al., 2016).
Previous studies have shown that the biochemical footprint of CB2 heteromers can show cross-antagonism as well as the attenuation of receptor signalling in PKB/Akt, ERK1/2, RhoA and cAMP pathways (see Introduction section 3.2.3). However, synergistic signalling effects have been reported for the CB2-CB1 heteromer in neurogenesis and for the CB2-GPR55 heteromer in ERK1/2 activation (Rodrigues et al., 2017; Balenga et al., 2011). Additionally, an increased CB1-mediated ERK1/2 activation is seen in the CB1-β_2AR heteromer (Hudson et al., 2010) and also in this work an increase in ERK1/2 activation was detected after co-stimulation of CB2 and βAR in Epac1-CB2-HEK cells. The observed reduction in βAR cAMP signalling in Epac1-CB2-HEK cells could be a potential feature of a CB2-βAR heteromer.

However, as the model uses the overexpression of both receptors it does not reflect the situation in Epac1-CB2-HEK cells, let alone in a physiological setting. β_2AR had to be transfected with higher plasmid amounts compared to CB2 for IP-experiments to achieve detectable protein expression reflecting possible plasmid competition (Stepanenko and Heng, 2017). Interaction studies based on FRET where a lower amount of heterologous receptor expression can be used, could specify the detection of a possible interaction, which should also be investigated for β_1AR. The use of receptor mutation/deletion constructs could provide knowledge of interaction-involved receptor domains and if the interaction is direct or indirect. Additionally, mutant receptors could serve as negative controls disrupting the putative heteromer.

To elucidate which factors are relevant for the observed functional crosstalk and if they constitute the biochemical footprint of a putative CB2-β_2AR heteromer, Epac1-CB2-HEK cells could be stimulated with selective PDE3, PDE4 and PKB/Akt inhibitors while observing the negative cAMP feedback during the CB2-βAR stimulation protocol. This

would allow to determine if PDE activity and the PKB/Akt pathway are involved in the negative cAMP feedback. Selective antagonists for β_1AR and β_2AR could further show the involvement of either receptor which is also of interest for the ERK1/2 activation assay and to investigate possible cross-antagonism. The disruption of the heteromer using mutated receptors should also abolish the observed functional crosstalk.

In conclusion, evidence for functional signalling crosstalk between CB2 and βAR is seen that might originate from a putative CB2-β_2AR heteromer or from the constitutive activity of CB2 in the used HEK cell models. Specifically in cAMP signalling where Epac1-CB2-HEK cells showed an attenuation of βAR signalling, the crosstalk was pronounced. Further research should aim to clarify the origin of the negative cAMP feedback after βAR stimulation and distinguish if the physical interaction between CB2 and β_2AR is also detectable in an endogenous system that shows CB2-βAR functional crosstalk. This could show the involvement of CB2 in the functional crosstalk between cannabinoid and β-adrenergic signalling that has been reported for the sympathetic and central nervous system (Schlicker et al., 1997; Pakdeechote et al., 2007) as well as for bone formation (Tam et al., 2008) and cardiac function (Ho and Kelly, 2017).

7.4 CB2 and βAR Effects on cAMP Signalling in Microglia

The investigation of CB2 and βAR mediated effects on cAMP signalling in primary mouse microglia via live cell FRET imaging in this work showed the detection of βAR signalling but indicated that there is no short-term influence of CB2 activation or blockage on the observed alteration of cAMP levels by βAR. The direct activation of CB2 in wildtype and CB2-deficient microglia did not reveal detectable changes in intracellular cAMP concentrations. A meta-analysis of expression data from previously published mouse microglia studies showed the robust detection of β_2AR and CB2 mRNA as well as β_1AR assuming that stimulation with the βAR agonist isoprenaline and CB2 agonist and inverse agonist JWH133 and AM630 should target the relevant receptors. Using wildtype and CB2-deficient animals, it was the aim to detect CB2-specific effects on microglial cAMP and functional crosstalk between CB2 and βAR as seen in Epac1-CB2-HEK cells.

From the detection of CX3CR1 and Iba-1 and the cAMP response to ISO in isolated primary microglia, it was seen that the obtained cells were heterogenous in their morphology and possibly also activation state. This can be explained with the microglia isolation and culturing method that was used in this work and that did not include the pre-sorting of brain cells or the addition of cytokines to the cell culture medium. A sorting of brain cells based on the surface markers CD11b and CD45 is often used to isolate microglia from other cells in the tissue and could result in a higher cell yield and correct identity of the obtained cells (Garcia et al., 2014).
Microglia rely on extracellular cues to regulate their status (Izquierdo et al., 2019) so the

addition of cytokines and factors that regulate microglia homeostasis would most likely result in a more homogenous cell population possibly also improving cell health (Ryan et al., 2017). The weak YFP signal of control cells isolated from $Cx3cr1^{YFP/+}$ transgenic animals and the de-ramified morphology of isolated cells suggests that isolated microglia were not homeostatic and possibly activated (Hickman et al., 2018).

During live cell FRET imaging, it was evident that isolated microglia cells were sensitive towards prolonged imaging periods and that the signal-to-noise ratio was below that of Epac1- or Epac1-CB2-HEK cells. The established CB2 activation protocol (FSK – CB2 agonist – AM630) was not applied in order to reduce imaging time and cells were simultaneously stimulated with ISO or ISO and JWH133/AM630. Due to the poor signal-to-noise, observed FRET changes were small compared to Epac1-CB2-HEK cells seen by the initial ISO_{max} peak and longer excitation times that had to be used. The lack of a detectable effect on cAMP signalling by CB2 agonist JWH133 in wildtype primary microglia could be linked to these issues during live cell FRET imaging.
Microglia have been reported to have low basal cAMP levels (Izquierdo et al., 2019), which is corroborated by the results from the RNA expression meta-analysis showing that among all analysed studies $G\alpha_{i/o}$-coupled GPCRs were the predominantly expressed GPCRs. Similar to Epac1-CB2-HEK cells, it might be that CB2-mediated decreases in cAMP are below the sensitivity minimum of the Epac1-camps FRET biosensor and therefore undetectable when directly stimulating CB2 with JWH133.

CB2 robustly triggers AC inhibition via $G\alpha_i$ subunits in recombinant systems such as Epac1-CB2-HEK cells, in endogenously expressing cells however, this has been shown difficult to detect (Beltramo, 2009). The expression of different regulators of cAMP signalling such as ACs, PDEs and G proteins can shape the cellular response to the activation of GPCRs. According to the meta-analysed mouse microglia RNAseq studies, AC_7 was robustly expressed in microglia. In microglia-related macrophages, B and T cells AC_7 is an important regulator of intracellular cAMP (Duan et al., 2010) and in addition to being stimulated by $G\beta\gamma$ (Sadana and Dessauer, 2009), it has been reported that this AC isoform can also be stimulated by $G\alpha_{13}$ in a synergistic mechanism with $G\alpha_s$ (Jiang et al., 2008, 2012). $G\alpha_{13}$ was found among the most robustly expressed G proteins in mouse microglia, next to the ubiquitous $G\alpha_s$, $G\alpha_{i2}$, $G\alpha_q$ and $G\alpha_{12}$ (Flock et al., 2017), so it might play a functional role in microglial cAMP signalling. In addition to the CB2-mediated inhibition of ACs (e.g. isoform 5 and 6), signalling via $G\beta\gamma$ subunits in microglia could stimulate AC_7 and other expressed AC isoforms potentially leading to a net increase in cAMP rather than a decrease most likely depending on the activation state of the cell (Ghosh et al., 2015).

For a T cell line, it has already been shown that CB1 and CB2 activation causes a short-term decrease in cAMP but a long-term increase in intracellular cAMP (Börner et al.,

2009). High intracellular cAMP levels reduce pro-inflammatory processes by inhibiting the activation of NF-κB in immune cells (Serezani et al., 2008; Ghosh et al., 2015), a function that has previously been associated with CB2 activation (Ramírez et al., 2005; Ehrhart et al., 2005; Klegeris et al., 2003). For microglia, it has been shown that pro-inflammatory cytokines like TNFα can increase the activity of PDE4B to decrease cAMP levels (Pearse and Hughes, 2016; Ghosh et al., 2012), highlighting that the dynamic regulation of cAMP is crucial to microglia function (Serezani et al., 2008; Ghosh et al., 2015; Pearse and Hughes, 2016) and CB2-mediated cAMP signalling could be of importance for this mechanism (Lin et al., 2017).

The limitation of this study is that CB2 expression levels in wildtype animals were not directly detected. The failure to measure a CB2 effect on cAMP levels could therefore originate from no or low CB2 expression as well as from the possibility that the CB2-mediated short-term effect might be too small to detect in microglia using the FRET biosensor Epac1-camps. Expression levels of CB2 should be reliably determined and preferably detected during live imaging by attaching a fluorescent tag to CB2 or pre-stimulating microglia with cytokines, such as IFNγ to induce a phenotype change that is associated with CB2 expression (Carlisle et al., 2002; Schmöle et al., 2015; López et al., 2018). Controlling for CB2 expression using mRNA analysis would also be a suitable approach to clarify expression levels in microglia from wildtype animals in this setup. Additionally, it could be tested if microglial cAMP levels are within the dynamic range of the Epac1-camps FRET sensor.

The stimulation of primary mouse microglia from wildtype and CB2-deficient animals with the βAR agonist ISO revealed that microglia from both genotypes showed heterogenous cAMP responses on a single cell level. Previous studies and the meta-analysis done in the scope of this work found that β_2AR is not only the most abundant β-adrenergic receptor, Gyoneva and Traynelis (2013) also report that its expression is dynamically down-regulated in activated microglia and involved in mediating microglia motility. In this study, the majority of wildtype and CB2-deficient microglia showed a transient cAMP increase after βAR stimulation with a negative feedback response similar to that of Epac1-CB2-HEK cells. A small proportion of measured cells showed either a persistent increase or a small decrease in cAMP, the latter suggesting that a decrease in cAMP was possible to detect in the analysed microglia cell culture or that live cell imaging issues were present.

The observed heterogeneity in microglial cAMP responses to ISO could be explained via the regulation of PDE3 and PDE4, that are known to control signalling from β_2AR (Nikolaev et al., 2006). PDE3 can be activated by the PI3K/Akt pathway and PKA (Schmidt et al., 2013; Han et al., 2006) and PDE4 activity can be increased by PKA, CaM kinase II as well as pro-inflammatory cytokines (Mika et al., 2015; Ghosh et al., 2012). Both

PDEs could potentially restrict β_2AR-mediated cAMP increases in the microglia. CB2-deficiency, however, had no detectable effect on the heterogeneity of βAR responses.

Epac1-CB2-HEK cells showed a marked difference in the cAMP response to ISO compared to Epac1-HEK cells and CB2 activation modulated the observed negative cAMP feedback to a small degree. For analysed microglia that showed a negative cAMP feedback in this study, neither genotype nor co-stimulation with CB2 agonist or inverse agonist JWH133 and AM630 altered the observed βAR cAMP responses or their frequency. This suggests that CB2 was either not expressed in the measured cells or not involved in βAR-mediated short-term cAMP signalling in microglia. Followingly, there was also no evidence of signalling crosstalk between CB2 and βAR in this system where CB2 and β_2AR should be endogenously expressed.

Although it was not possible to detect changes in intracellular cAMP levels upon CB2 activation or blockage in this study, potential future studies could investigate the role of CB2 in the dynamic regulation of cAMP levels in microglia, specifically the possibility of a CB2-mediated long-term increase in cAMP that could trigger anti-inflammatory processes.

8 Conclusion and Outlook

In this work, selected functions and signalling properties of the cannabinoid receptor 2 have been investigated with a focus on the role of CB2 during adult hippocampal neurogenesis in mice and CB2-mediated cAMP signalling and signalling crosstalk with the β-adrenergic system in a HEK293 cell model and in primary mouse microglia.

The investigated regulation of adult neurogenesis by CB2 revealed that although previous research found proliferative effects of CB2 activation on neural progenitor cells and neurogenesis in the dentate gyrus, animals without basal CB2 signalling did not show an impairment in cell proliferation or reduction in plasticity-relevant populations of neural progenitors in the hippocampus. This suggests that the role of CB2 in neural progenitors and specifically its overlap or distinction to CB1 signalling requires further research that shows in which physiological but also pathophysiological situation CB2 function acts on adult neurogenesis in the hippocampus. The involvement of microglial CB2 function, that may be regulated during ageing or depending on pathological cues, might also be of relevance for CB2 effects on adult neurogenesis.

In the scope of this work, a cell model was generated that allows for the live cell FRET imaging of CB2-mediated cAMP dynamics using the cAMP biosensor Epac1-camps. This model proved valuable in the detection of CB2 agonist-elicited inhibition of cAMP production via $G\alpha_i$ subunits and their blockage with a CB2 inverse agonist. The cell's dynamic response to the stimuli was analysed on a single cell level providing insights on the nature of heterologous CB2 expression systems that most likely show constitutive activity, and contributes to the understanding of $G\alpha_i$-mediated GPCR signalling in living cells. With Epac1-CB2-HEK cells, it was also possible to investigate the modulation of βAR cAMP signalling through CB2 presence and activity, that attenuated βAR-mediated cAMP production. βAR and CB2 co-activity enhanced ERK1/2 activation and CB2 was shown to interact directly or indirectly with the β_2-adrenergic receptor. The attenuation of βAR cAMP signalling and the increased ERK1/2 activation could be features of a putative CB2-β_2AR, that have also been described previously for other CB2 heteromers.

The continued investigation of CB2 function and interactions in a live cell model system with intact feedback mechanisms and the possibility to analyse cellular responses on a single cell level with high temporal resolution provides many opportunities to clarify, discover, and manipulate molecular mechanisms that are targeted by CB2. However, fu-

ture studies should also aim to optimise technical aspects, such as the monitoring of CB2 expression during live cell imaging.

With the investigation of adult mouse microglia, a primary cell model was investigated where CB2 and also β_2AR signalling are relevant. The meta-analysis of publicly available RNAseq data sets from adult mouse microglia, that was done in this work, provided assistance in discussing the observed results from the live cell FRET imaging of microglia from wildtype and CB2-deficient animals with ubiquitous Epac1-camps expression. Direct effects of CB2 activation or CB2-mediated modulations of βAR signalling were not detected, however, the live imaging of cAMP dynamics in adult microglia was feasible and also showed that βAR responses differed on a single cell level. Similar to Epac1-CB2-HEK cells, βAR activation predominantly showed a negative cAMP feedback. The presence of this feedback in microglia could be an important mechanism in the response to the endogenous βAR ligand norepinephrine. Furthermore, this work illustrates that to detect CB2-mediated inhibition of cAMP production, it has to be ensured that CB2 is expressed in a given analysed cell and that the expected changes in intracellular cAMP are within the dynamic range of the FRET-sensor.

In conclusion, the investigation of CB2 function in this work provides new insights into the role of CB2 in adult neurogenesis and, while using live imaging techniques to detect CB2-mediated cAMP signalling, it shows a putative functional crosstalk and interaction between CB2 and βAR in the generated cell model Epac1-CB2-HEK as well as the detection of βAR-mediated cAMP signalling in adult mouse microglia. Further, the results of this study also highlight the challenges of the single live cell analysis of cAMP levels using FRET-based biosensors to detect signalling of $G\alpha_i$-coupled GPCRs. Future research should try to implement optimised FRET imaging for primary cells that endogenously express CB2 and are potentially important for CB2 function *in vivo* in the CNS, such as microglia and neural progenitor cells, in order to study CB2-mediated cAMP signalling in a more physiological setting. Using a cell model like Epac1-CB2-HEK cells, new CB2 ligands could be evaluated in living cells and subsequently used on primary cells with endogenous CB2. The use of CB2-reporter mice could also ensure the association of observed effects to CB2 function.

The investigation of CB2 function and its interactions with other GPCRs and signal transducers in a neurobiological context harbours great potential to understand molecular mechanism behind physiological and pathophysiological conditions of the central nervous system.

9 Materials and Methods

9.1 Materials

9.1.1 Chemicals and Reagents

Chemicals

Table 9.1. Chemicals and reagents used in this work.

Reagent	Source	Identifier
2-arachidonoyl glycerol (2-AG)	Cayman	Cat# 62160, PubChem ID: 5282280
2-Propanol	Th. Geyer	Cat# 1157.5000, PubChem ID: 3776
Acrylamide solution (40 %, 37.5:1)	AppliChem	Cat# A1577, PubChem ID: 6579
AM630	Tocris	Cat# 1120, PubChem ID: 4302963
Anti-FLAG® M2 Affinity Gel	Sigma-Aldrich	Cat# A2220
β-caryophyllene (BCP)	Sigma-Aldrich	Cat# C9653, PubChem ID: 5281515
β-glycerophosphate disodium salt hydrate	Sigma-Aldrich	Cat# G9422, PubChem ID: 22251426
Bromophenole blue	AppliChem	Cat# A3640, PubChem ID: 8272
Calcium chloride 2-hydrate $CaCl_2$ X $2H_2O$	AppliChem	Cat#A1873, PubChem ID: 24844
n-dodecyl β-D-maltoside (DDM)	Sigma-Aldrich	Cat# D4641, PubChem ID: 114880
Dimethyl sulfoxide (DMSO)	Sigma-Aldrich	Cat# D2650, PubChem ID: 679
DL-dithiothreitol	Sigma-Aldrich	Cat# D0632, PubChem ID: 446094

Table 9.1. Chemicals and reagents used in this work.

Reagent	Source	Identifier
Ethylenediaminetetraacetic acid (EDTA) disodium salt 2-hydrate	Th. Geyer	Cat# 2281, PubChem ID: 44120005
Ethanol (EtOH)	Th. Geyer	Cat# 2209.5000, PubChem ID: 702
Ethylene glycol	Sigma-Aldrich	Cat# 324558, PubChem ID: 174
Forskolin (FSK)	Sigma-Aldrich	Cat# F6886, PubChem ID: 47936
Glycerol	Sigma-Aldrich	Cat# 15523, PubChem ID: 753
Glycine	Sigma-Aldrich	Cat# G8898, PubChem ID: 750
HEPES, pH 7.5	Sigma-Aldrich	Cat# H0887, PubChem ID: 23831
HU308	Tocris	Cat# 3088, PubChem ID: 11553430
Isoprenaline hydrochloride	Sigma-Aldrich	Cat# I5627, PubChem ID: 3779
JWH133	Tocris	Cat# 1343, PubChem ID: 6918505
Ketanest ® S (esketamine)	Pfizer	PubChem ID: 182137
Leupeptin	Sigma-Aldrich	Cat# L2884, PubChem ID: 72429
Magnesium chloride 6-hydrate ($MgCl_2$ X $6H_2O$)	AppliChem	Cat# 141396, PubChem ID: 24644
Methanol (MeOH)	Th. Geyer	Cat# 1462.2511, PubChem ID: 887
Normal goat serum	Cell Signaling Technology	Cat# 5425
PageRuler^{TM} Prestained Protein Ladder	Thermo Fisher Scientific	Cat# 26617
Roti®-Histofix 4% (4% phosphate-buffered formaldehyde (PFA))	Carl Roth	Cat#P087, PubChem ID: 712
Phenylmethylsulfonyl fluoride (PMSF)	Roche	Cat# 10837091001, PubChem ID: 4784

Table 9.1. Chemicals and reagents used in this work.

Reagent	Source	Identifier
cOmplete™ (protease inhibitor cocktail)	Roche	Cat# 4693116001
Poly-L-lysine hydrobromide (PLL)	Sigma-Aldrich	Cat# P6282, PubChem ID: 72363
Potassium chloride (KCl)	Sigma-Aldrich	Cat# P9541, PubChem ID: 4873
ProLong™ Gold Antifade Mountant	Sigma-Aldrich	Cat# P36934
ProLong™ Gold Antifade Mountant with DAPI	Sigma-Aldrich	Cat# P36935
Protein G-Sepharose Fast Flow	GE Healthcare	Cat# 17-0618-01
Polyvinylpyrrolidone (PVP)	Sigma-Aldrich	Cat# PVP40, PubChem ID: 6917
Rompun ® (xylazine)	Bayer	PubChem ID: 5707
Skim Milk Powder (MP)	Sigma-Aldrich	Cat# 70166
Sodium azide	Sigma-Aldrich	Cat# S2002, PubChem ID: 33557
Sodium chloride (NaCl)	Sigma-Aldrich	Cat# 31434, PubChem ID: 5234
NaCl solution (0.9%)	Braun	Cat# 235 0748
Tri-sodium citrate dihydrate	Merck	Cat# 1064480500, PubChem ID: 71474
Sodium dihydrogen phosphate (NaH_2PO_4)	AppliChem	Cat# A3902, PubChem ID: 24204
Sodium dodecylsulfate (SDS)	AppliChem	Cat# A2263, PubChem ID: 3423265
Sodium flouride (NaF)	Sigma-Aldrich	Cat# S7920, PubChem ID: 5235
Sodium hydrogen phosphate (Na_2HPO_4)	Merck	Cat# 1.06580.0500, PubChem ID: 24203
Sodium hydroxide (NaOH)	J.T.Baker	Cat#10528240, PubChem ID: 14798
Sucrose	Sigma-Aldrich	Cat# 50389, PubChem ID: 5988
TEMED	AppliChem	Cat# A1148, PubChem ID: 8037

Table 9.1. Chemicals and reagents used in this work.

Reagent	Source	Identifier
Trizma® base (Tris)	Sigma-Aldrich	Cat# T1503, PubChem ID: 6503
Triton® X-100	AppliChem	Cat# A4975, PubChem ID: 5590
Tween® 20	AppliChem	Cat# A4974, PubChem ID: 443314

Cell Culture Reagents

Table 9.2. Cell culture reagents used in this work.

Reagent	Source	Identifier
Dulbecco's Modified Eagle Medium (DMEM)	Gibco	Cat# 41966-029
Hank's Balanced Salt Solution (HBSS) (without MgCl and CaCl)	Sigma-Aldrich	Cat# H6648
Dulbecco's Phosphate-Buffered Saline (DPBS)	Sigma-Aldrich	Cat# D8537
0.25 % Trypsin/EDTA	Sigma-Aldrich	Cat# T4049
Opti-MEM™	Gibco	Cat# 31985-062
Lipofectamine®2000	Life Technologies	Cat# 11668-019
Penicillin-Streptomycin (P/S)	Sigma-Aldrich	Cat# P4333
Hygromycin B	Roth	Cat# CP12.2, PubChem ID: 56928061
G-418	Roche	Cat#4727878001, PubChem ID: 123865
Fetal Bovine Serum (FBS)	Pan Biotech	Cat#P30-3312
Trypsin	Sigma-Aldrich	Cat#T7409 PubChem ID: 5311489

Antibodies

Table 9.3. Antibodies used in this work. IP - immunoprecipitation, IHC - immunohistochemistry, WB - Western Blot.

Antibody	Source	Identifier	Working Concentration
Rabbit anti-CB2	Santa Cruz Biotech.	Cat# sc-25494, RRID:AB_2082784	IHC: 1:300 in DPBS, WB: 1:500 in TBST
Rabbit anti-DCX	Synaptic Systems	Cat# 326 003, RRID:AB_2620067	IHC: 1:700 in DPBS
Guinea pig anti-calretinin	Synaptic Systems	Cat# 214 104, RRID:AB_10635160	IHC: 1:500 in DPBS
Rabbit anti-FLAG	Sigma-Aldrich	Cat# F7425, RRID:AB_439687	WB: 1:1000 in TBST
Mouse anti-FLAG® M2	Sigma-Aldrich	Cat# F1804, RRID:AB_262044	IHC: 1:300 in DPBS
Goat anti-mouse IgG, Alexa Fluor® 488	Thermo Fisher Scientific	Cat# R37120, RRID:AB_2556548	IHC: 1:500 in DPBS
Goat anti-mouse IgG, Alexa Fluor® 594	Thermo Fisher Scientific	Cat# R37121, RRID:AB_2556549	IHC: 1:500 in DPBS
Goat anti-rabbit IgG, Alexa Fluor® 488	Thermo Fisher Scientific	Cat# R37116, RRID:AB_2556544	IHC: 1:500 in DPBS
Goat anti-rabbit IgG, Alexa Fluor® 594	Thermo Fisher Scientific	Cat# R37117, RRID:AB_2556545	IHC: 1:500 in DPBS
Goat anti-guinea pig IgG, Alexa Fluor® 594	Thermo Fisher Scientific	Cat# A-11076, RRID:AB_2534120	IHC: 1:500 in DPBS
Rabbit anti-HA	Sigma-Aldrich	Cat# H6908, RRID:AB_260070	WB: 1:1000 in TBST
Mouse anti-HA	Sigma-Aldrich	Cat# H3663, RRID:AB_262051	IHC: 1:300 in DPBS, IP: 1:200
Rabbit anti-phospho-ERK1/2	Cell Signaling Tech.	Cat# 4370, RRID:AB_2315112	WB: 1:2000 in TBST/1% MP
Mouse anti-ERK1/2	Cell Signaling Tech.	Cat# 9107, RRID:AB_10695739	WB: 1:2000 in TBST/1% MP
Donkey anti-mouse IgG-IRDye® 680LT	LI-COR Biosciences	Cat# 926-68022, RRID:AB_10715072	WB: 1:10000 in TBST
Donkey anti-mouse IgG-IRDye® 800CW	LI-COR Biosciences	Cat# 926-32212, RRID:AB_621847	WB: 1:10000 in TBST

Table 9.3. Antibodies used in this work. IP - immunoprecipitation, IHC - immunohistochemistry, WB - Western Blot.

Antibody	Source	Identifier	Working Concentration
Donkey anti-rabbit IgG-IRDye® 680LT	LI-COR Biosciences	Cat# 926-68023, RRID:AB_10706167	WB: 1:10000 in TBST
Donkey anti-rabbit IgG-IRDye® 800CW	LI-COR Biosciences	Cat# 926-32213, RRID:AB_621848	WB: 1:10000 in TBST
Rabbit polyclonal anti-Ki67	Thermo Fisher Scientific	Cat# PA5-19462, RRID:AB_10981523	IHC: 1:500 in DPBS
Rabbit anti-actin	Sigma-Aldrich	Cat# A2066, RRID:AB_476693	WB: 1:1000 in TBST
Rabbit polyclonal anti-Iba1	Wako	Cat# 019-19741, RRID:AB_839504	IHC: 1:300 in DPBS
Mouse monoclonal anti-GFP	Millipore	Cat# MAB3580, RRID: AB_94936	IHC: 1:300 in DPBS
Rabbit polyclonal anti-β_2AR	Santa Cruz Biotech.	Cat# sc-569, RRID:AB_630926	IHC: 1:300 in DPBS

9.1.2 Animals, Cell Lines, and Plasmids

Mouse Strains

Table 9.4. Mouse strains used in this work.

Strain	Source	Identifier
CAG-Epac1-camps (FVB/N)	Kindly donated by Prof. V. Nikolaev	Calebiro et al. (2009)
B6.129P2-Cnr2^{tm1Dgen}/J	Jackson Laboratory	Cat# JAX:005786, RRID:IMSR_JAX:005786
B6.129P2(Cg)-Cx3cr1$^{tm2.1(cre/ERT2)Litt}$/WganJ	Kindly donated by Dr. L. Laprell	Cat# JAX:021160, RRID:IMSR_JAX:021160

Human Cell Lines

Table 9.5. Human cell lines used in this work.

Cell Line	Source	Identifier
HEK293	CLS	Cat# 300192/p777_HEK293, RRID:CVCL_0045
Epac1-camps HEK293	Kindly donated by Prof. V. Nikolaev	
Epac1-camps FLAG-hCB2 HEK293	This work	

Recombinant DNA Plasmids

Table 9.6. Recombinant DNA plasmids used in this work.

Plasmid	Source	Identifier
pcDNA3.1(+)-FLAG-hCB2(Q-H)	Karsak lab	
pcDNA3.1(+)-HA-hADRB2	Karsak lab	
pcDNA3.1(+)	Thermo Fisher Scientific	Cat# V79020

9.1.3 Devices and Software

FRET Imaging Setup

Table 9.7. FRET imaging setup.

Device	Source	Identifier
DM IRB inverted microscope	Leica	
Attofluor^{TM} Cell Chamber	Thermo Fisher Scientific	Cat# A7816
Plan-NEOFLUAR 63X/1.25 oil objective	Zeiss	Cat# 440460
pE-100 440 nm LED	CoolLED	Cat# AB4631
CoolSNAP MYO CCD camera	Photometrics	
DV2 beam splitter	Photometrics	
Duemilanove microcontroller	Arduino	
05-EM filter set (505 dcxr dichroic mirror, D480/30, D535/40)	Photometrics	

Other Devices

Table 9.8. Other devices used in this work.

Device	Source	Identifier
Axio Imager M1 epi-fluorescent microscope	Zeiss	
FV1000 confocal microscope	Olympus	
Odyssey® CLx Western blot imaging system	LI-COR Biosciences	

Software Tools

Table 9.9. Software tools used in this work.

Software	Source	Identifier
FluoView FV-1000	Olympus	ver. 4.2a
GREIN	Mahi et al. (2019)	
Illustrator	Adobe	CC 2015
ImageJ	Schneider et al. (2012)	ver. 1.43
ImageJ Plugin: FRET analysis	Sprenger et al. (2012)	
ImageJ Plugin: MicroManager		ver. 1.4.5
ImageJ Plugin: MultiStackReg		ver. 1.45
Image Studio Lite	LI-COR Biosciences	ver. 5.2
Excel	Microsoft Corporation	ver. 14
Fiji	Schindelin et al. (2012)	
JabRef		ver. 4.3.1
MatCol	Khushi et al. (2017)	
Photoshop	Adobe	CC 2015
Prism	GraphPad Software	ver. 8.0.2
R	The R Foundation	ver. 3.5.1
R package: edgeR	Robinson et al. (2009)	
R package: org.Mm.eg.db	Carlson (2019)	
R package: plyr	Wickham (2011)	ver. 1.8.4
R package: zoo	Zeileis and Grothendieck (2005)	ver. 1.8-5
R Studio	RStudio, Inc.	ver. 1.1.383
Stereo Investigator	MBF Bioscience	

TeXstudio		ver. 2.12.14
Word	Microsoft Corporation	ver. 14

9.1.4 Buffers, Solutions and Gels

0.2 % DDM cell lysis buffer

Substance	Concentration
HEPES, pH 7.5	5 mM
NaCl	150 mM
Glycerol	10 %
EDTA (in ddH$_2$O), pH 8.0	1 mM
DDM	0.2 % w/v
Leupeptin	1 µM
PMSF (in EtOH)	1 mM
NaF	20 mM
β-glycerophosphate	20 mM
Protease inhibitor cocktail	2 tablets
in ddH$_2$O	

6X SDS loading buffer (adapted from Laemmli (1970))

Substance	Concentration
Tris (in ddH$_2$O), pH 6.8	100 mM
SDS	4 % w/v
Glycerol	60 %
Bromophenole blue	1 knife point
DL-dithiothreitol	100 mM
in ddH$_2$O	

10X SDS-PAGE running buffer

Substance	Concentration
Tris	0.25 M
Glycine	2 M
SDS	1 % w/v
in ddH$_2$O	

10X SDS-PAGE transfer buffer without MeOH

Substance	Concentration
Tris	0.25 M
Glycine	2 M
in ddH$_2$O	

1X SDS-PAGE transfer buffer

Substance	Concentration
10X SDS-PAGE transfer buffer without MeOH	1X
MeOH	20 %
in ddH$_2$O	

FRET imaging buffer

Substance	Concentration
NaCl	144 mM
KCl	5.4 mM
MgCl$_2$ X 6H$_2$O	1 mM
CaCl$_2$ X 2H$_2$O	1 mM
HEPES (in ddH$_2$O, pH 7.4 with NaOH)	10 mM
adjust to pH 7.4	
in ddH$_2$O	

25X Tris-buffered saline (TBS)

Substance	Concentration
Tris	250 mM
NaCl	3.75 M
in ddH$_2$O	

1X Tris-buffered saline with Tween-20 (TBST)

Substance	Concentration
25X TBS	1X
Tween® 20	0.025 % v/v
in ddH$_2$O	

Western Blot blocking buffer

Substance	Concentration
Skim Milk Powder	5 % w/v
in TBST	

Polyacrylamid Resolving Gel 10%

Substance	Concentration
Tris, pH 8.8	380 mM
Acrylamide	10 %
SDS	0.2 %
APS	0.25 mg/mL
TEMED	0.2 % v/v
in ddH$_2$O	

Polyacrylamid Stacking Gel

Substance	Concentration
Tris, pH 6.8	130 mM
Acrylamide	4.5 %
SDS	0.1 %
APS	0.25 mg/mL
TEMED	0.4 % v/v
in ddH$_2$O	

Cell freezing medium

Substance	Concentration
FBS	20 % v/v
DMSO	10 % v/v
in DMEM	

Cell culture medium

Substance	Concentration
FBS	10 % v/v
P/S	1 % v/v
in DMEM	

Phosphate buffer

Substance	Concentration
NaH$_2$PO$_4$	26.5 mM
Na$_2$HPO$_4$	77 mM
NaCl	300 mM
adjust to pH 7.2	
in ddH$_2$O	

Cryoprotectant solution for vibratome sections

Substance	Concentration
Phosphate buffer, pH 7.2	50 % v/v
Sucrose	30 % w/v
PVP	1 % w/v
Ethylene glycol	30 % v/v
in ddH$_2$O	

Immunohistochemistry (IHC) blocking solution

Substance	Concentration
Normal goat serum	5 %
Triton® X-100	0.2 %
Sodium azide	0.02 %
in DPBS	

9.2 Methods

9.2.1 Animals

All animals used in this study were housed in a 12 h:12 h light-dark cycle with water and food pellets *ad libitum* at a temperature of 21 °C. Housing facilities and animal handling were in accordance with the German and European Community laws on protection of experimental animals and approved by the local authorities of the City of Hamburg. Mouse strains used are listed in Table 9.4 and indicated for each experimental procedure.

9.2.2 Preparation of Mouse Brain Sections

Eight female 16 to 17 week-old *Cnr2^{tm1Dgen}* (DeltagenInc, 2005) CB2-deficient and wild-type mice were deeply anesthetised with 120 µg/g body weight esketamine and 16 µg/g body weight xylazine intra-peritoneally in sterile physiological 0.9 % NaCl solution and then transcardially perfused with 25 ml 4 % PFA. Whole brains were harvested and stored in 4 % PFA at 4 °C until use, but at least 24 h. Fixed brains were cut on a vibratome at 40 µm section thickness from the rostral beginning of the hippocampus until the caudal end in series of ten. Sections were collected in 24-well plates filled with cryoprotectant solution at 4 °C until immunohistochemistry.

9.2.3 Immunohistochemistry of Mouse Brain Sections

One series of 10 brain sections (distance between sections: 400 µm) per animal were transferred from cryoprotectant to cold Dulbecco's phosphate-buffered saline (DPBS) in 24-well plates and washed three times. Antigen retrieval was performed in 10 mM sodium citrate (in ddH$_2$O, pH 9) at 80 °C in an incubator for 30 min. Tissue sections were then cooled at room temperature, washed with DPBS and blocked with IHC blocking solution for 45 min at room temperature on a shaker and then incubated with primary antibody against DCX and CR or against Ki67 (working concentration see Table 9.3) in DPBS over night at 4 °C on a shaker.

After incubation with the primary antibody, brain sections were washed three times with DPBS for each 5 min on a shaker at room temperature. Fluorescent-dye conjugated secondary antibodies (anti-rabbit IgG Alexa Fluor® 488, anti-guinea pig IgG Alexa Fluor® 594) were prepared in DPBS according to used primary antibodies and sections were incubated with the secondary antibody (Ab)-solution for 2 h in the dark at room temperature on a shaker. Sections were again washed three time with DPBS for each 15 min on a shaker and then carefully transferred to objectives. ProLong^{TM} Gold Antifade Mountant with DAPI was applied and cover slips were carefully placed on the sections avoiding air bubbles. The mounted sections were left to dry at room temperature in the dark for about 24 h and then transferred to boxes and stored at 4 °C until imaging.

9.2.4 Quantification of Neuronal Progenitor Cell Populations

Blinded quantification of DCX+, DCX+/CR+ and Ki67+ neuronal progenitor cells in the subgranular zone of the dentate gyrus in 40 µm-thick brain sections was carried out on an epi-fluorescence microscope using the software tool Stereo Investigator. For each section and brain hemisphere an overview image of the complete DG with clearly distinguishable infra- and suprapyramidal blades was acquired using the DAPI staining to determine if the hemisphere is quantifiable. Exclusion criteria were the overlapping or damage of tissue. In each hemisphere and blade all positive cells (DCX+, Ki67+) and double-positive (DCX+/CR+) in the SGZ were counted in a focal plane of 20 µm. Using ImageJ, the area of the complete GCL and SGZ of the DG was calculated for each hemisphere and blade seperately. The total sample volume was then determined by multiplying the GCL area with the thickness of the focal plane (20 µm). All hippocampal sample volumes and cell counts were summed for each animal and positive counts per volume (in mm^3) for DCX+ and Ki67+ were determined. From DCX+/CR+ counts, the percentage of double-positives from all DCX+ cells was calculated for each animal.

9.2.5 Preparation of Poly-L-Lysine-Coated Glass Coverslips

22 mm glass cover slips were placed in 6-well-plates (12 mm coverslips for 24-well-plates) and 0.1 mg/mL poly-L-lysin (PLL) solution in ddH_2O was pipetted onto the coverslip covering the majority of the surface. Glass coverslips were incubated for at least 30 min or up to 1 h at room temperature under the cell culture hood. Coverslips were then washed three times with ddH_2O and kept at room temperature until use.

9.2.6 Isolation and Culture of Primary Mouse Microglial Cells

Isolation and culture of primary mouse microglia was adapted from Witting and Möller (2011). Four- to eight-week-old male and female mice (n = 14) from matings of $Cnr2^{tm1Dgen}$ and $CAG\text{-}Epac1\text{-}camps$ transgenic mice (Calebiro et al., 2009) ($CB2^{+/+}$ or $CB2^{-/-}$ and $Epac1\text{-}camps^{+/-}$) and one $Cx3cr1^{tm2.1(cre/ERT2)Litt/+}$ mouse were used. Two mice ($CB2^{-/-}$ and wildtype littermate) per isolation were killed using CO_2 and then transcardially perfused with HBSS (here without MgCl or CaCl). Each brain was carefully removed and placed into separate petri dishes filled with cold HBSS. Olfactory bulb and cerebellum were cut off and brains were divided along the sagittal suture. The midbrain was removed and the cortex and hippocampus were transferred into separate chilled falcon tubes with 5 ml HBSS.
Under the cell culture hood, the brain tissue was washed three times with 5 ml HBSS saving 1 ml to 2 ml from the last wash. In the tube, the tissue was manually crushed using the blunt end of a pair of scissors. 1 ml 0.25 % trypsin in HBSS (without MgCl or CaCl) was pipetted into each tube and incubated for 10 min at 37 °C in a water bath. 10 ml cell culture medium was added to stop the reaction and the tissue was homogenised by

pipetting up and down with the same serological pipette. A 5 ml serological pipette and a glass pasteur pipette were coated with fetal bovine serum (FBS) and the tissue was homogenised further with the 5 ml pipette and then with the pasteur pipette. The homogenate was then titrated through a 70 μm cell strainer and centrifuged for 10 min at 200g. The supernatant was removed and the cell pellet was resuspended in 24 ml cell culture medium. Cells were plated on two 6-well-plates with PLL-coated glass cover slips and incubated at 37 °C and 5 % CO_2. After 24 h the medium was changed by aspirating the old medium, washing the cells three times with warm DPBS and supplying them with new cell culture medium. Primary microglia cells were cultured for 14 d and the medium was changed every fourth day.

9.2.7 HEK293 cell culture and preparation for downstream assays

All cells were maintained at 37 °C and 5 % CO_2. HEK293 were kept in DMEM supplemented with 10 % FBS and 1 % penicillin/streptomycin (P/S) and split 1:10 using 0.25 % trypsin/EDTA every second to third day. HEK293 cells stably expressing FRET-cAMP-biosensor Epac1-camps were kept in the described HEK293-medium with additional 400 μg/μl hygromycin B. For double stably transfected HEK293 with Epac1-camps and FLAG-hCB2, DMEM plus 10 % FBS and 1 % P/S was additionally supplemented with 400 μg/μl hygromycin B and 600 μg/μl G418. Both stably transfected cell lines were split using 0.05 % trypsin/EDTA in a dilution of 1:6 to 1:8 every third to fourth day. Volumes of cell media were varied according to dish/plate size (see Table 9.26).

Table 9.26. Used media volumes in cell culture experiments

Dish/Plate Size	Volume [ml]
10 cm	10
6-well	2
24-well	0.5
96-well	0.1

Cryo-preserved 1 ml-tubes with cells in freezing medium were carefully thawed in a 37 °C water bath under gentle agitation for about 30 s. Cells were then immediately resuspended in 4 ml warm medium and centrifuged at 1000 rpm for 5 min. The supernatant was aspirated and the pellet was resuspended in 10 ml warm medium and plated on a 10 cm-dish.

For freezing, confluent cells on 10 cm-dishes were trypsinised and centrifuged at 1000 rpm for 5 min. The pellet was then carefully resuspended in 1 ml freezing medium per confluent 10 cm-dish and each 1 ml of the cell suspension was pipetted into a cryo-tube. The tubes were transferred into a freezing container filled with isopropanol and placed in a −80 °C freezer to cool down at a rate of 1 °C/min. On the next day, cryo-preserved cells were transferred to a liquid nitrogen tank for long-term storage.

The preparation of cell lysates for downstream assays such as Western Blot was done

by removing the medium and applying ice-cold DDM lysis buffer directly onto the cells. The lysates were then transferred into reaction tubes, homogenised with a 27G syringe, incubated for 30 min at 4 °C on a rotor and centrifuged for 15 min at 13 000 rpm and 4 °C. The supernatant was used immediately for further assays or stored at −20 °C.

9.2.8 Transfection of HEK293 Cells with HA-hβ_2AR and FLAG-hCB2

HEK293 were plated on 6-well plates at a density of 0.1×10^6 cells per well without the use of P/S and 24 h. When cells were about 50 % to 60 % confluent, they were transfected using 500 ng pcDNA 3.1(+)-FLAG-hCB2(Q-H) and 3 µg pcDNA 3.1(+)-HA-hB2AR (500 ng for immunocytochemistry stainings) (single transfections filled up with empty vector pcDNA3.1(+)) per well in a 1:2 DNA to Lipofectamine®2000 ratio with OptiMEM according to the manufacturer's protocol. After another 24 h-incubation the medium was aspirated and cells were lysed with DDM lysis buffer for co-IP or fixed with 4 %PFA for 20 min at room temperature on a shaker and stored in DPBS at 4 °C for immunocytochemistry.

9.2.9 Immunoprecipitaion of FLAG- and HA-tagged Receptor Constructs

For immunoprecipitation (IP) of FLAG- and HA-tagged receptor constructs 20 µl protein lysate (input) was mixed with 4 µl 6X Laemmli buffer. 200 µl protein lysate were used for HA- and FLAG-IP. For the HA-IP, each sample was mixed with mouse anti-HA antibody in n-dodecyl β-D-maltoside (DDM) lysis buffer at an end concentration of 1:200 and incubated over night on a rotor at 4 °C. For each HA-IP-sample 10 µl Protein-G sepharose beads and for each FLAG-IP-sample 8 µl mouse anti-FLAG® M2 Affinity Gel beads were pipetted into 500 µl DDM lysis buffer and washed three times. During the last washing step, all remaining liquid was aspirated with a 27G syringe and 100 µl DDM lysis buffer for each HA-IP- or FLAG-IP-sample were carefully added to the beads and pipette-mixed. 100 µl of each IP-bead mixture were then added to the assigned samples and incubated at 4 °C for 1 h on a rotor. After incubation, the beads of all samples were washed three times with DDM lysis buffer and in the last washing step all remaining liquid was aspirated and the beads were mixed with 18 µl 6X Laemmli buffer and incubated for 10 min at 70 °C. IP-samples were spun down and the supernatant as well as the input samples were used Western blot.

9.2.10 SDS-Polyacrylamide Gel Electrophoresis and Immunoblotting

10 % polyacrylamid resolving gels were prepared in 50 ml-tubes and ca. 8 ml per gel were carefully poured into a casting frame of 1.5 mm gel thickness. Per gel, 500 µl isopropanol were added and the gel was left to polymerise for about 30 min at room temperature while the stacking gel was prepared. After polymerisation of the resolving gel, the isopropanol was poured off and the stacking gel was carefully pipetted into the casting

frame up until the top of the casting frame. 10- or 15-well combs were added while avoiding air bubbles and the gel was left to polymerise for about 20 min at room temperature. Polymerised gels were then either used immediately or stored in a sealed plastic bag wrapped in wet tissue at 4 °C for about 5 to 7 days.

For SDS-PAGE, up to 4 gels were assembled in the running chamber supplied with SDS-PAGE running buffer. The combs were removed and each well was rinsed with buffer before the prepared protein samples and 4 µl of the protein ladder were loaded into each gel. Gels were run at 80 V for the first 10 min and then set to 110 V until the running front reached the end of the gel. With sponges, filter paper, the gel and a nitrocellulose membrane, the transfer sandwich was assembled in a transfer chamber filled with cold transfer buffer. The proteins were then transferred onto the nitrocellulose membrane at 95 V for 2 h at 4 °C.

After the successful transfer of proteins, indicated by a visible protein ladder, the membrane was blocked in Western blot blocking solution for 1 h at room temperature on a shaker. Following blocking, membranes were incubated over night at 4 °C on a shaker in primary antibody solution. Depending on the primary antibody the composition of the antibody solution varied (see Table 9.1.1). Then membranes were washed three times with TBST for 5 min at room temperature on a shaker and then incubated with either IRDye® 680LT- or IRDye® 800CW-coupled secondary antibodies in TBST (see Table 9.1.1) for 1 h at room temperature on a shaker. Membranes were then washed two times with TBST and one time with TBS for 15 min at room temperature on a shaker. The detection of target protein bands from the wet membrane was done using the Odyssey® CLx imaging system and band intensities were quantified using Image Studio Lite.

9.2.11 Immunocytochemistry and Object-Based Co-Localisation Analysis

Cells on coverslips were washed with DPBS and then fixed with 4 % PFA for 20 min at room temperature on a shaker. HEK293 transfected with FLAG-hCB2 and HA-hB2AR, Epac1- and Epac1-CB2-HEK cells were then blocked with 5 % normal goat serum in DPBS for 1 h at room temperature on a shaker. For primary microglia, the blocking and primary antibody solutions were supplied with 0.3 % Triton® X-100.

Primary antibodies used for all HEK293 cell model systems were rabbit anti-CB2, rabbit anti-β_2AR, mouse anti-HA and rabbit anti-FLAG in the indicated concentrations, and primary microglia were stained with rabbit anti-Iba-1 and mouse anti-GFP (also recognises YFP (Assinck et al., 2017)) (see Table 9.1.1). Fixed cells were incubated with primary antibody for 24 h at 4 °C on a shaker and then washed three times for 5 min with cold DPBS. Secondary antibody solutions were prepared with anti-mouse IgG, Alexa Fluor® 488 and 594 and anti-rabbit IgG, Alexa Fluor® 488 and 594 in DPBS and cells were incubated for 2 h at room temperature on a shaker in the dark.

Coverslips were then washed three times for 15 min with DPBS and mounted onto glass slides with ProLong™ Gold Antifade Mountant medium (without DAPI for Epac1- and

Epac1-CB2-HEK cells) and dried at room temperature over night in the dark. Slides were then stored at 4 °C until imaging on a confocal microscope. Acquired image z-stacks of FLAG-hCB2 and HA-hβ_2AR co-transfected HEK293 were analysed for object-based co-localisation of CB2 and HA, as well as FLAG and β_2AR with MatCol on default settings and the percentage of co-localising pixels from the total pixel amount was calculated.

9.2.12 Generation of HEK293 Cells Stably Expressing Epac1-camps and FLAG-hCB2

Epac1-HEK cells were plated on 6-well-plates at a density of 1×10^5 cells per well without the use of P/S or hygromycin B and 24 h after seeding when cells were about 50 % to 60 % confluent, they were transfected with either 1 µg pcDNA 3.1(+)-FLAG-hCB2(Q-H) or 1 µg pcDNA3.1(+) per well in a 1:2 desoxyribonucleic acid (DNA) to Lipofectamine®2000 ratio with OptiMEM according to the manufacturer's protocol. After another 24 h-incubation the medium was changed to DMEM supplemented with 10 % FBS, 1 % P/S, 400 µg/µl hygromycin B and 800 µg/µl G418 (as determined in previous kill-curve experiment) for the selection of clones stably expressing both Epac1-camps and FLAG-hCB2 or the control plasmid. Clones were selected for 14 d and the medium was changed every third day. Surviving clones were collected, counted in a Neubauer-chamber, diluted down to 10 cells/ml and plated on a 96-well plate in selection medium. The medium was changed every third day and as soon as the cells in a well reached 100 % confluency, they were transferred to a 24-well and subsequently to a 6-well plate. Colonies in confluent 6-well plate wells were split 1:2 and the remaining cells were analysed via SDS-PAGE for FLAG-hCB2 expression (see Methods section 9.2.10). Positive colonies were further propagated to 10 cm-dishes and frozen.

9.2.13 ERK1/2 Activation Assay

Epac1-CB2-HEK cells were plated on 24-well-plates at a density of 6×10^3 cells in cell culture medium. After 48 h incubation, the medium was changed to DMEM without any supplements for 4 h. βAR- and CB2-ligands (isoprenaline, JWH133 and AM630) were prepared in dimethyl sulfoxide (DMSO) and diluted if necessary. 50 µl of medium from each well were saved and mixed with the different ligands keeping DMSO at an end concentration of 0.1 %. The stimulation aliqouts were quickly pipetted back into the wells and the plate was incubated for 5 min. After stimulation, the medium was quickly aspirated and the cells were lysed with 80 µl ice-cold DDM lysis buffer per well. 30 µl protein lysate were then mixed with 6 µl 6X Laemmli buffer, boiled at 95 °C for 5 min, loaded into a 10 % SDS-gel with 10 wells in series and analysed on the Odyssey® CLx imaging system (see Methods section 9.2.10). The membranes were blocked with Western blot blocking solution and incubated with mouse anti-ERK1/2 and rabbit anti-pERK1/2 primary antibodies (see Table 9.1.1). After detection and quantification of protein bands the

ratio between phosphorylated ERK1/2- and total ERK1/2-band intensity ($\frac{pERK}{ERK}$) for each sample was formed and log$_2$-transformed. For each blot, the log$_2$-transformed DMSO value was subtracted from each sample value on that individual blot for normalisation.

9.2.14 Live Cell FRET imaging

Live cell FRET imaging was carried out as previously described (Kraft and Nikolaev, 2017; Sprenger et al., 2012; Börner et al., 2011). Epac1- and Epac1-CB2-HEK cells were plated on PLL-coated 22 mm glass cover slips in 6-well-plates at a density of 0.1×10^6 cells per well and incubated for 48 h.

On the imaging day, coverslips with Epac1-, Epac1-CB2-HEK cells or primary mouse microglia were transferred into a cell imaging chamber, washed one time using FRET imaging buffer and then kept in a minimum of 400 µl FRET imaging buffer at room temperature during imaging. The imaging chamber was secured on the stage of an inverted microscope equipped with a 63X oil objective. Cells were excited using a 440 nm LED connected to an Arduino board and fluorescent emission was detected with a dual-emission photometry system using a CCD camera and a beam splitter with a filter set for CFP and YFP. Excitation time and image acquisition were controlled and synchronised using the Micro-Manager plugin for ImageJ.

Images were acquired every 20 s with 10 % to 15 %LED power, 50 ms to 100 ms excitation time depending on the expression of Epac1-camps and binning was set to 4. Live fluorescence intensities and the raw FRET ratio were monitored during the recording and stimulants were applied after a baseline was reached. Cell stimulants (dissolved in DMSO and further diluted in FRET imaging buffer) were then carefully added to the cell imaging chamber in appropriate concentrations in a volume of each 400 µl without exceeding the maximum chamber capacity of 1.6 ml (maximum concentration of DMSO on cells: 0.05%).

9.2.15 Experimental Data Analysis

FRET Data Analysis

Acquired time lapse emission channel images were processed using ImageJ and following calculations and FRET response analyses were done using self-made scripts in R. For image noise reduction a Kalman stack filter was applied and using the MultiStackReg plugin (rigid body transformation) the two channels were aligned. ROIs on cells were drawn where Epac1-camps expression was homogenous and movement was minimal throughout the recording. Integrated density, area and average grey value of each ROI for each frame were measured and the total corrected cellular fluorescence (TCCF) was calculated according to McCloy et al. (2014):

$$TCCF = ROI_{IntDen} - ROI_{Area} \times BG_{AveGrey}$$

After the individual channels were inspected for excessive photobleaching and correct opposing fluorescence intensity changes, the FRET ratio R was calculated as follows:

$$R = \frac{TCCF_{YFP}}{TCCF_{CFP}} - B$$

Where B is the bleedthrough correction factor of CFP emission into the YFP channel determined for the imaging setup. For statistical analysis and data visualisation, the FRET ratio for each ROI over time was normalised to its pre-stimulation baseline R_0, subtracted from 1 and multiplied by 100 in order to depict the decrease in FRET upon increased intracellular cAMP levels as a percentage increase or vice versa. It was calculated as follows:

$$\Delta R_t[\%] = (1 - \frac{R_t}{R_0}) \times 100$$

For each FRET response after application of a specific stimulant local maxima and minima were detected and for each of these response curves the maximum slope as well as the time to 50 % of the signal's amplitude were determined. The max. slope values are always depicted without a sign. Plots featuring max. slope values are supplied with an information on the direction of the response.

For CB2 activation experiments (see Results section 6.2.1) in Epac1-CB2-HEK cells, ROIs/-cells showing at least 10 % cAMP inhibition after CB2 agonist application and a blockage of the inhibition via AM630 (max. slope of response: $\geq$ 0.01) are considered responders (R). Cells with less than 10 % cAMP inhibition after agonist stimulation but a clear response to AM630 show a response pattern of high constitutive activity (CA) of CB2 receptors. If a cell showed no response to either CB2 agonist or inverse agonist/antagonist with a linear increase of ΔR_t after reaching the FSK baseline comparable to Epac1-HEK cells, the cell is categorised as a non-responder (N). To avoid the pitfalls of pseudoreplication in recordings with multiple cells from Epac1-HEK and Epac1-CB2-HEK cells, the FRET response parameters of a minimum of three cells with the same response pattern in one recording were averaged.

The inhibition of FSK-mediated cyclic AMP production by CB2 agonists was calculated as follows:

$$cAMP_{inhib}[\%] = (\frac{\Delta R_{Ago}}{\Delta R_{FSK}} - 1) \times 100$$

Accordingly, the negative cAMP feedback after isoprenaline stimulation in Results section 6.3.1 and 6.4.3 was calculated as follows:

$$feedback[\%] = (\frac{\Delta R_{ISO_{fb}}}{\Delta R_{ISO_{max}}} - 1) \times 100$$

Statistical Analysis

All statistical analysis was carried out using GraphPad Prism and applied statistical test to estimate differences between sample groups are given with the result figures in the

Results chapters 5 and 6. The Shapiro-Wilk test was used to determine the normality of a given sample population. Epac1-HEK and Epac1-CB2-HEK cell FRET data was analysed using Nested-models with ROIs/cells nested within recordings.

9.2.16 Meta-Analysis of RNAseq Data from adult mouse microglia

Meta-analysis of published RNAseq data from adult mouse microglia at different ages was carried out using the GREP2 pipeline with the web-platform GREIN and the R packages *edgeR* and *org.Mm.eg.db*. For the selection of RNAseq data the web-platform GREIN was used, that offers processed RNAseq data from the genomics data repository GEO. The database was searched for experiments performed in *Mus musculus* and the keyword "microglia". Each GSE search result was screened for the availability of untreated microglia control samples. A detailed list of included studies (GSE, n = 18) and individual samples (GSM, n= 132) and their source animals is given in the Appendix 10.5.

Raw gene counts for the relevant samples were downloaded and analysed using custom-made R scripts. Genes with low or no expression (cpm $\geq$ 2 in at least three different samples) were filtered and gene counts were normalised using the TMM method from *edgeR*. Normalised cpm were added with a pseudocount of 0.25 and then $\log_2$-transformed ($\log_2$(cpm)) and summarised over all samples. Gene lists were then grouped for GPCR class A and cAMP pathway-related signalling proteins according to Atwood and Mackie (2010) and median-ranked.

Bibliography

Agarwal, S. R., P.-C. Yang, M. Rice, C. A. Singer, V. O. Nikolaev, M. J. Lohse, C. E. Clancy, and R. D. Harvey
2014. Role of membrane microdomains in compartmentation of cAMP signaling. *PLoS ONE*, 9(4):e95835.

Aguado, T., J. Palazuelos, K. Monory, N. Stella, B. Cravatt, B. Lutz, G. Marsicano, Z. Kokaia, M. Guzmán, and I. Galve-Roperh
2006. The endocannabinoid system promotes astroglial differentiation by acting on neural progenitor cells. *Journal of Neuroscience*, 26(5):1551–1561.

Ahlquist, R. P.
1948. A study of the adrenotropic receptors. *American Journal of Physiology*, 153(3):586–600.

Aimone, J. B., Y. Li, S. W. Lee, G. D. Clemenson, W. Deng, and F. H. Gage
2014. Regulation and function of adult neurogenesis: from genes to cognition. *Physiological Reviews*, 94(4):991–1026.

Alberti, T. B., W. L. R. Barbosa, J. L. F. Vieira, N. R. B. Raposo, and R. C. Dutra
2017. (-)-β-caryophyllene, a CB2 receptor-selective phytocannabinoid, suppresses motor paralysis and neuroinflammation in a murine model of multiple sclerosis. *International Journal of Molecular Sciences*, 18.

Altman, J. and G. D. Das
1965. Autoradiographic and histological evidence of postnatal hippocampal neurogenesis in rats. *The Journal of Comparative Neurology*, 124:319–335.

Ashton, J. C. and M. Glass
2007. The cannabinoid CB2 receptor as a target for inflammation-dependent neurodegeneration. *Current Neuropharmacology*, 5:73–80.

Assinck, P., G. J. Duncan, J. R. Plemel, M. J. Lee, J. A. Stratton, S. B. Manesh, J. Liu, L. M. Ramer, S. H. Kang, D. E. Bergles, J. Biernaskie, and W. Tetzlaff
2017. Myelinogenic plasticity of oligodendrocyte precursor cells following spinal cord contusion injury. *The Journal of Neuroscience*, 37(36):8635–8654.

Atwood, B. K., J. Lopez, J. Wager-Miller, K. Mackie, and A. Straiker
2011. Expression of G-protein-coupled receptors and related proteins in HEK293, AtT20, BV2, and N18 cell lines as revealed by microarray analysis. *BMC Genomics*, 12(1):14.

Atwood, B. K. and K. Mackie
2010. CB2: A cannabinoid receptor with an identity crisis. *British Journal of Pharmacology*, 160(3):467–479.

Atwood, B. K., J. Wager-Miller, C. Haskins, A. Straiker, and K. Mackie
2012. Functional selectivity in CB2 cannabinoid receptor signaling and regulation: implications for the therapeutic potential of CB2 ligands. *Molecular Pharmacology*, 81(2):250–263.

Avraham, H. K., S. Jiang, Y. Fu, E. Rockenstein, A. Makriyannis, A. Zvonok, E. Masliah, and S. Avraham
2013. The cannabinoid CB2receptor agonist AM1241 enhances neurogenesis in GFAP/gp120 transgenic mice displaying deficits in neurogenesis. *British Journal of*

Pharmacology, 171(2):468–479.

Badhwar, A., J. P. Lerch, E. Hamel, and J. G. Sled
2013. Impaired structural correlates of memory in Alzheimer's disease mice. *NeuroImage: Clinical*, 3:290–300.

Baek, J.-H., C. L. Darlington, P. F. Smith, and J. C. Ashton
2013. Antibody testing for brain immunohistochemistry: Brain immunolabeling for the cannabinoid CB2 receptor. *Journal of Neuroscience Methods*, 216(2):87–95.

Baillie, G. S., A. Sood, I. McPhee, I. Gall, S. J. Perry, R. J. Lefkowitz, and M. D. Houslay
2003. β-arrestin-mediated PDE4 cAMP phosphodiesterase recruitment regulates beta-adrenoceptor switching from Gs to Gi. *Proceedings of the National Academy of Sciences of the United States of America*, 100:940–945.

Bakker, R., P. Tiesinga, and R. Kötter
2015. The scalable brain atlas: Instant web-based access to public brain atlases and related content. *Neuroinformatics*, 13:353–366.

Balenga, N. A., E. Martínez-Pinilla, J. Kargl, R. Schröder, M. Peinhaupt, W. Platzer, Z. Balint, M. Zamarbide, I. G. Dopeso-Reyes, A. Ricobaraza, et al.
2014. Heteromerization of GPR55 and cannabinoid CB2 receptors modulates signalling. *British Journal of Pharmacology*, 171(23):5387–5406.

Balenga, N. A. B., E. Aflaki, J. Kargl, W. Platzer, R. Schröder, S. Blättermann, E. Kostenis, A. J. Brown, A. Heinemann, and M. Waldhoer
2011. GPR55 regulates cannabinoid 2 receptor-mediated responses in human neutrophils. *Cell Research*, 21:1452–1469.

Bauer, M., A. Chicca, M. Tamborrini, D. Eisen, R. Lerner, B. Lutz, O. Poetz, G. Pluschke, and J. Gertsch
2012. Identification and quantification of a new family of peptide endocannabinoids (Pepcans) showing negative allosteric modulation at CB1 receptors. *The Journal of Biological Chemistry*, 287:36944–36967.

Becker, S.
2016. Neurogenesis and pattern separation: time for a divorce. *Wiley Interdisciplinary Reviews: Cognitive Science*, 8(3):e1427.

Beltramo, M.
2009. Cannabinoid type 2 receptor as a target for chronic pain. *Mini-Reviews in Medicinal Chemistry*, 9(1):11–25.

Benito, C., R. M. Tolon, M. R. Pazos, E. Nunez, A. I. Castillo, and J. Romero
2008. Cannabinoid CB2 receptors in human brain inflammation. *British Journal of Pharmacology*, 153(2):277–285.

Besnard, A. and A. Sahay
2015. Adult hippocampal neurogenesis, fear generalization, and stress. *Neuropsychopharmacology*, 41(1):24–44.

Betolngar, D.-B., M. Erard, H. Pasquier, Y. Bousmah, A. Diop-Sy, E. Guiot, P. Vincent, and F. Mérola
2015. pH sensitivity of FRET reporters based on cyan and yellow fluorescent proteins. *Analytical and Bioanalytical Chemistry*, 407(14):4183–4193.

Bettiga, A., M. Aureli, G. Colciago, V. Murdica, M. Moschini, R. Lucianò, D. Canals, Y. Hannun, P. Hedlund, G. Lavorgna, R. Colombo, R. Bassi, M. Samarani, F. Montorsi, A. Salonia, and F. Benigni
2017. Bladder cancer cell growth and motility implicate cannabinoid 2 receptor-mediated modifications of sphingolipids metabolism. *Scientific Reports*, 7(1):42157.

Boldrini, M., C. A. Fulmore, A. N. Tartt, L. R. Simeon, I. Pavlova, V. Poposka, G. B. Rosok-

lija, A. Stankov, V. Arango, A. J. Dwork, R. Hen, and J. J. Mann
2018. Human hippocampal neurogenesis persists throughout aging. *Cell Stem Cell*, 22(4):589–599.e5.

Bolognini, D., M. G. Cascio, D. Parolaro, and R. G. Pertwee
2012. AM630 behaves as a protean ligand at the human cannabinoid CB2 receptor. *British Journal of Pharmacology*, 165(8):2561–2574.

Bonfanti, L. and J. Nacher
2012. New scenarios for neuronal structural plasticity in non-neurogenic brain parenchyma: The case of cortical layer II immature neurons. *Progress in Neurobiology*, 98(1):1–15.

Bonnet, N., D. D. Pierroz, and S. L. Ferrari
2008. Adrenergic control of bone remodeling and its implications for the treatment of osteoporosis. *Journal of Musculoskeletal & Neuronal Interactions*, 8:94–104.

Bouaboula, M., N. Desnoyer, P. Carayon, T. Combes, and P. Casellas
1999. Gi protein modulation induced by a selective inverse agonist for the peripheral cannabinoid receptor CB2: implication for intracellular signalization cross-regulation. *Molecular Pharmacology*, 55:473–480.

Bouaboula, M., C. Poinot-Chazel, J. Marchand, X. Canat, B. Bourrié, M. Rinaldi-Carmona, B. Calandra, G. Fur, and P. Casellas
1996. Signaling pathway associated with stimulation of CB2 peripheral cannabinoid receptor. *European Journal of Biochemistry*, 237(3):704–711.

Bouaboula, M., M. Rinaldi, P. Carayon, C. Carillon, B. Delpech, D. Shire, G. Le Fur, and P. Casellas
1993. Cannabinoid-receptor expression in human leukocytes. *European Journal of Biochemistry*, 214:173–180.

Boularan, C. and C. Gales
2015. Cardiac cAMP: production, hydrolysis, modulation and detection. *Frontiers in Pharmacology*, 6.

Brandt, M. D., S. Jessberger, B. Steiner, G. Kronenberg, K. Reuter, A. Bick-Sander, W. von der Behrens, and G. Kempermann
2003. Transient calretinin expression defines early postmitotic step of neuronal differentiation in adult hippocampal neurogenesis of mice. *Molecular and Cellular Neuroscience*, 24(3):603–613.

Bravo-Ferrer, I., M. I. Cuartero, J. G. Zarruk, J. M. Pradillo, O. Hurtado, V. G. Romera, J. Díaz-Alonso, J. M. García-Segura, M. Guzmán, I. Lizasoain, I. Galve-Roperh, and M. A. Moro
2016. Cannabinoid type-2 receptor drives neurogenesis and improves functional outcome after stroke. *Stroke*, 48(1):204–212.

Brown, G. C. and A. Vilalta
2015. How microglia kill neurons. *Brain Research*, 1628:288–297.

Bruss, M. D., W. Richter, K. Horner, S.-L. C. Jin, and M. Conti
2008. Critical role of PDE4D in β_2-adrenoceptor-dependent cAMP signaling in mouse embryonic fibroblasts. *The Journal of Biological Chemistry*, 283:22430–22442.

Brust, T. F., J. M. Conley, and V. J. Watts
2015. G$\alpha_{i/o}$-coupled receptor-mediated sensitization of adenylyl cyclase: 40 years later. *European Journal of Pharmacology*, 763:223–232.

Buckley, N. E., K. L. McCoy, E. Mezey, T. Bonner, A. Zimmer, C. C. Felder, M. Glass, and A. Zimmer
2000. Immunomodulation by cannabinoids is absent in mice deficient for the cannabinoid CB2 receptor. *European Journal of Pharmacology*, 396(2-3):141–149.

Butovsky, O., M. P. Jedrychowski, C. S. Moore, R. Cialic, A. J. Lanser, G. Gabriely, T. Koeglsperger, B. Dake, P. M. Wu, C. E. Doykan, Z. Fanek, L. Liu, Z. Chen, J. D. Rothstein, R. M. Ransohoff, S. P. Gygi, J. P. Antel, and H. L. Weiner
2013. Identification of a unique TGF-β-dependent molecular and functional signature in microglia. *Nature Neuroscience*, 17(1):131–143.

Börner, C., M. Smida, V. Höllt, B. Schraven, and J. Kraus
2009. Cannabinoid receptor type 1-and 2-mediated increase in cyclic AMP inhibits T cell receptor-triggered signaling. *Journal of Biological Chemistry*, 284(51):35450–35460.

Börner, S., F. Schwede, A. Schlipp, F. Berisha, D. Calebiro, M. J. Lohse, and V. O. Nikolaev
2011. FRET measurements of intracellular cAMP concentrations and cAMP analog permeability in intact cells. *Nature Protocols*, 6(4):427–438.

Cabral, G. A., E. S. Raborn, L. Griffin, J. Dennis, and F. Marciano-Cabral
2008. CB2 receptors in the brain: role in central immune function. *British Journal of Pharmacology*, 153:240–251.

Calebiro, D., V. O. Nikolaev, M. C. Gagliani, T. de Filippis, C. Dees, C. Tacchetti, L. Persani, and M. J. Lohse
2009. Persistent cAMP-signals triggered by internalized g-protein-coupled receptors. *PLoS Biology*, 7(8):e1000172.

Calebiro, D., V. O. Nikolaev, and M. J. Lohse
2010. Imaging of persistent cAMP signaling by internalized G-protein-coupled receptors. *Journal of Molecular Endocrinology*, 45(1):1–8.

Callén, L., E. Moreno, P. Barroso-Chinea, D. Moreno-Delgado, A. Cortés, J. Mallol, V. Casadó, J. L. Lanciego, R. Franco, C. Lluis, et al.
2012. Cannabinoid receptors CB1and CB2form functional heteromers in brain. *Journal of Biological Chemistry*, 287(25):20851–20865.

Campbell, A. P. and A. V. Smrcka
2018. Targeting G-protein-coupled receptor signalling by blocking G proteins. *Nature Reviews Drug Discovery*, 17(11):789–803.

Carlisle, S. J., F. Marciano-Cabral, A. Staab, C. Ludwick, and G. A. Cabral
2002. Differential expression of the CB2 cannabinoid receptor by rodent macrophages and macrophage-like cells in relation to cell activation. *International Immunopharmacology*, 2(1):69–82.

Carlson, M.
2019. org.mm.eg.db: Genome wide annotation for mouse. R package version 3.8.2.

Cassano, T., S. Calcagnini, L. Pace, F. De Marco, A. Romano, and S. Gaetani
2017. Cannabinoid receptor 2 signaling in neurodegenerative disorders: From pathogenesis to a promising therapeutic target. *Frontiers in Neuroscience*, 11.

Chen-Izu, Y., R. P. Xiao, L. T. Izu, H. Cheng, M. Kuschel, H. Spurgeon, and E. G. Lakatta
2000. Gi-dependent localization of β_2-adrenergic receptor signaling to L-type Ca(2+) channels. *Biophysical Journal*, 79:2547–2556.

Chiu, I. M., E. T. A. Morimoto, H. Goodarzi, J. T. Liao, S. O'Keeffe, H. P. Phatnani, M. Muratet, M. C. Carroll, S. Levy, S. Tavazoie, R. M. Myers, and T. Maniatis
2013. A neurodegeneration-specific gene-expression signature of acutely isolated microglia from an amyotrophic lateral sclerosis mouse model. *Cell Reports*, 4(2):385–401.

Coke, C. J., K. A. Scarlett, M. A. Chetram, K. J. Jones, B. J. Sandifer, A. S. Davis, A. I. Marcus, and C. V. Hinton
2016. Simultaneous activation of induced heterodimerization between CXCR4 chemokine receptor and cannabinoid receptor 2 (CB2) reveals a mechanism for regulation of tumor progression. *Journal of Biological Chemistry*, 291(19):9991–10005.

Cronk, J. C., N. C. Derecki, E. Ji, Y. Xu, A. E. Lampano, I. Smirnov, W. Baker, G. T. Norris,

I. Marin, N. Coddington, Y. Wolf, S. D. Turner, A. Aderem, A. L. Klibanov, T. H. Harris, S. Jung, V. Litvak, and J. Kipnis
2015. Methyl-CpG binding protein 2 regulates microglia and macrophage gene expression in response to inflammatory stimuli. *Immunity*, 42(4):679–691.

Daaka, Y., L. M. Luttrell, and R. J. Lefkowitz
1997. Switching of the coupling of the β_2-adrenergic receptor to different G proteins by protein kinase A. *Nature*, 390:88–91.

Davis, T. L., T. M. Bonacci, S. R. Sprang, and A. V. Smrcka
2005. Structural and molecular characterization of a preferred protein interaction surface on g protein $\beta\gamma$ subunits. *Biochemistry*, 44(31):10593–10604.

de Ligt, R. A., A. P. Kourounakis, and A. P. IJzerman
2000. Inverse agonism at G protein-coupled receptors: (patho)physiological relevance and implications for drug discovery. *British Journal of Pharmacology*, 130:1–12.

Degasperi, A., M. R. Birtwistle, N. Volinsky, J. Rauch, W. Kolch, and B. N. Kholodenko
2014. Evaluating strategies to normalise biological replicates of Western Blot data. *PLoS ONE*, 9(1):e87293.

DeltagenInc
2005. NIH initiative supporting placement of Deltagen, Inc. mice into public repositories. MGI Direct Data Submission.

Desroches, J., S. Charron, J.-F. Bouchard, and P. Beaulieu
2014. Endocannabinoids decrease neuropathic pain-related behavior in mice through the activation of one or both peripheral CB1 and CB2 receptors. *Neuropharmacology*, 77:441–452.

Devane, W. A., L. Hanus, A. Breuer, R. G. Pertwee, L. A. Stevenson, G. Griffin, D. Gibson, A. Mandelbaum, A. Etinger, and R. Mechoulam
1992. Isolation and structure of a brain constituent that binds to the cannabinoid receptor. *Science*, 258:1946–1949.

Dey, J., M. T. Alam, S. Chandra, S. Gandhi, and P. P. Tripathi
2019. Recalibrating the existence of new neurons in adult brain. *ACS Chemical Neuroscience*.

Dhopeshwarkar, A. and K. Mackie
2014. CB2 cannabinoid receptors as a therapeutic target-what does the future hold? *Molecular Pharmacology*, 86:430–437.

Dhopeshwarkar, A. and K. Mackie
2016. Functional selectivity of CB2 cannabinoid receptor ligands at a canonical and non-canonical pathway. *Journal of Pharmacology and Experimental Therapeutics*, Pp. jpet–116.

Downer, E. J.
2014. High hopes for CB2 receptors in neurogenesis. *British Journal of Pharmacology*, 171(6):1345–1346.

Doze, V. A. and D. M. Perez
2012. G-protein-coupled receptors in adult neurogenesis. *Pharmacological Reviews*, 64(3):645–675.

Duan, B., R. Davis, E. L. Sadat, J. Collins, P. C. Sternweis, D. Yuan, and L. I. Jiang
2010. Distinct roles of adenylyl cyclase VII in regulating the immune responses in mice. *The Journal of Immunology*, 185(1):335–344.

Duan, M., H. Yao, Y. Cai, K. Liao, P. Seth, and S. Buch
2014. HIV-1 tat disrupts CX3CL1-CX3CR1 axis in microglia via the NF-κBYY1 pathway. *Current HIV Research*, 12(3):189–200.

Dumitru, C. A., I. E. Sandalcioglu, and M. Karsak

2018. Cannabinoids in glioblastoma therapy: New applications for old drugs. *Frontiers in Molecular Neuroscience*, 11:159.

Eason, M. G., H. Kurose, B. D. Holt, J. R. Raymond, and S. B. Liggett
1992. Simultaneous coupling of α_2-adrenergic receptors to two G-proteins with opposing effects. *The Journal of Biological Chemistry*, 267:15795–15801.

Ehrhart, J., D. Obregon, T. Mori, H. Hou, N. Sun, Y. Bai, T. Klein, F. Fernandez, J. Tan, and R. D. Shytle
2005. Stimulation of cannabinoid receptor 2 suppresses microglial activation. *Journal of Neuroinflammation*, 2(1):29.

El Khoury, J., S. E. Hickman, C. A. Thomas, L. Cao, S. C. Silverstein, and J. D. Loike
1996. Scavenger receptor-mediated adhesion of microglia to β-amyloid fibrils. *Nature*, 382:716–719.

Eljaschewitsch, E., A. Witting, C. Mawrin, T. Lee, P. M. Schmidt, S. Wolf, H. Hoertnagl, C. S. Raine, R. Schneider-Stock, R. Nitsch, and O. Ullrich
2006. The endocannabinoid anandamide protects neurons during CNS inflammation by induction of MKP-1 in microglial cells. *Neuron*, 49:67–79.

Emery, A. C., M. V. Eiden, and L. E. Eiden
2012. A new site and mechanism of action for the widely used adenylate cyclase inhibitor SQ22,536. *Molecular Pharmacology*, 83(1):95–105.

Eriksson, P. S., E. Perfilieva, T. Björk-Eriksson, A. M. Alborn, C. Nordborg, D. A. Peterson, and F. H. Gage
1998. Neurogenesis in the adult human hippocampus. *Nature Medicine*, 4:1313–1317.

Ettinger, A. and T. Wittmann
2014. Fluorescence live cell imaging. *Methods in Cell Biology*, 123:77–94.

Fakhfouri, G., A. Ahmadiani, R. Rahimian, A. A. Grolla, F. Moradi, and A. Haeri
2012. WIN55212-2 attenuates amyloid-β-induced neuroinflammation in rats through activation of cannabinoid receptors and PPAR-γ pathway. *Neuropharmacology*, 63(4):653–666.

Felce, J. H., S. L. Latty, R. G. Knox, S. R. Mattick, Y. Lui, S. F. Lee, D. Klenerman, and S. J. Davis
2017. Receptor quaternary organization explains G-protein-coupled receptor family structure. *Cell Reports*, 20(11):2654–2665.

Felder, C. C., K. E. Joyce, E. M. Briley, J. Mansouri, K. Mackie, O. Blond, Y. Lai, A. L. Ma, and R. L. Mitchell
1995. Comparison of the pharmacology and signal transduction of the human cannabinoid CB1 and CB2 receptors. *Molecular Pharmacology*, 48:443–450.

Fertig, B. A. and G. S. Baillie
2018. PDE4-mediated cAMP signalling. *Journal of Cardiovascular Development and Disease*, 5.

Flock, T., A. S. Hauser, N. Lund, D. E. Gloriam, S. Balaji, and M. M. Babu
2017. Selectivity determinants of GPCR-G-protein binding. *Nature*, 545:317–322.

Friedman, B. A., K. Srinivasan, G. Ayalon, W. J. Meilandt, H. Lin, M. A. Huntley, Y. Cao, S.-H. Lee, P. C. G. Haddick, H. Ngu, Z. Modrusan, J. L. Larson, J. S. Kaminker, M. P. van der Brug, and D. V. Hansen
2018. Diverse brain myeloid expression profiles reveal distinct microglial activation states and aspects of Alzheimer's disease not evident in mouse models. *Cell Reports*, 22(3):832–847.

Friedman, J., B. Babu, and R. B. Clark
2002. β_2-adrenergic receptor lacking the cyclic AMP-dependent protein kinase consensus sites fully activates extracellular signal-regulated kinase 1/2 in human embry-

onic kidney 293 cells: lack of evidence for Gs/Gi switching. *Molecular Pharmacology*, 62:1094–1102.

Froese, A. and V. O. Nikolaev
2015. Imaging alterations of cardiomyocyte cAMP microdomains in disease. *Frontiers In Pharmacology*, 6.

Förster, T.
1948. Zwischenmolekulare Energiewanderung und Fluoreszenz. *Annalen der Physik*, 437(1):55–75.

Förster, T.
1965. Transfer mechanisms of electronic excitation energy. *Modern Quantum Chemistry*, 3:93–137.

Galiègue, S., S. Mary, J. Marchand, D. Dussossoy, D. Carrière, P. Carayon, M. Bouaboula, D. Shire, G. Le Fur, and P. Casellas
1995. Expression of central and peripheral cannabinoid receptors in human immune tissues and leukocyte subpopulations. *European Journal of Biochemistry*, 232:54–61.

Garcia, A. D. R., N. B. Doan, T. Imura, T. G. Bush, and M. V. Sofroniew
2004. GFAP-expressing progenitors are the principal source of constitutive neurogenesis in adult mouse forebrain. *Nature Neuroscience*, 7(11):1233–1241.

Garcia, J. A., S. M. Cardona, and A. E. Cardona
2014. Isolation and analysis of mouse microglial cells. *Current Protocols in Immunology*, 104:Unit 14.35.

García-Arencibia, M., S. González, E. de Lago, J. A. Ramos, R. Mechoulam, and J. Fernández-Ruiz
2007. Evaluation of the neuroprotective effect of cannabinoids in a rat model of Parkinson's disease: Importance of antioxidant and cannabinoid receptor-independent properties. *Brain Research*, 1134:162–170.

Gertsch, J., M. Leonti, S. Raduner, I. Racz, J.-Z. Chen, X.-Q. Xie, K.-H. Altmann, M. Karsak, and A. Zimmer
2008. β-caryophyllene is a dietary cannabinoid. *Proceedings of the National Academy of Sciences*, 105(26):9099–9104.

Ghosh, M., V. Aguirre, K. Wai, H. Felfly, W. D. Dietrich, and D. D. Pearse
2015. The interplay between cyclic AMP, MAPK, and NF-κB pathways in response to proinflammatory signals in microglia. *BioMed Research International*, 2015.

Ghosh, M., D. Garcia-Castillo, V. Aguirre, R. Golshani, C. M. Atkins, H. M. Bramlett, W. D. Dietrich, and D. D. Pearse
2012. Proinflammatory cytokine regulation of cyclic AMP-phosphodiesterase 4 signaling in microglia in vitro and following CNS injury. *Glia*, 60(12):1839–1859.

Glass, M. and C. C. Felder
1997. Concurrent stimulation of cannabinoid CB1 and dopamine D2 receptors augments cAMP accumulation in striatal neurons: evidence for a Gs linkage to the CB1 receptor. *The Journal of Neuroscience*, 17:5327–5333.

Goddard, A. D. and A. Watts
2012. Contributions of fluorescence techniques to understanding G-protein-coupled receptor dimerisation. *Biophysical Reviews*, 4(4):291–298.

Gomes, I., M. A. Ayoub, W. Fujita, W. C. Jaeger, K. D. G. Pfleger, and L. A. Devi
2016. G protein-coupled receptor heteromers. *Annual Review of Pharmacology and Toxicology*, 56:403–425.

Gomes, I., B. A. Jordan, A. Gupta, N. Trapaidze, V. Nagy, and L. A. Devi
2000. Heterodimerization of μ and δ opioid receptors: A role in opiate synergy. *The Journal of Neuroscience*, 20:RC110.

Gonçalves, J. T., S. T. Schafer, and F. H. Gage
2016. Adult neurogenesis in the hippocampus: From stem cells to behavior. *Cell*, 167(4):897–914.

Gosselin, D., V. M. Link, C. E. Romanoski, G. J. Fonseca, D. Z. Eichenfield, N. J. Spann, J. D. Stender, H. B. Chun, H. Garner, F. Geissmann, and C. K. Glass
2014. Environment drives selection and function of enhancers controlling tissue-specific macrophage identities. *Cell*, 159(6):1327–1340.

Gosselin, D., D. Skola, N. G. Coufal, I. R. Holtman, J. C. M. Schlachetzki, E. Sajti, B. N. Jaeger, C. O'Connor, C. Fitzpatrick, M. P. Pasillas, M. Pena, A. Adair, D. D. Gonda, M. L. Levy, R. M. Ransohoff, F. H. Gage, and C. K. Glass
2017. An environment-dependent transcriptional network specifies human microglia identity. *Science*, 356(6344):eaal3222.

Grundmann, M., N. Merten, D. Malfacini, A. Inoue, P. Preis, K. Simon, N. Rüttiger, N. Ziegler, T. Benkel, N. K. Schmitt, S. Ishida, I. Müller, R. Reher, K. Kawakami, A. Inoue, U. Rick, T. Kühl, D. Imhof, J. Aoki, G. M. König, C. Hoffmann, J. Gomeza, J. Wess, and E. Kostenis
2018. Lack of β-arrestin signaling in the absence of active G-proteins. *Nature Communications*, 9(1):341.

Gurevich, V. V. and E. V. Gurevich
2018. GPCRs and signal transducers: Interaction stoichiometry. *Trends in Pharmacological Sciences*.

Gyoneva, S. and S. F. Traynelis
2013. Norepinephrine modulates the motility of resting and activated microglia via different adrenergic receptors. *Journal of Biological Chemistry*, 288(21):15291–15302.

Gómez-Gálvez, Y., C. Palomo-Garo, J. Fernández-Ruiz, and C. García
2016. Potential of the cannabinoid CB2 receptor as a pharmacological target against inflammation in Parkinson's disease. *Progress in Neuro-Psychopharmacology and Biological Psychiatry*, 64:200–208.

Han, S. J., S. Vaccari, T. Nedachi, C. B. Andersen, K. S. Kovacina, R. A. Roth, and M. Conti
2006. Protein kinase B/Akt phosphorylation of PDE3A and its role in mammalian oocyte maturation. *The EMBO Journal*, 25:5716–5725.

Hanamsagar, R., M. D. Alter, C. S. Block, H. Sullivan, J. L. Bolton, and S. D. Bilbo
2017. Generation of a microglial developmental index in mice and in humans reveals a sex difference in maturation and immune reactivity. *Glia*, 65(9):1504–1520.

Harding, S. D., J. L. Sharman, E. Faccenda, C. Southan, A. J. Pawson, S. Ireland, A. J. G. Gray, L. Bruce, S. P. H. Alexander, S. Anderton, C. Bryant, A. P. Davenport, C. Doerig, D. Fabbro, F. Levi-Schaffer, M. Spedding, J. A. Davies, and NC-IUPHAR
2017. The IUPHAR/BPS guide to PHARMACOLOGY in 2018: updates and expansion to encompass the new guide to IMMUNOPHARMACOLOGY. *Nucleic Acids Research*, 46(D1):D1091–D1106.

Harrison, J. K., Y. Jiang, S. Chen, Y. Xia, D. Maciejewski, R. K. McNamara, W. J. Streit, M. N. Salafranca, S. Adhikari, D. A. Thompson, P. Botti, K. B. Bacon, and L. Feng
1998. Role for neuronally derived fractalkine in mediating interactions between neurons and CX3CR1-expressing microglia. *Proceedings of the National Academy of Sciences of the United States of America*, 95:10896–10901.

Haynes, S. E., G. Hollopeter, G. Yang, D. Kurpius, M. E. Dailey, W.-B. Gan, and D. Julius
2006. The P2Y12 receptor regulates microglial activation by extracellular nucleotides. *Nature Neuroscience*, 9(12):1512–1519.

Hernandez, M. X., S. Jiang, T. A. Cole, S.-H. Chu, M. I. Fonseca, M. J. Fang, L. A. Hohs-

field, M. D. Torres, K. N. Green, R. A. Wetsel, A. Mortazavi, and A. J. Tenner
2017. Prevention of C5aR1 signaling delays microglial inflammatory polarization, favors clearance pathways and suppresses cognitive loss. *Molecular Neurodegeneration*, 12(1):66.

Hickman, S., S. Izzy, P. Sen, L. Morsett, and J. El Khoury
2018. Microglia in neurodegeneration. *Nature Neuroscience*, 21:1359–1369.

Hill, S. J.
2006. G-protein-coupled receptors: past, present and future. *British Journal of Pharmacology*, 147 Suppl 1:S27–S37.

Ho, W. S. V. and M. E. M. Kelly
2017. Cannabinoids in the cardiovascular system. *Advances in Pharmacology*, 80:329–366.

Horgusluoglu, E., K. Nudelman, K. Nho, and A. J. Saykin
2016. Adult neurogenesis and neurodegenerative diseases: A systems biology perspective. *American Journal of Medical Genetics Part B: Neuropsychiatric Genetics*, 174(1):93–112.

Hudson, B. D., T. E. Hébert, and M. E. M. Kelly
2010. Physical and functional interaction between CB1 cannabinoid receptors and β_2-adrenoceptors. *British Journal of Pharmacology*, 160(3):627–642.

Hwang, H.-W., Y. Saito, C. Y. Park, N. E. Blachère, Y. Tajima, J. J. Fak, I. Zucker-Scharff, and R. B. Darnell
2017. cTag-PAPERCLIP reveals alternative polyadenylation promotes cell-type specific protein diversity and shifts araf isoforms with microglia activation. *Neuron*, 95:1334–1349.e5.

Ibsen, M. S., M. Connor, and M. Glass
2017. Cannabinoid CB1 and CB2 receptor signaling and bias. *Cannabis and Cannabinoid Research*, 2(1):48–60.

Imai, Y. and S. Kohsaka
2002. Intracellular signaling in M-CSF-induced microglia activation: Role of Iba-1. *Glia*, 40(2):164–174.

Insel, P. A. and R. S. Ostrom
2003. Forskolin as a tool for examining adenylyl cyclase expression, regulation, and G protein signaling. *Cellular and Molecular Neurobiology*, 23:305–314.

Ito, D., K. Tanaka, S. Suzuki, T. Dembo, and Y. Fukuuchi
2001. Enhanced expression of Iba-1, ionized calcium-binding adapter molecule 1, after transient focal cerebral ischemia in rat brain. *Stroke*, 32:1208–1215.

Izquierdo, P., D. Attwell, and C. Madry
2019. Ion channels and receptors as determinants of microglial function. *Trends in Neurosciences*, 42:278–292.

Jiang, L. I., J. Collins, R. Davis, I. D. Fraser, and P. C. Sternweis
2008. Regulation of camp responses by the g12/13 pathway converges on adenylyl cyclase vii. *The Journal of biological chemistry*, 283:23429–23439.

Jiang, L. I., J. E. Wang, and P. C. Sternweis
2012. Regions on adenylyl cyclase VII required for selective regulation by the G13 pathway. In Duan et al. (2010), Pp. 587–593.

Jinno, S.
2011. Decline in adult neurogenesis during aging follows a topographic pattern in the mouse hippocampus. *The Journal of Comparative Neurology*, 519:451–466.

Joseph, B. and J. L. Venero
2013. A brief overview of multitalented microglia. *Methods iIn Molecular Biology*, 1041:3–8.

Kalla, R., M. Bohatschek, C. U. A. Kloss, J. Krol, X. Von Maltzan, and G. Raivich
2003. Loss of microglial ramification in microglia-astrocyte cocultures: involvement of adenylate cyclase, calcium, phosphatase, and G_i-protein systems. *Glia*, 41:50–63.

Karsak, M., M. Cohen-Solal, J. Freudenberg, A. Ostertag, C. Morieux, U. Kornak, J. Essig, E. Erxlebe, I. Bab, C. Kubisch, et al.
2005. Cannabinoid receptor type 2 gene is associated with human osteoporosis. *Human Molecular Genetics*, 14(22):3389–3396.

Karsak, M., E. Gaffal, R. Date, L. Wang-Eckhardt, J. Rehnelt, S. Petrosino, K. Starowicz, R. Steuder, E. Schlicker, B. Cravatt, et al.
2007. Attenuation of allergic contact dermatitis through the endocannabinoid system. *Science*, 316(5830):1494–1497.

Katsnelson, M. A., L. G. Rucker, H. M. Russo, and G. R. Dubyak
2015. K+ efflux agonists induce NLRP3 inflammasome activation independently of Ca2+ signaling. *The Journal of Immunology*, 194(8):3937–3952.

Kempermann, G.
2011. Seven principles in the regulation of adult neurogenesis. *European Journal of Neuroscience*, 33(6):1018–1024.

Kempermann, G., S. Jessberger, B. Steiner, and G. Kronenberg
2004. Milestones of neuronal development in the adult hippocampus. *Trends in Neurosciences*, 27(8):447–452.

Kenakin, T.
2001. Inverse, protean, and ligand-selective agonism: matters of receptor conformation. *FASEB Journal*, 15:598–611.

Keravis, T. and C. Lugnier
2012. Cyclic nucleotide phosphodiesterase (PDE) isozymes as targets of the intracellular signalling network: benefits of PDE inhibitors in various diseases and perspectives for future therapeutic developments. *British Journal of Pharmacology*, 165(5):1288–1305.

Khushi, M., C. E. Napier, C. M. Smyth, R. R. Reddel, and J. W. Arthur
2017. MatCol: a tool to measure fluorescence signal colocalisation in biological systems. *Scientific Reports*, 7(1):8879.

Klarenbeek, J., J. Goedhart, A. van Batenburg, D. Groenewald, and K. Jalink
2015. Fourth-generation Epac-based FRET sensors for cAMP feature exceptional brightness, photostability and dynamic range: Characterization of dedicated sensors for FLIM, for ratiometry and with high affinity. *PLoS ONE*, 10(4):e0122513.

Klarenbeek, J. B., J. Goedhart, M. A. Hink, T. W. J. Gadella, and K. Jalink
2011. A mTurquoise-based cAMP sensor for both FLIM and ratiometric read-out has improved dynamic range. *PLoS ONE*, 6(4):e19170.

Klegeris, A., C. J. Bissonnette, and P. L. McGeer
2003. Reduction of human monocytic cell neurotoxicity and cytokine secretion by ligands of the cannabinoid-type CB2 receptor. *British Journal of Pharmacology*, 139:775–786.

Knoth, R., I. Singec, M. Ditter, G. Pantazis, P. Capetian, R. P. Meyer, V. Horvat, B. Volk, and G. Kempermann
2010. Murine features of neurogenesis in the human hippocampus across the lifespan from 0 to 100 years. *PLoS ONE*, 5(1):e8809.

Kraft, A. E. and V. O. Nikolaev
2017. FRET microscopy for real-time visualization of second messengers in living cells. *Methods in Molecular Biology*, 1563:85–90.

Krasemann, S., C. Madore, R. Cialic, C. Baufeld, N. Calcagno, R. El Fatimy, L. Beckers, E. O'Loughlin, Y. Xu, Z. Fanek, D. J. Greco, S. T. Smith, G. Tweet, Z. Humulock, T. Zrzavy, P. Conde-Sanroman, M. Gacias, Z. Weng, H. Chen, E. Tjon, F. Mazaheri,

K. Hartmann, A. Madi, J. D. Ulrich, M. Glatzel, A. Worthmann, J. Heeren, B. Budnik, C. Lemere, T. Ikezu, F. L. Heppner, V. Litvak, D. M. Holtzman, H. Lassmann, H. L. Weiner, J. Ochando, C. Haass, and O. Butovsky
2017. The TREM2-APOE pathway drives the transcriptional phenotype of dysfunctional microglia in neurodegenerative diseases. *Immunity*, 47:566–581.e9.

Ladarre, D., A. B. Roland, S. Biedzinski, A. Ricobaraza, and Z. Lenkei
2014. Polarized cellular patterns of endocannabinoid production and detection shape cannabinoid signaling in neurons. *Frontiers in cellular neuroscience*, 8:426.

Laemmli, U. K.
1970. Cleavage of structural proteins during the assembly of the head of bacteriophage T4. *Nature*, 227:680–685.

Lauckner, J. E., B. Hille, and K. Mackie
2005. The cannabinoid agonist WIN55,212-2 increases intracellular calcium via CB1 receptor coupling to Gq/11 G proteins. *Proceedings of the National Academy of Sciences of the United States of America*, 102:19144–19149.

Lawson, L. J., V. H. Perry, P. Dri, and S. Gordon
1990. Heterogeneity in the distribution and morphology of microglia in the normal adult mouse brain. *Neuroscience*, 39(1):151–170.

Lee, H. and S. Thuret
2018. Adult human hippocampal neurogenesis: Controversy and evidence. *Trends in Molecular Medicine*.

Lee, S.-H., R. Hollingsworth, H.-Y. Kwon, N. Lee, and C. Y. Chung
2012. β-arrestin 2-dependent activation of ERK1/2 is required for ADP-induced paxillin phosphorylation at Ser(83) and microglia chemotaxis. *Glia*, 60:1366–1377.

Li, Q., Z. Cheng, L. Zhou, S. Darmanis, N. Neff, J. Okamoto, G. Gulati, M. L. Bennett, L. O. Sun, L. E. Clarke, et al.
2019a. Developmental heterogeneity of microglia and brain myeloid cells revealed by deep single-cell RNA sequencing. *Neuron*, 101(2):207–223.e10.

Li, Q., Z. Cheng, L. Zhou, S. Darmanis, N. F. Neff, J. Okamoto, G. Gulati, M. L. Bennett, L. O. Sun, L. E. Clarke, J. Marschallinger, G. Yu, S. R. Quake, T. Wyss-Coray, and B. A. Barres
2019b. Developmental heterogeneity of microglia and brain myeloid cells revealed by deep single-cell RNA sequencing. *Neuron*, 101(2):207–223.e10.

Lim, Y. H., A. Bacchiocchi, J. Qiu, R. Straub, A. Bruckner, L. Bercovitch, D. Narayan, Y. C. for Mendelian Genomics, J. McNiff, C. Ko, L. Robinson-Bostom, R. Antaya, R. Halaban, and K. A. Choate
2016. GNA14 somatic mutation causes congenital and sporadic vascular tumors by MAPK activation. *The American Journal of Human Genetics*, 99(2):443–450.

Lin, L., T. Yihao, F. Zhou, N. Yin, T. Qiang, Z. Haowen, C. Qianwei, T. Jun, Z. Yuan, Z. Gang, F. Hua, Y. Yunfeng, and C. Zhi
2017. Inflammatory regulation by driving microglial M2 polarization: Neuroprotective effects of cannabinoid receptor-2 activation in intracerebral hemorrhage. *Frontiers in Immunology*, 8:112.

Lipp, H.-P. and L. Bonfanti
2016. Adult neurogenesis in mammals: variations and confusions. *Brain, Behavior and Evolution*, 87(3):205–221.

Liu, Q.-R., C.-H. Pan, A. Hishimoto, C.-Y. Li, Z.-X. Xi, A. Llorente-Berzal, M.-P. Viveros, H. Ishiguro, T. Arinami, E. S. Onaivi, et al.
2009. Species differences in cannabinoid receptor 2 (cnr2 gene): identification of novel human and rodent cb2 isoforms, differential tissue expression and regulation

by cannabinoid receptor ligands. *Genes, Brain and Behavior*, 8(5):519–530.

Luttrell, L. M., J. Wang, B. Plouffe, J. S. Smith, L. Yamani, S. Kaur, P.-Y. Jean-Charles, C. Gauthier, M.-H. Lee, B. Pani, J. Kim, S. Ahn, S. Rajagopal, E. Reiter, M. Bouvier, S. K. Shenoy, S. A. Laporte, H. A. Rockman, and R. J. Lefkowitz
2018. Manifold roles of β-arrestins in GPCR signaling elucidated with siRNA and CRISPR/Cas9. *Science Signaling*, 11(549):eaat7650.

López, A., N. Aparicio, M. R. Pazos, M. T. Grande, M. A. Barreda-Manso, I. Benito-Cuesta, C. Vázquez, M. Amores, G. Ruiz-Pérez, E. García-García, M. Beatka, R. M. Tolón, B. N. Dittel, C. J. Hillard, and J. Romero
2018. Cannabinoid CB2 receptors in the mouse brain: relevance for Alzheimer's disease. *Journal of Neuroinflammation*, 15:158.

Mahi, N. A., M. F. Najafabadi, M. Pilarczyk, M. Kouril, and M. Medvedovic
2019. GREIN: An interactive web platform for re-analyzing GEO RNA-seq data. *Scientific Reports*, 9(1):7580.

Malfitano, A. M., S. Basu, K. Maresz, M. Bifulco, and B. N. Dittel
2014. What we know and do not know about the cannabinoid receptor 2 (CB2). *Seminars in Immunology*, 26(5):369–379.

Mancini, I., R. Brusa, G. Quadrato, C. Foglia, P. Scandroglio, L. S. Silverman, D. Tulshian, A. Reggiani, and M. Beltramo
2009. Constitutive activity of cannabinoid-2 (CB2) receptors plays an essential role in the protean agonism of (+)AM1241 and L768242. *British Journal of Pharmacology*, 158:382–391.

Marchalant, Y., P. W. Brownjohn, A. Bonnet, T. Kleffmann, and J. C. Ashton
2014. Validating antibodies to the cannabinoid CB2 receptor antibody sensitivity is not evidence of antibody specificity. *Journal of Histochemistry & Cytochemistry*, 62(6):395–404.

Maresz, K., E. J. Carrier, E. D. Ponomarev, C. J. Hillard, and B. N. Dittel
2005. Modulation of the cannabinoid CB2 receptor in microglial cells in response to inflammatory stimuli. *Journal of Neurochemistry*, 95(2):437–445.

Martín-Moreno, A. M., B. Brera, C. Spuch, E. Carro, L. García-García, M. Delgado, M. A. Pozo, N. G. Innamorato, A. Cuadrado, and M. L. de Ceballos
2012. Prolonged oral cannabinoid administration prevents neuroinflammation, lowers β-amyloid levels and improves cognitive performance in Tg APP 2576 mice. *Journal of Neuroinflammation*, 9:8.

Matcovitch-Natan, O., D. R. Winter, A. Giladi, S. Vargas Aguilar, A. Spinrad, S. Sarrazin, H. Ben-Yehuda, E. David, F. Zelada González, P. Perrin, H. Keren-Shaul, M. Gury, D. Lara-Astaiso, C. A. Thaiss, M. Cohen, K. Bahar Halpern, K. Baruch, A. Deczkowska, E. Lorenzo-Vivas, S. Itzkovitz, E. Elinav, M. H. Sieweke, M. Schwartz, and I. Amit
2016. Microglia development follows a stepwise program to regulate brain homeostasis. *Science*, 353(6301):aad8670.

Matsuda, L. A., S. J. Lolait, M. J. Brownstein, A. C. Young, and T. I. Bonner
1990. Structure of a cannabinoid receptor and functional expression of the cloned cDNA. *Nature*, 346:561–564.

McCarthy, G. M., S. P. Farris, Y. A. Blednov, R. A. Harris, and R. D. Mayfield
2018. Microglial-specific transcriptome changes following chronic alcohol consumption. *Neuropharmacology*, 128:416–424.

McCloy, R. A., S. Rogers, C. E. Caldon, T. Lorca, A. Castro, and A. Burgess
2014. Partial inhibition of Cdk1 in G 2 phase overrides the SAC and decouples mitotic events. *Cell Cycle*, 13:1400–1412.

Melsom, C. B., O. Orstavik, J.-B. Osnes, T. Skomedal, F. O. Levy, and K. A. Krobert

2014. Gα$_i$-proteins regulate adenylyl cyclase activity independent of receptor activation. *PLoS ONE*, 9(9):e106608.

Meng, J., J. L. Glick, P. Polakis, and P. J. Casey
1999. Functional interaction between Gα$_z$ and Rap1GAP suggests a novel form of cellular cross-talk. *The Journal of Biological Chemistry*, 274:36663–36669.

Mika, D., W. Richter, and M. Conti
2015. A CaMKII/PDE4D negative feedback regulates cAMP signaling. *Proceedings of the National Academy of Sciences of the United States of America*, 112:2023–2028.

Milligan, G.
2003. Constitutive activity and inverse agonists of G protein-coupled receptors: a current perspective. *Molecular Pharmacology*, 64:1271–1276.

Milligan, G., R. A. Bond, and M. Lee
1995. Inverse agonism: pharmacological curiosity or potential therapeutic strategy? *Trends in Pharmacological Sciences*, 16:10–13.

Minami, S. S., S.-W. Min, G. Krabbe, C. Wang, Y. Zhou, R. Asgarov, Y. Li, L. H. Martens, L. P. Elia, M. E. Ward, L. Mucke, R. V. Farese, and L. Gan
2014. Progranulin protects against amyloid β deposition and toxicity in Alzheimer's disease mouse models. *Nature Medicine*, 20:1157–1164.

Molina-Holgado, F., A. Rubio-Araiz, D. García-Ovejero, R. J. Williams, J. D. Moore, A. Arévalo-Martín, O. Gómez-Torres, and E. Molina-Holgado
2007a. CB2 cannabinoid receptors promote mouse neural stem cell proliferation. *The European Journal of Neuroscience*, 25:629–634.

Molina-Holgado, F., A. Rubio-Araiz, D. García-Ovejero, R. J. Williams, J. D. Moore, Arévalo-Martín, O. Gómez-Torres, and E. Molina-Holgado
2007b. Cb2 cannabinoid receptors promote mouse neural stem cell proliferation. *European Journal of Neuroscience*, 25(3):629–634.

Moreno-Jiménez, E. P., M. Flor-García, J. Terreros-Roncal, A. Rábano, F. Cafini, N. Pallas-Bazarra, J. Ávila, and M. Llorens-Martín
2019. Adult hippocampal neurogenesis is abundant in neurologically healthy subjects and drops sharply in patients with Alzheimer's disease. *Nature Medicine*, 25:554–560.

Mori, I., Y. Imai, S. Kohsaka, and Y. Kimura
2000. Upregulated expression of Iba1 molecules in the central nervous system of mice in response to neurovirulent influenza A virus infection. *Microbiology and Immunology*, 44:729–735.

Morrens, J., W. Van Den Broeck, and G. Kempermann
2012. Glial cells in adult neurogenesis. *Glia*, 60(2):159–174.

Mukherjee, S., V. Jansen, J. F. Jikeli, H. Hamzeh, L. Alvarez, M. Dombrowski, M. Balbach, T. Strünker, R. Seifert, U. B. Kaupp, et al.
2016. A novel biosensor to study cAMP dynamics in cilia and flagella. *eLife*, 5:e14052.

Munro, S., K. L. Thomas, and M. Abu-Shaar
1993. Molecular characterization of a peripheral receptor for cannabinoids. *Nature*, 365:61–65.

Nada, M.-B., L. Slomianka, A. L. Vyssotski, and H.-P. Lipp
2010. Early age-related changes in adult hippocampal neurogenesis in C57 mice. *Neurobiology of Aging*, 31(1):151–161.

Navarro, G., D. Borroto-Escuela, E. Angelats, I. Etayo, I. Reyes-Resina, M. Pulido-Salgado, A. I. Rodríguez-Pérez, E. I. Canela, J. Saura, J. L. Lanciego, J. L. Labandeira-García, C. A. Saura, K. Fuxe, and R. Franco
2018a. Receptor-heteromer mediated regulation of endocannabinoid signaling in activated microglia. role of CB1 and CB2 receptors and relevance for Alzheimer's disease

and levodopa-induced dyskinesia. *Brain, Behavior, and Immunity*, 67:139–151.

Navarro, G., K. Varani, I. Reyes-Resina, V. Sánchez de Medina, R. Rivas-Santisteban, C. Sánchez-Carnerero Callado, F. Vincenzi, S. Casano, C. Ferreiro-Vera, E. I. Canela, P. A. Borea, X. Nadal, and R. Franco
2018b. Cannabigerol action at cannabinoid CB1 and CB2 receptors and at CB1-CB2 heteroreceptor complexes. *Frontiers in Pharmacology*, 9:632.

Neher, J. J. and C. Cunningham
2019. Priming microglia for innate immune memory in the brain. *Trends in Immunology*, 40:358–374.

Nicola, Z., K. Fabel, and G. Kempermann
2015. Development of the adult neurogenic niche in the hippocampus of mice. *Frontiers in Neuroanatomy*, 9:53.

Nikolaev, V. O., M. Bünemann, L. Hein, A. Hannawacker, and M. J. Lohse
2004a. Novel single chain cAMP sensors for receptor-induced signal propagation. *Journal of Biological Chemistry*, 279(36):37215–37218.

Nikolaev, V. O., M. Bünemann, E. Schmitteckert, M. J. Lohse, and S. Engelhardt
2006. Cyclic AMP imaging in adult cardiac myocytes reveals far-reaching beta1-adrenergic but locally confined β_2-adrenergic receptor-mediated signaling. *Circulation Research*, 99:1084–1091.

Nikolaev, V. O., S. Gambaryan, S. Engelhardt, U. Walter, and M. J. Lohse
2004b. Real-time monitoring of the PDE2 activity of live cells. *Journal of Biological Chemistry*, 280(3):1716–1719.

Nikolaev, V. O. and M. J. Lohse
2006. Monitoring of cAMP synthesis and degradation in living cells. *Physiology*, 21(2):86–92.

Nimmerjahn, A., F. Kirchhoff, and F. Helmchen
2005. Resting microglial cells are highly dynamic surveillants of brain parenchyma in vivo. *Science*, 308:1314–1318.

Noctor, S. C., A. C. Flint, T. A. Weissman, R. S. Dammerman, and A. R. Kriegstein
2001. Neurons derived from radial glial cells establish radial units in neocortex. *Nature*, 409(6821):714–720.

Noristani, H. N., Y. N. Gerber, J.-C. Sabourin, M. Le Corre, N. Lonjon, N. Mestre-Frances, H. E. Hirbec, and F. E. Perrin
2017. RNA-Seq analysis of microglia reveals time-dependent activation of specific genetic programs following spinal cord injury. *Frontiers in Molecular Neuroscience*, 10:90.

Northup, J. K., P. C. Sternweis, M. D. Smigel, L. S. Schleifer, E. M. Ross, and A. G. Gilman
1980. Purification of the regulatory component of adenylate cyclase. *Proceedings of the National Academy of Sciences of the United States of America*, 77:6516–6520.

Ofek, O., M. Attar-Namdar, V. Kram, M. Dvir-Ginzberg, R. Mechoulam, A. Zimmer, B. Frenkel, E. Shohami, and I. Bab
2011. CB2 cannabinoid receptor targets mitogenic Gi protein-cyclin D1 axis in osteoblasts. *Journal of Bone and Mineral Research*, 26(2):308–316.

Ofek, O., M. Karsak, N. Leclerc, M. Fogel, B. Frenkel, K. Wright, J. Tam, M. Attar-Namdar, V. Kram, E. Shohami, et al.
2006. Peripheral cannabinoid receptor, CB2, regulates bone mass. *Proceedings of the National Academy of Sciences of the United States of America*, 103(3):696–701.

Offermanns, S., E. Heiler, K. Spicher, and G. Schultz
1994. G_q and G_{11} are concurrently activated by bombesin and vasopressin in Swiss 3T3 cells. *FEBS Letters*, 349:201–204.

Oldham, W. M. and H. E. Hamm

2008. Heterotrimeric G-protein activation by G-protein-coupled receptors. *Nature Reviews Molecular Cell Biology*, 9(1):60–71.

O'Rourke, J. G., L. Bogdanik, A. Yáñez, D. Lall, A. J. Wolf, A. K. M. G. Muhammad, R. Ho, S. Carmona, J. P. Vit, J. Zarrow, K. J. Kim, S. Bell, M. B. Harms, T. M. Miller, C. A. Dangler, D. M. Underhill, H. S. Goodridge, C. M. Lutz, and R. H. Baloh
2016. C9orf72 is required for proper macrophage and microglial function in mice. *Science*, 351(6279):1324–1329.

Orr, A. G., A. L. Orr, X.-J. Li, R. E. Gross, and S. F. Traynelis
2009. Adenosine A_{2A} receptor mediates microglial process retraction. *Nature Neuroscience*, 12(7):872–878.

Pacher, P. and R. Mechoulam
2011. Is lipid signaling through cannabinoid 2 receptors part of a protective system? *Progress in Lipid Research*, 50(2):193–211.

Pakdeechote, P., W. R. Dunn, and V. Ralevic
2007. Cannabinoids inhibit noradrenergic and purinergic sympathetic cotransmission in the rat isolated mesenteric arterial bed. *British journal of pharmacology*, 152:725–733.

Palazuelos, J., T. Aguado, A. Egia, R. Mechoulam, M. Guzmán, and I. Galve-Roperh
2006. Non-psychoactive CB2 cannabinoid agonists stimulate neural progenitor proliferation. *The FASEB Journal*, 20(13):2405–2407.

Palazuelos, J., Z. Ortega, J. Díaz-Alonso, M. Guzmán, and I. Galve-Roperh
2012. CB2 cannabinoid receptors promote neural progenitor cell proliferation via mTORC1 signaling. *Journal of Biological Chemistry*, 287(2):1198–1209.

Pearse, D. D. and Z. A. Hughes
2016. Pde4b as a microglia target to reduce neuroinflammation. *Glia*, 64:1698–1709.

Pereira, J. P., J. An, Y. Xu, Y. Huang, and J. G. Cyster
2009. Cannabinoid receptor 2 mediates the retention of immature B cells in bone marrow sinusoids. *Nature Immunology*, 10(4):403–411.

Pertwee, R. G.
2015. Endocannabinoids and their pharmacological actions. In *Endocannabinoids*, Pp. 1–37. Springer.

Pertwee, R. G., A. C. Howlett, M. E. Abood, S. P. H. Alexander, V. Di Marzo, M. R. Elphick, P. J. Greasley, H. S. Hansen, G. Kunos, K. Mackie, et al.
2010. International Union of Basic and Clinical Pharmacology. LXXIX. Cannabinoid receptors and their ligands: beyond CB1 and CB2. *Pharmacological Reviews*, 62(4):588–631.

Petrucci, V., A. Chicca, S. Glasmacher, J. Paloczi, Z. Cao, P. Pacher, and J. Gertsch
2017. Pepcan-12 (RVD-hemopressin) is a CB2 receptor positive allosteric modulator constitutively secreted by adrenals and in liver upon tissue damage. *Scientific Reports*, 7(1).

Plümpe, T., D. Ehninger, B. Steiner, F. Klempin, S. Jessberger, M. Brandt, B. Römer, G. R. Rodriguez, G. Kronenberg, and G. Kempermann
2006. Variability of doublecortin-associated dendrite maturation in adult hippocampal neurogenesis is independent of the regulation of precursor cell proliferation. *BMC Neuroscience*, 7(1):77.

Prather, P. L., N. A. Martin, C. S. Breivogel, and S. R. Childers
2000. Activation of cannabinoid receptors in rat brain by WIN 55212-2 produces coupling to multiple G protein alpha-subunits with different potencies. *Molecular Pharmacology*, 57:1000–1010.

Prenderville, J. A., M. Kelly, and E. J. Downer
2015. The role of cannabinoids in adult neurogenesis. *British Journal of Pharmacology*,

172(16):3950–3963.

Quraishi, S. A. and C. A. Paladini
  2016. A central move for CB2 receptors. *Neuron*, 90(4):670–671.

Ramírez, B. G., C. Blázquez, T. Gómez del Pulgar, M. Guzmán, and M. L. de Ceballos
  2005. Prevention of Alzheimer's disease pathology by cannabinoids: neuroprotection mediated by blockade of microglial activation. *The Journal of Neuroscience*, 25:1904–1913.

Rhee, M.-H., I. Nevo, T. Avidor-Reiss, R. Levy, and Z. Vogel
  2000. Differential superactivation of adenylyl cyclase isozymes after chronic activation of the CB1 cannabinoid receptor. *Molecular Pharmacology*, 57(4):746–752.

Ridley, A. J.
  2015. Rho GTPase signalling in cell migration. *Current Opinion in Cell Biology*, 36:103–112.

Robichaux, W. G. and X. Cheng
  2018. Intracellular cAMP sensor EPAC: Physiology, pathophysiology, and therapeutics development. *Physiological Reviews*, 98:919–1053.

Robinson, M. D., D. J. McCarthy, and G. K. Smyth
  2009. edgeR: a bioconductor package for differential expression analysis of digital gene expression data. *Bioinformatics*, 26(1):139–140.

Rodrigues, R. S., F. F. Ribeiro, F. Ferreira, S. H. Vaz, A. M. Sebastião, and S. Xapelli
  2017. Interaction between cannabinoid type 1 and type 2 receptors in the modulation of subventricular zone and dentate gyrus neurogenesis. *Frontiers in Pharmacology*, 8:516.

Rogers, N.
  2015. Cannabinoid receptor with an'identity crisis' gets a second look. *Nature Medicine*, 21(9):966–967.

Rom, S. and Y. Persidsky
  2013. Cannabinoid receptor 2: potential role in immunomodulation and neuroinflammation. *Journal of Neuroimmune Pharmacology*, 8(3):608–620.

Ryan, K. J., C. C. White, K. Patel, J. Xu, M. Olah, J. M. Replogle, M. Frangieh, M. Cimpean, P. Winn, A. McHenry, B. J. Kaskow, G. Chan, N. Cuerdon, D. A. Bennett, J. D. Boyd, J. Imitola, W. Elyaman, P. L. De Jager, and E. M. Bradshaw
  2017. A human microglia-like cellular model for assessing the effects of neurodegenerative disease gene variants. *Science Translational Medicine*, 9(421):eaai7635.

Río Hortega, P.
  1918. Noticia de un nuevo y fácil método para la coloración de la neuroglia y el tejido conjuntivo. *Trab Lab Invest Biol*, 15:367–378.

Sadana, R. and C. W. Dessauer
  2009. Physiological roles for G protein-regulated adenylyl cyclase isoforms: Insights from knockout and overexpression studies. *Neurosignals*, 17(1):5–22.

Safaiyan, S., N. Kannaiyan, N. Snaidero, S. Brioschi, K. Biber, S. Yona, A. L. Edinger, S. Jung, M. J. Rossner, and M. Simons
  2016. Age-related myelin degradation burdens the clearance function of microglia during aging. *Nature Neuroscience*, 19(8):995–998.

Sarfaraz, S., V. M. Adhami, D. N. Syed, F. Afaq, and H. Mukhtar
  2008. Cannabinoids for cancer treatment: progress and promise. *Cancer Research*, 68:339–342.

Sassone-Corsi, P.
  2012. The cyclic AMP pathway. *Cold Spring Harbor Perspectives in Biology*, 4(12):a011148–a011148.

Sato, J., N. Makita, and T. Iiri

2016. Inverse agonism: the classic concept of GPCRs revisited. *Endocrine Journal*, 63(6):507–514.

Scarlett, K. A., E.-S. Z. White, C. J. Coke, J. R. Carter, L. K. Bryant, and C. V. Hinton
2018. Agonist-induced CXCR4 and CB2 heterodimerization inhibits gα13/RhoA-mediated migration. *Molecular Cancer Research*, 16(4):728–739.

Schindelin, J., I. Arganda-Carreras, E. Frise, V. Kaynig, M. Longair, T. Pietzsch, S. Preibisch, C. Rueden, S. Saalfeld, B. Schmid, J.-Y. Tinevez, D. J. White, V. Hartenstein, K. Eliceiri, P. Tomancak, and A. Cardona
2012. Fiji: an open-source platform for biological-image analysis. *Nature Methods*, 9(7):676–682.

Schlicker, E., J. Timm, J. Zentner, and M. Göthert
1997. Cannabinoid CB1 receptor-mediated inhibition of noradrenaline release in the human and guinea-pig hippocampus. *Naunyn-Schmiedeberg's Archives of Pharmacology*, 356:583–589.

Schmidt, C., N. Schneble, J. P. Müller, R. Bauer, A. Perino, R. Marone, S. D. Rybalkin, M. P. Wymann, E. Hirsch, and R. Wetzker
2013. Phosphoinositide 3-kinase γ mediates microglial phagocytosis via lipid kinase-independent control of cAMP. *Neuroscience*, 233:44–53.

Schmöle, A.-C., R. Lundt, B. Gennequin, H. Schrage, E. Beins, A. Krämer, T. Zimmer, A. Limmer, A. Zimmer, and D.-M. Otte
2015. Expression analysis of CB2-GFP BAC transgenic mice. *PloS ONE*, 10(9):e0138986.

Schneider, C. A., W. S. Rasband, and K. W. Eliceiri
2012. NIH image to ImageJ: 25 years of image analysis. *Nature Methods*, 9:671–675.

Sellner, S., R. Paricio-Montesinos, A. Spieß, A. Masuch, D. Erny, L. A. Harsan, D. v. Elverfeldt, M. Schwabenland, K. Biber, O. Staszewski, et al.
2016. Microglial CX3CR1 promotes adult neurogenesis by inhibiting Sirt 1/p65 signaling independent of CX3CL1. *Acta Neuropathologica Communications*, 4(1):102.

Serezani, C. H., M. N. Ballinger, D. M. Aronoff, and M. Peters-Golden
2008. Cyclic AMP: master regulator of innate immune cell function. *American Journal Of Respiratory Cell And Molecular Biology*, 39:127–132.

Shen, A., M. Nieves-Cintron, Y. Deng, Q. Shi, D. Chowdhury, J. Qi, J. W. Hell, M. F. Navedo, and Y. K. Xiang
2018. Functionally distinct and selectively phosphorylated GPCR subpopulations co-exist in a single cell. *Nature Communications*, 9:1050.

Shenoy, S. K., M. T. Drake, C. D. Nelson, D. A. Houtz, K. Xiao, S. Madabushi, E. Reiter, R. T. Premont, O. Lichtarge, and R. J. Lefkowitz
2005. β-arrestin-dependent, G protein-independent ERK1/2 activation by the β_2 adrenergic receptor. *Journal of Biological Chemistry*, 281(2):1261–1273.

Siehler, S.
2009. Regulation of RhoGEF proteins by G12/13-coupled receptors. *British Journal of Pharmacology*, 158:41–49.

Sierra, S., N. Luquin, A. J. Rico, V. Gómez-Bautista, E. Roda, I. G. Dopeso-Reyes, A. Vázquez, E. Martínez-Pinilla, J. L. Labandeira-García, R. Franco, and J. L. Lanciego
2015. Detection of cannabinoid receptors CB1 and CB2 within basal ganglia output neurons in macaques: changes following experimental parkinsonism. *Brain Structure & Function*, 220:2721–2738.

Sisay, S., G. Pryce, S. J. Jackson, C. Tanner, R. A. Ross, G. J. Michael, D. L. Selwood, G. Giovannoni, and D. Baker
2013. Genetic background can result in a marked or minimal effect of gene knockout (GPR55 and CB2 receptor) in experimental autoimmune encephalomyelitis models of

multiple sclerosis. *PloS ONE*, 8:e76907.

Sledziński, P., J. Zeyland, R. Słomski, and A. Nowak
2018. The current state and future perspectives of cannabinoids in cancer biology. *Cancer Medicine*, 7:765–775.

Snyder, J. S., S. C. Ferrante, and H. A. Cameron
2012. Late maturation of adult-born neurons in the temporal dentate gyrus. *PLoS ONE*, 7(11):e48757.

Snyder, J. S., P. Ramchand, S. Rabbett, R. Radik, J. M. Wojtowicz, and H. A. Cameron
2011. Septo-temporal gradients of neurogenesis and activity in 13-month-old rats. *Neurobiology of Aging*, 32:1149–1156.

Soethoudt, M., U. Grether, J. Fingerle, T. W. Grim, F. Fezza, L. de Petrocellis, C. Ullmer, B. Rothenhäusler, C. Perret, N. van Gils, D. Finlay, C. MacDonald, A. Chicca, M. D. Gens, J. Stuart, H. de Vries, N. Mastrangelo, L. Xia, G. Alachouzos, M. P. Baggelaar, A. Martella, E. D. Mock, H. Deng, L. H. Heitman, M. Connor, V. Di Marzo, J. Gertsch, A. H. Lichtman, M. Maccarrone, P. Pacher, M. Glass, and M. van der Stelt
2017. Cannabinoid CB2 receptor ligand profiling reveals biased signalling and off-target activity. *Nature Communications*, 8:13958.

Sophocleous, A., S. Marino, D. Kabir, S. H. Ralston, and A. I. Idris
2017. Combined deficiency of the Cnr1 and Cnr2 receptors protects against age-related bone loss by osteoclast inhibition. *Aging Cell*.

Sorrells, S. F., M. F. Paredes, A. Cebrian-Silla, K. Sandoval, D. Qi, K. W. Kelley, D. James, S. Mayer, J. Chang, K. I. Auguste, E. F. Chang, A. J. Gutierrez, A. R. Kriegstein, G. W. Mathern, M. C. Oldham, E. J. Huang, J. M. Garcia-Verdugo, Z. Yang, and A. Alvarez-Buylla
2018. Human hippocampal neurogenesis drops sharply in children to undetectable levels in adults. *Nature*, 555:377–381.

Spiering, D., J. J. Bravo-Cordero, Y. Moshfegh, V. Miskolci, and L. Hodgson
2013. Quantitative ratiometric imaging of FRET-biosensors in living cells. *Methods in Cell Biology*, 114:593–609.

Sprenger, J. U., R. K. Perera, K. R. Götz, and V. O. Nikolaev
2012. FRET microscopy for real-time monitoring of signaling events in live cells using unimolecular biosensors. *Journal of Visualized Experiments*, (66).

Srinivasan, K., B. A. Friedman, J. L. Larson, B. E. Lauffer, L. D. Goldstein, L. L. Appling, J. Borneo, C. Poon, T. Ho, F. Cai, P. Steiner, M. P. van der Brug, Z. Modrusan, J. S. Kaminker, and D. V. Hansen
2016. Untangling the brain's neuroinflammatory and neurodegenerative transcriptional responses. *Nature Communications*, 7(1):11295.

Sriram, K. and P. A. Insel
2018. G-protein-coupled receptors as targets for approved drugs: How many targets and how many drugs? *Molecular Pharmacology*, 93(4):251–258.

Stella, N., P. Schweitzer, and D. Piomelli
1997. A second endogenous cannabinoid that modulates long-term potentiation. *Nature*, 388:773–778.

Stempel, A. V., A. Stumpf, H.-Y. Zhang, T. Özdoğan, U. Pannasch, A.-K. Theis, D.-M. Otte, A. Wojtalla, I. Rácz, A. Ponomarenko, et al.
2016. Cannabinoid type 2 receptors mediate a cell type-specific plasticity in the hippocampus. *Neuron*, 90(4):795–809.

Stepanenko, A. A. and H. H. Heng
2017. Transient and stable vector transfection: Pitfalls, off-target effects, artifacts. *Mutation Research*, 773:91–103.

Stevens, R. C., V. Cherezov, V. Katritch, R. Abagyan, P. Kuhn, H. Rosen, and K. Wüthrich
2012. The GPCR network: a large-scale collaboration to determine human GPCR structure and function. *Nature Reviews Drug Discovery*, 12(1):25–34.

Storch, U., J. Straub, S. Erdogmus, T. Gudermann, and M. Mederos Y Schnitzler
2017. Dynamic monitoring of Gi/o-protein-mediated decreases of intracellular cAMP by FRET-based Epac sensors. *Pflügers Archiv - European Journal of Physiology*, 469(5-6):725–737.

Stumpf, A., D. Parthier, R. P. Sammons, A. V. Stempel, J. Breustedt, B. R. Rost, and D. Schmitz
2018. Cannabinoid type 2 receptors mediate a cell type-specific self-inhibition in cortical neurons. *Neuropharmacology*, 139:217–225.

Sunahara, R. K.
2002. Isoforms of mammalian adenylyl cyclase: Multiplicities of signaling. *Molecular Interventions*, 2(3):168–184.

Sutherland, E. W. and T. W. Rall
1958. Fractionation and characterization of a cyclic adenine ribonucleotide formed by tissue particles. *Journal of Biological Chemistry*, 232:1077–1091.

Syrovatkina, V., K. O. Alegre, R. Dey, and X.-Y. Huang
2016. Regulation, signaling, and physiological functions of G-proteins. *Journal of Molecular Biology*, 428(19):3850–3868.

Sánchez, C., M. L. de Ceballos, T. Gomez del Pulgar, D. Rueda, C. Corbacho, G. Velasco, I. Galve-Roperh, J. W. Huffman, S. Ramón y Cajal, and M. Guzmán
2001. Inhibition of glioma growth in vivo by selective activation of the CB2 cannabinoid receptor. *Cancer Research*, 61:5784–5789.

Tam, J., V. Trembovler, V. Di Marzo, S. Petrosino, G. Leo, A. Alexandrovich, E. Regev, N. Casap, A. Shteyer, C. Ledent, M. Karsak, A. Zimmer, R. Mechoulam, R. Yirmiya, E. Shohami, and I. Bab
2008. The cannabinoid CB1 receptor regulates bone formation by modulating adrenergic signaling. *FASEB Journal*, 22:285–294.

Tanaka, Y., T. Horinouchi, and K. Koike
2005. New insights into β-adrenoceptors in smooth muscle: distribution of receptor subtypes and molecular mechanisms triggering muscle relaxation. *Clinical and Experimental Pharmacology & Physiology*, 32:503–514.

Tao, Y., L. Li, B. Jiang, Z. Feng, L. Yang, J. Tang, Q. Chen, J. Zhang, Q. Tan, H. Feng, et al.
2016. Cannabinoid receptor-2 stimulation suppresses neuroinflammation by regulating microglial M1/M2 polarization through the cAMP/PKA pathway in an experimental GMH rat model. *Brain, Behavior, and Immunity*.

Taussig, R., J. A. Iniguez-Lluhi, and A. G. Gilman
1993. Inhibition of adenylyl cyclase by Gi alpha. *Science*, 261:218–221.

Taussig, R., W. J. Tang, J. R. Hepler, and A. G. Gilman
1994. Distinct patterns of bidirectional regulation of mammalian adenylyl cyclases. *Journal of Biological Chemistry*, 269:6093–6100.

Tubio, M. R., N. Fernandez, C. P. Fitzsimons, S. Copsel, S. Santiago, C. Shayo, C. Davio, and F. Monczor
2010. Expression of a G protein-coupled receptor leads to attenuation of signaling by other GPCRs: experimental evidence for a spontaneous GPCR constitutive inactive form. *Journal of Biological Chemistry*, 285:14990–14998.

Turcotte, C., M.-R. Blanchet, M. Laviolette, and N. Flamand
2016. The CB2 receptor and its role as a regulator of inflammation. *Cellular and Molecular Life Sciences*, 73:4449–4470.

Van Sickle, M. D., M. Duncan, P. J. Kingsley, A. Mouihate, P. Urbani, K. Mackie, N. Stella, A. Makriyannis, D. Piomelli, J. S. Davison, et al.
  2005. Identification and functional characterization of brainstem cannabinoid cb2 receptors. *Science*, 310(5746):329–332.

Varol, D., A. Mildner, T. Blank, A. Shemer, N. Barashi, S. Yona, E. David, S. Boura-Halfon, Y. Segal-Hayoun, L. Chappell-Maor, H. Keren-Shaul, D. Leshkowitz, E. Hornstein, M. Fuhrmann, I. Amit, N. Maggio, M. Prinz, and S. Jung
  2017. Dicer deficiency differentially impacts microglia of the developing and adult brain. *Immunity*, 46:1030–1044.e8.

Vasek, M. J., C. Garber, D. Dorsey, D. M. Durrant, B. Bollman, A. Soung, J. Yu, C. Perez-Torres, A. Frouin, D. K. Wilton, K. Funk, B. K. DeMasters, X. Jiang, J. R. Bowen, S. Mennerick, J. K. Robinson, J. R. Garbow, K. L. Tyler, M. S. Suthar, R. E. Schmidt, B. Stevens, and R. S. Klein
  2016. A complement-microglial axis drives synapse loss during virus-induced memory impairment. *Nature*, 534:538–543.

Venkatakrishnan, A. J., X. Deupi, G. Lebon, C. G. Tate, G. F. Schertler, and M. M. Babu
  2013. Molecular signatures of G-protein-coupled receptors. *Nature*, 494(7436):185–194.

Waagstein, F., A. Hjalmarson, E. Varnauskas, and I. Wallentin
  1975. Effect of chronic beta-adrenergic receptor blockade in congestive cardiomyopathy. *British Heart Journal*, 37:1022–1036.

Wachter, S. B. and E. M. Gilbert
  2012. Beta-adrenergic receptors, from their discovery and characterization through their manipulation to beneficial clinical application. *Cardiology*, 122:104–112.

Wacker, D., R. C. Stevens, and B. L. Roth
  2017. How ligands illuminate GPCR molecular pharmacology. *Cell*, 170(3):414–427.

Wang, W., Y. Qiao, and Z. Li
  2018. New insights into modes of GPCR activation. *Trends in Pharmacological Sciences*, 39:367–386.

Watts, V. J. and K. A. Neve
  2005. Sensitization of adenylate cyclase by $G\alpha_{i/o}$-coupled receptors. *Pharmacology & Therapeutics*, 106(3):405–421.

Weresa, J., A. Pędzińska-Betiuk, R. Kossakowski, and B. Malinowska
  2019. Cannabinoid CB1 and CB2 receptors antagonists AM251 and AM630 differentially modulate the chronotropic and inotropic effects of isoprenaline in isolated rat atria. *Pharmacological Reports*, 71(1):82–89.

Wettschureck, N. and S. Offermanns
  2005. Mammalian G proteins and their cell type specific functions. *Physiological Reviews*, 85(4):1159–1204.

Wickham, H.
  2011. The split-apply-combine strategy for data analysis. *Journal of Statistical Software*, 40(1):1–29.

Willoughby, D. and D. M. Cooper
  2008. Live-cell imaging of cAMP dynamics. *Nature Methods*, 5(1):29–36.

Witherow, D. S., Q. Wang, K. Levay, J. L. Cabrera, J. Chen, G. B. Willars, and V. Z. Slepak
  2000. Complexes of the G protein subunit $G\beta 5$ with the regulators of G protein signaling RGS7 and RGS9. *Journal of Biological Chemistry*, 275(32):24872–24880.

Witting, A. and T. Möller
  2011. Microglia cell culture: A primer for the novice. *Methods in Molecular Biology (Clifton, N.J.)*, 758:49–66.

Woehler, A., J. Wlodarczyk, and E. Neher

2010. Signal/noise analysis of FRET-based sensors. *Biophysical Journal*, 99:2344–2354.

Wolf, S. A., A. Bick-Sander, K. Fabel, P. Leal-Galicia, S. Tauber, G. Ramirez-Rodriguez, A. Müller, A. Melnik, T. P. Waltinger, O. Ullrich, et al.
2010. Cannabinoid receptor CB1 mediates baseline and activity-induced survival of new neurons in adult hippocampal neurogenesis. *Cell Communication and Signaling*, 8(1):1.

Wootten, D., A. Christopoulos, M. Marti-Solano, M. M. Babu, and P. M. Sexton
2018. Mechanisms of signalling and biased agonism in G-protein-coupled receptors. *Nature Reviews Molecular Cell Biology*, 19(10):638–653.

Xin, W., W. P. Feinstein, A. L. Britain, C. D. Ochoa, B. Zhu, W. Richter, S. J. Leavesley, and T. C. Rich
2015. Estimating the magnitude of near-membrane PDE4 activity in living cells. *American Journal of Physiology. Cell Physiology*, 309:C415–C424.

Zamah, A. M., M. Delahunty, L. M. Luttrell, and R. J. Lefkowitz
2002. Protein kinase A-mediated phosphorylation of the β_2-adrenergic receptor regulates its coupling to Gs and Gi. demonstration in a reconstituted system. *Journal of Biological Chemistry*, 277:31249–31256.

Zeileis, A. and G. Grothendieck
2005. zoo: S3 infrastructure for regular and irregular time series. *Journal of Statistical Software*, 14(6):1–27.

Zhang, H.-Y., M. Gao, Q.-R. Liu, G.-H. Bi, X. Li, H.-J. Yang, E. L. Gardner, J. Wu, and Z.-X. Xi
2014. Cannabinoid CB2 receptors modulate midbrain dopamine neuronal activity and dopamine-related behavior in mice. *Proceedings of the National Academy of Sciences*, 111(46):E5007–E5015.

Zoratti, C., D. Kipmen-Korgun, K. Osibow, R. Malli, and W. F. Graier
2003. Anandamide initiates Ca(2+) signaling via CB2 receptor linked to phospholipase C in calf pulmonary endothelial cells. *British Journal of Pharmacology*, 140:1351–1362.

10 Appendix

10.1 List of Hazardous Substances

List of hazardous substances according to GHS that were used in this work.

Table 10.1. List of hazardous substances according to GHS used in this work.

Substance	Pictogram	H statement	P statement
2-Propanol		H225, H319, H336	P210, P241, P280, P303+P361+P353, P305+P351+P338, P405, P501
Acrylamide		H301 H312+H332, H315, H317, H319, H340, H350, H361f, H372	P201, P280, P302+P352, P305+P351+P338
DL-dithiothreitol		H302, H421	P264, P270, P273, P280, P301+P312+P330, P501
Ethanol		H225, H319	P210, P240, P241, P260, P280, P303+P361+P353, P501
Roti®-Histofix 4% (phosphate-buffered formaldehyde 4%)		H302, H317, H341, H350	P261, P280, P302+P352, P308+P313
Methanol		H225, H301, H311, H331, H370	P210, P280, P301+P310, P303+P361+P353, P304+P340, P405, P501
Phenylmethyl-sulfonyl fluoride		H301, H314	P260, P280, P301+P310+P330, P303+P361+P353, P304+P340+P310, P305+P351+P338+P310

Table 10.1. List of hazardous substances according to GHS used in this work.

Substance	Pictogram	H statement	P statement
Xylazine		H301	P264, P270, P301+P310, P321, P330, P405, and P501
Sodium azide		H300+H310, H373, H410	P273, P280, P301+P310+P330, P302+P352+P310, P391, P501
Sodium dodecylsulfate		H228, H302+H332, H315, H318, H335, H412	P210, P280, P302+P352, P304+P341, P305+P351+P338
Sodium flouride		H301, H315, H319	P264, P270, P280, P301+P310+P330, P337+P313, P501
Sodium hydroxide		H290, H314	P234, P280, P301+P330+P331, P303+P361+P353, P305+P351+P338, P310
TEMED		H225, H302+H332, H314	P210, P233, P280, P301+P330+P331, P305+P351+P338
Triton® X-100		H302, H318, H411	P273, P280, P305+P351+P338, P310

10.2 Direct CB2 stimulation and Vehicle Control in Epac1-CB2-HEK cells
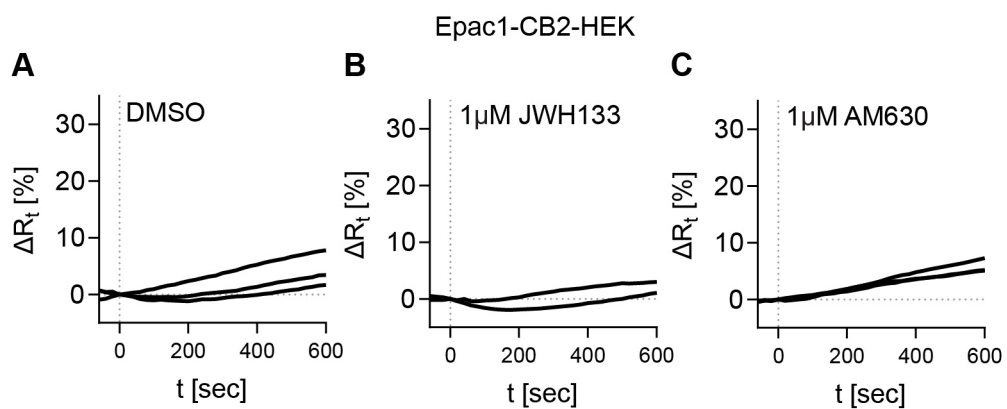
Figure 10.1. FRET responses to direct CB2 stimulation and vehicle control in Epac1-CB2-HEK cells. Time-dependent FRET ratio (ΔR_t) traces of Epac1-CB2-HEK cells stimulated with 1 µM JWH133, 1 µM AM630, and 0.1 % DMSO as indicated. Line plots represent the mean of all ROIs/cells in one recording.
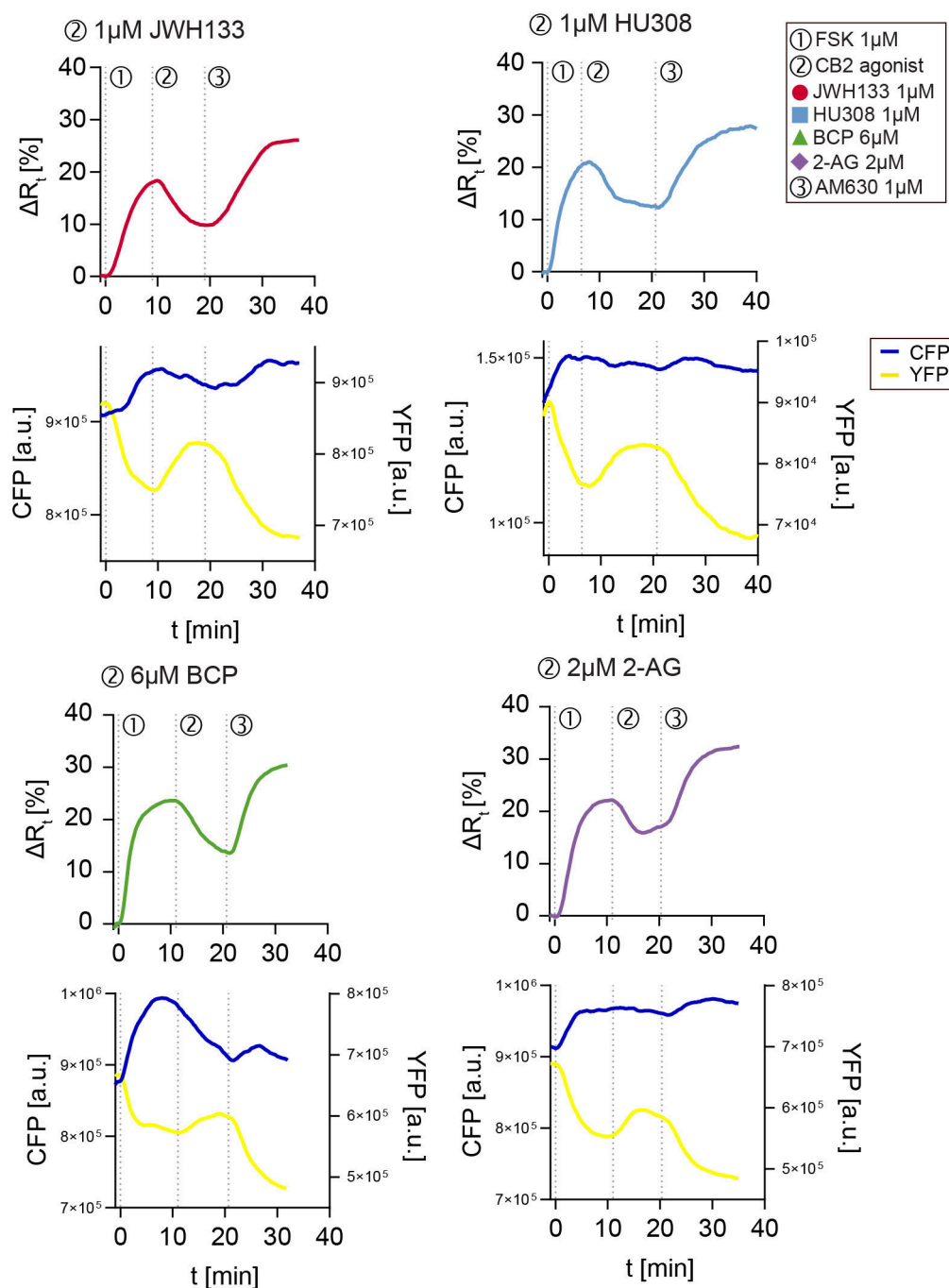
10.3 Single Channels from Representative FRET Recordings

Figure 10.2. Single channels CFP and YFP from CB2 agonist stimulation protocol in Epac1-CB2-HEK cells. Plots from representative FRET measurements in Figure 6.6A in Results section 6.2.2 and corresponding single emission channels CFP (blue) and YFP(yellow).
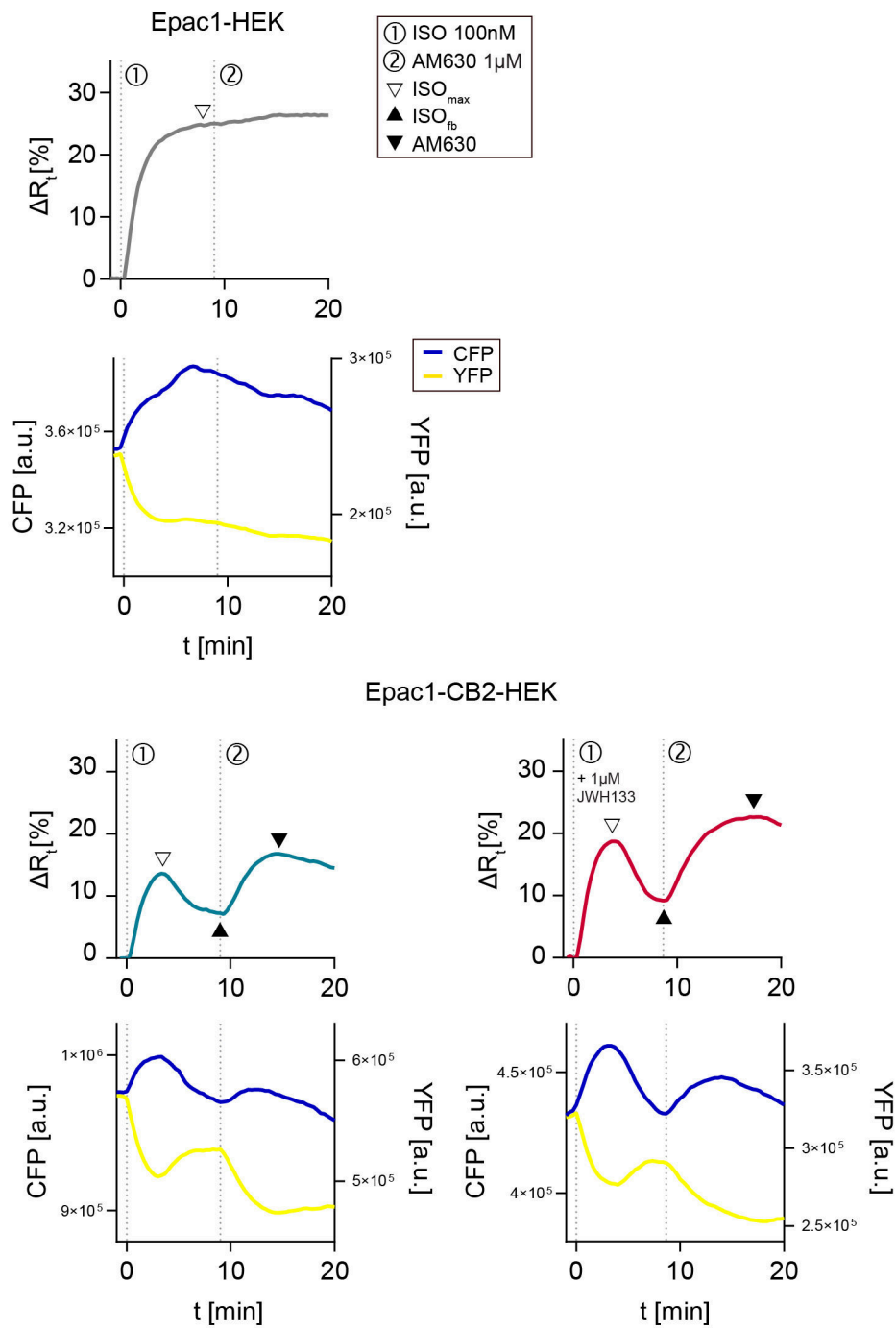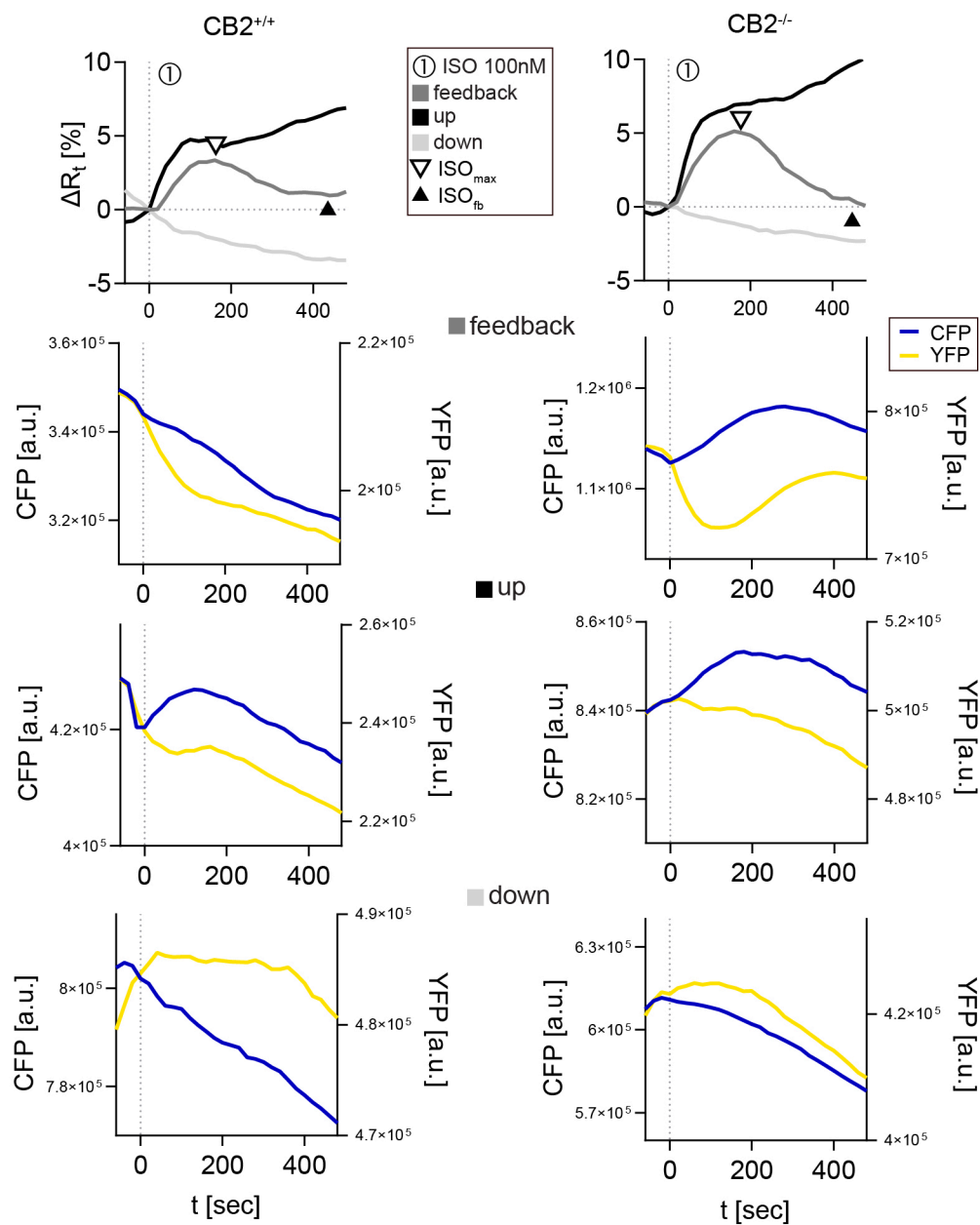
Figure 10.3. Single channels CFP and YFP from CB2 and βAR stimulation in Epac1-CB2-HEK cells. Plots from representative FRET measurements in Figure 6.7A in Results section 6.3.1 and corresponding single emission channels CFP (blue) and YFP(yellow).
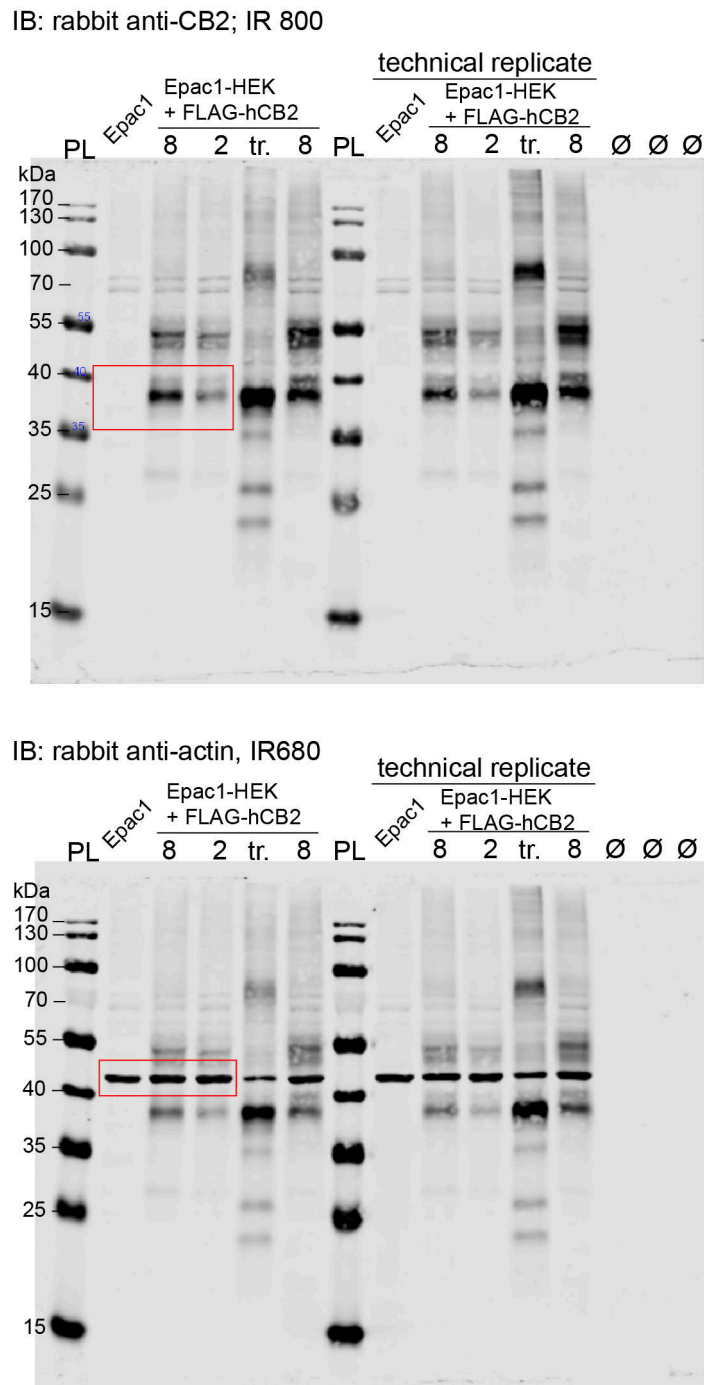
Figure 10.4. Single channels CFP and YFP from βAR stimulation in adult microglia from wildtype and CB2-deficient mice. Plots from representative FRET measurements in Figure 6.13C in Results section 6.4.3 and corresponding single emission channels CFP (blue) and YFP(yellow).

10.4 Original Western Blot images

Epac1-HEK
IB: rabbit anti-CB2; IR 800

Epac1-HEK
IB: rabbit anti-actin, IR 800

Figure 10.5. Original Western Blot images from Figure 6.1A in Results section 6.1.1. PL - protein ladder, IB - immunoblotting.

Figure 10.6. Original Western Blot images from Figure 6.1B in Results section 6.1.1. PL - protein ladder, IB - immunoblotting.

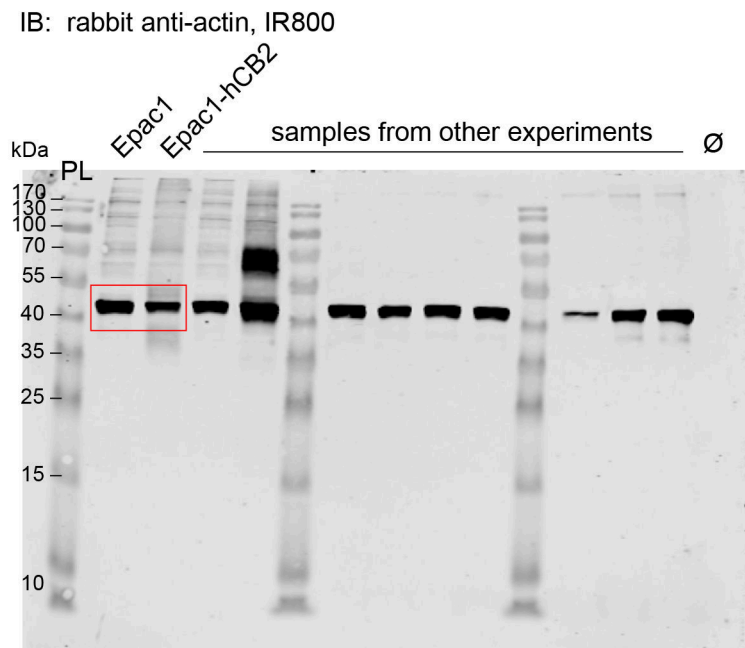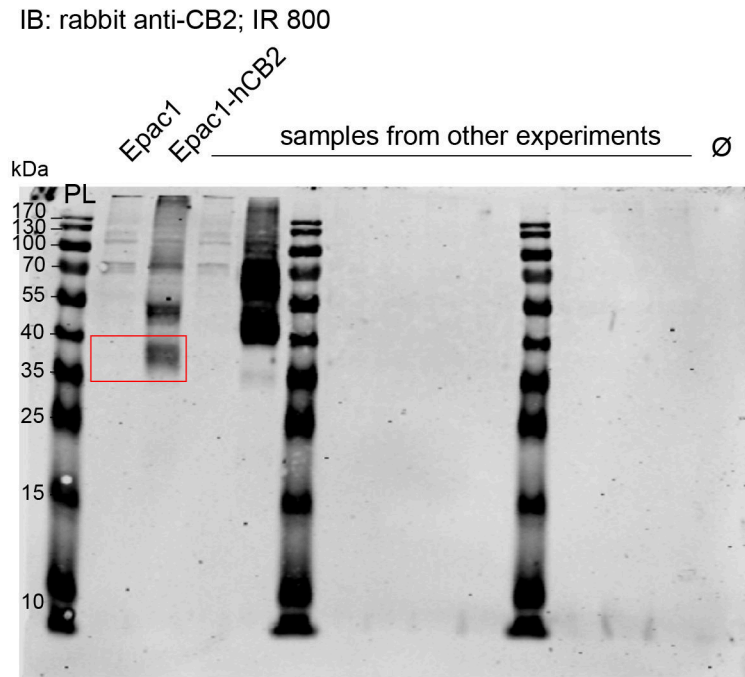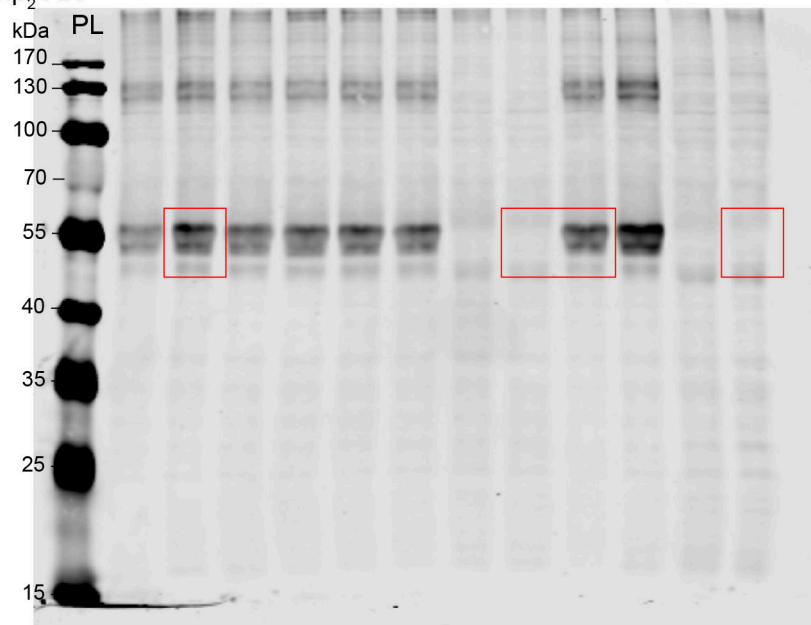**Figure 10.7. Original Western Blot images from Figure 6.1C in Results section 6.1.1.** PL - protein ladder, IB - immunoblotting.
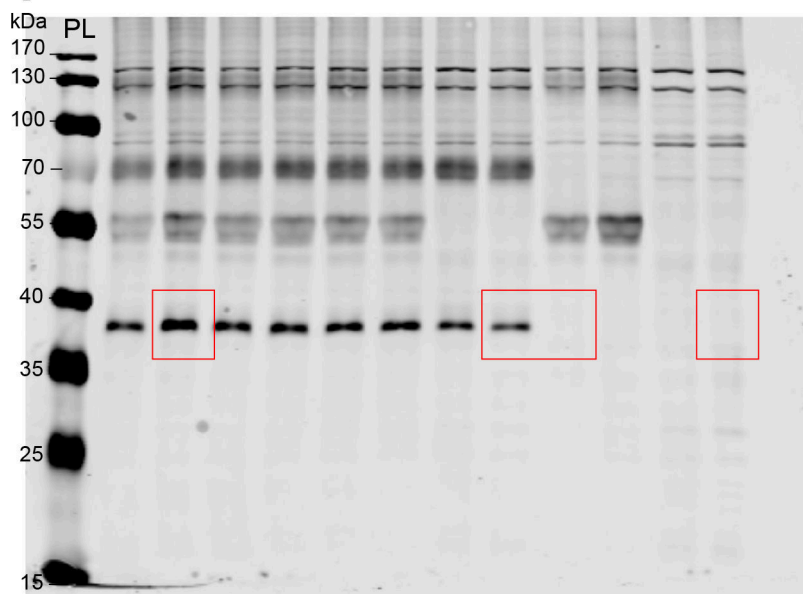
Figure 10.8. Original Western Blot images from Figure 6.8A Input in Results section 6.3.2. Input samples for FLAG-IP. PL - protein ladder, IB - immunoblotting, IP - immunoprecipitation.

IP: anti-FLAG, IB: rabbit anti-HA, IR 680

FLAG-hCB2   +   +   +   +   +   +   +   +   -   -

HA-hβ$_2$-AR   +   +   +   +   +   +   -   -   +   +   pcDNA3.1

IP: anti-FLAG, IB: rabbit anti-FLAG, IR 680

FLAG-hCB2   +   +   +   +   +   +   +   +   -   -

HA-hβ$_2$-AR   +   +   +   +   +   +   -   -   +   +   pcDNA3.1

Figure 10.9. Original Western Blot images from Figure 6.8A FLAG-IP in Results section 6.3.2. PL - protein ladder, IB - immunoblotting, IP - immunoprecipitation.
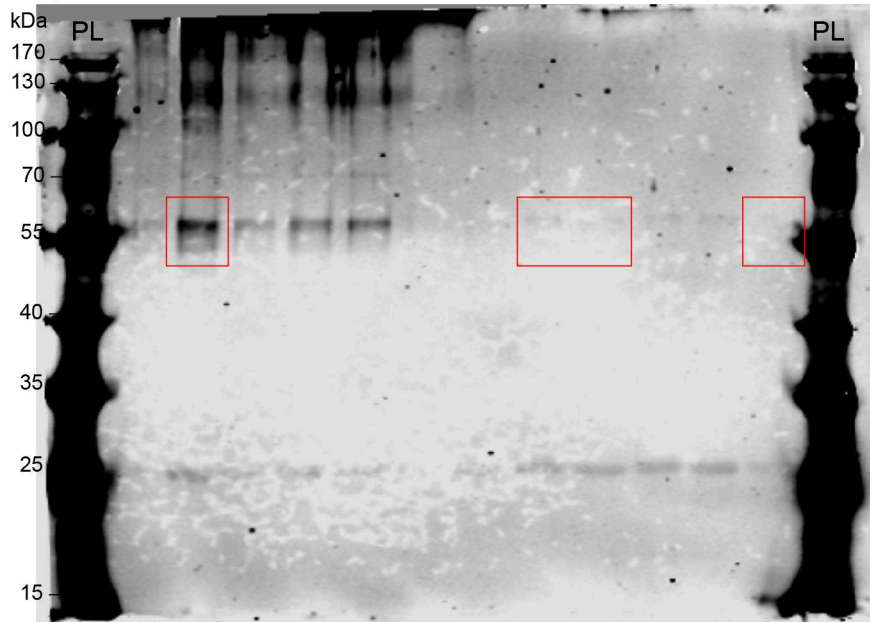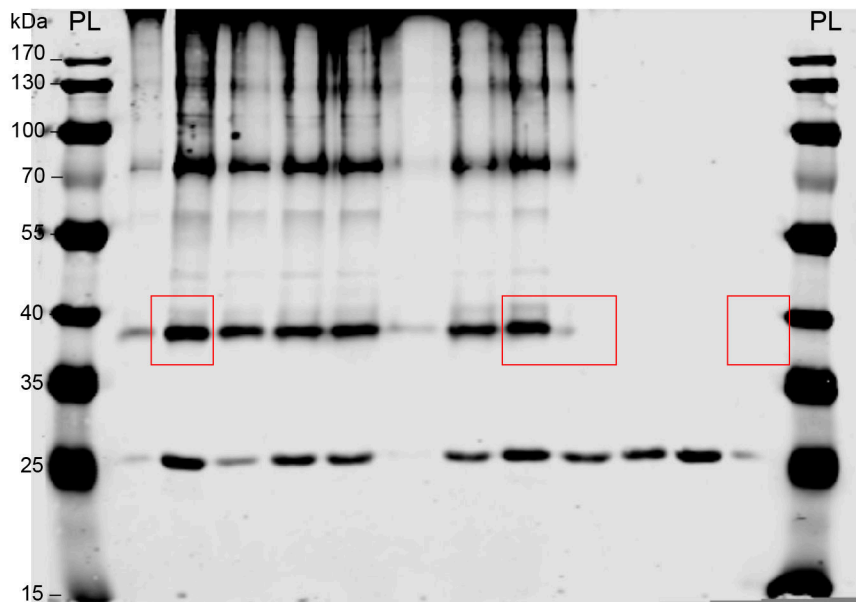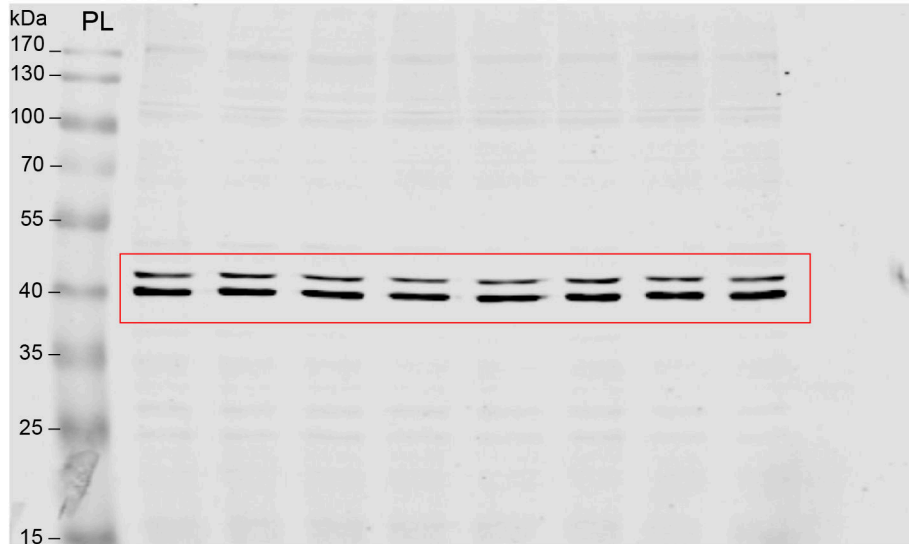
Figure 10.10. Original Western Blot images from Figure 6.8B Input in Results section 6.3.2. Input samples for HA-IP. PL - protein ladder, IB - immunoblotting, IP - immunoprecipitation.

Epac1-HEK, IB: mouse anti-ERK1/2, IR 800

1µM JWH133	+	-	+	+	+	-	-	
100nM ISO	-	+	+	+	-	+	-	DMSO
1µM AM630	-	-	-	+	+	+	+	Ø

Epac1-HEK, IB: rabbit anti-pERK1/2, IR 680

1µM JWH133	+	-	+	+	+	-	-	
100nM ISO	-	+	+	+	-	+	-	DMSO
1µM AM630	-	-	-	+	+	+	+	Ø

Figure 10.11. Original Western Blot images from Figure 6.10A in Results section 6.3.3. Epac1-HEK cells. PL - protein ladder, IB - immunoblotting, IP - immunoprecipitation.

Epac1-CB2-HEK, IB: mouse anti-ERK1/2, IR 800

1µM JWH133	+	-	+	+	+	-	-		
100nM ISO	-	+	+	+	-	+	-	DMSO	
1µM AM630	-	-	-	+	+	+	+		Ø

Epac1-CB2-HEK, IB: rabbit anti-pERK1/2, IR 680

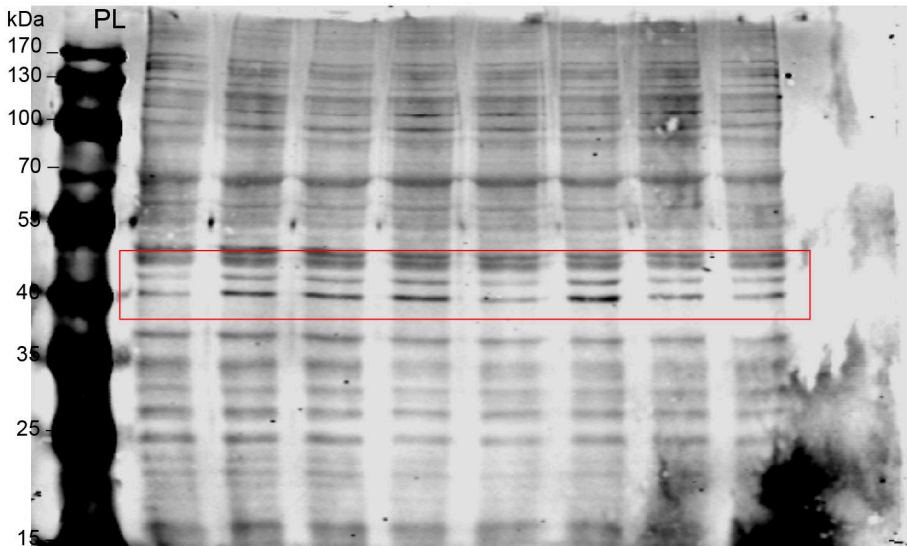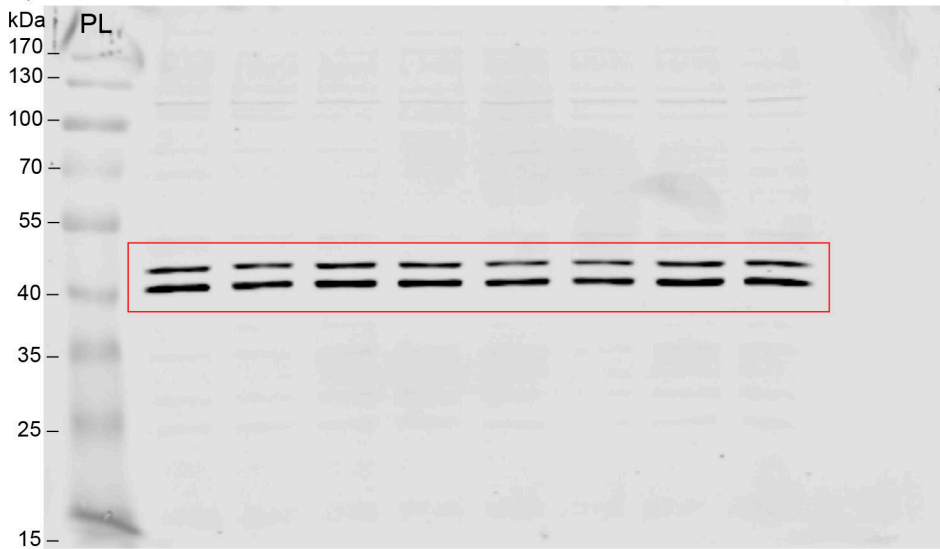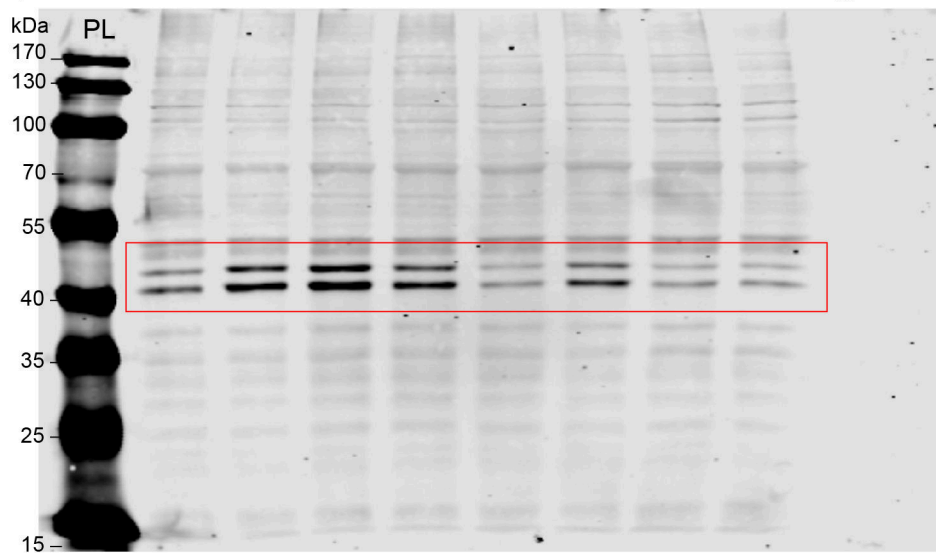| 1µM JWH133 | + | - | + | + | + | - | - | | |
| 100nM ISO | - | + | + | + | - | + | - | DMSO | |
| 1µM AM630 | - | - | - | + | + | + | + | | Ø |

Figure 10.12. Original Western Blot images from Figure 6.10A in Results section 6.3.3. Epac1-CB2-HEK cells. PL - protein ladder, IB - immunoblotting, IP - immunoprecipitation.

10.5 Meta-Analysis of RNAseq Expression Data

A detailed list of included studies (GSE) and individual samples (GSM) used in the meta-analysis of RNAseq expression data from adult mouse microglia in Results section 6.4.1.

Table 10.2. RNAseq studies included in meta-analsis in Results section 6.4.1. WT - wildtype, n.s. - not specified, wk - weeks.

GSM	Age [wk]	Tissue	Strain	Genotype	Sex	Treatment	Sorting	GSE	Reference
1061164-1061173, 1061182	9, 14, 18, 21	spinal cord	B6SJLF1/J, C57BL/6	WT	n.s.	none	CD11b+	43366	Chiu et al. (2013)
1533927	8-9	brain	C57BL/6J	WT	n.s.	none	CD11b+, CD45 low	62826	Gosselin et al. (2014)
1617046, 1617047, 1617052-1617055	10-12	brain	C57BL/6J	WT	n.s.	none	CD11b+, CD45 low	66211	Cronk et al. (2015)
1947165, 1947166, 1947172, 1947176, 1947185	8-10	brain	C57BL/6	WT	male	vehicle	CD11b+, GFAP low	75246	Srinivasan et al. (2016)
2055998-2056000, 2056007-2056010	13, 73	spinal cord	C57BL/6	$C9orf72^{+/+}$	n.s.	none	CD11b+	77681	O'Rourke et al. (2016)

Table 10.2. RNAseq studies included in meta-analsis in Results section 6.4.1. WT - wildtype, n.s. - not specified, wk - weeks.

GSM	Age [wk]	Tissue	Strain	Genotype	Sex	Treatment	Sorting	GSE	Reference
2104029, 2104030, 2104033-2104036	8	spinal cord, cortex, hippocampus	C57BL/6J	$Cx3cr1^{GFP/+}$	n.s.	none	CD45 int,CD11b int, GFP+	79812	Matcovitch-Natan et al. (2016)
2146911-2146916, 2146919, 2146920	10, 13, 65	brain	C57BL/6	WT	n.s.	none	CD11b+, CD45 int	81230	Safaiyan et al. (2016)
2373562, 2373565, 2373569, 2373571-2373573	60, 65	cortex	C57BL/6	$Cx3cr1^{GFP/+}$ PS2APP neg	n.s.	none	GFP+	89482	Friedman et al. (2018)
2642943-2642947	n.s.	brain	C57BL/6	WT	n.s.	none	CD11b+, CD45 low	89960	Gosselin et al. (2017)
2422380-2422388, 2422390, 2422395-2422398	6-8	cortex	C57BL/6	WT	male	water, saline injected	CD11b+	91387	McCarthy et al. (2018)
2463007-2463014	8, 21, 30, 43-47	brain	C57BL/6	$Cx3cr1^{GFP/+}$, $Ccr2^{RFP/+}$	both	behavioural testing	GFP+, RFP+	93824	Hernandez et al. (2017)
2683273-2683275	n.s.	brain	C57BL/6	$Cx3cr1$-Cre	n.s.	PBS	CD11b+	94054	Hwang et al. (2017)

Table 10.2. RNAseq studies included in meta-analsis in Results section 6.4.1. WT - wildtype, n.s. - not specified, wk - weeks.

GSM	Age [wk]	Tissue	Strain	Genotype	Sex	Treatment	Sorting	GSE	Reference
2528062-2528064	12	spinal cord	C57BL/6	$Cx3cr1^{GFP/+}$	male	none	GFP+	96055	Noristani et al. (2017)
2588502, 2588503, 2588513-2588515	6-8	brain, spinal cord	C57BL/6	$Cx3cr1$-Cre, $Dicer^{fl/fl}$	both	none	CD45 int, CD11b+, F4/80+, Ly6C-, Ly6G-	98142	Varol et al. (2017)
2648792-2648798, 2648823-2648827	8	hippocampus	C57BL/6N	WT	both	Saline injected	CD11b+	99622	Hanamsagar et al. (2017)
3490835-3490846	8	cortex, cerebellum, hippocampus, striatum	C57BL/6N	WT	n.s	none	CD45 low,CD11b+, TMEM119+	123021	Li et al. (2019b)
3555561-3555566	8	brain	C57BL/6J	WT	both	none	CD45 int, CD11b+	124829	ImmGen ULI

Table 10.2. RNAseq studies included in meta-analsis in Results section 6.4.1. WT - wildtype, n.s. - not specified, wk - weeks.

GSM	Age [wk]	Tissue	Strain	Genotype	Sex	Treatment	Sorting	GSE	Reference
3455331-3455339, 3455409, 3455410, 3455418-3455420	8, 25	cortex, cerebellum, hippocampus, spinal cord	C57BL/6J	WT	n.s	none	CD45 int, CD11b+, CD64+, CX3CR1+, F4/80 low	122108	ImmGen ULI

11 Acknowledgements

First of all, I would like to thank Prof. Dr. Meliha Karsak for offering me this project and the PhD position in her lab introducing me to the world of cannabinoid receptors. Thank you for all the help, feedback and support over the years. I learned a lot during my PhD time and I am grateful for that.

I would also like to thank Prof. Dr. Zoya Ignatova for kindly agreeing on being my co-supervisor and thesis committee member and for all the valuable feedback on my work.

I like to thank Prof. Dr. Viacheslav Nikolaev for being a member of my thesis committee and for the valuable feedback on my work as well as for all the help to set up the cAMP FRET imaging in the lab, that made this work possible. Thank you for giving me the plasmid, cell line and the animals and allowing me to do the first experiments in your lab. I learned a lot about the method from you and everyone in your lab and appreciated this opportunity very much.

A special thank you goes to all my colleagues in the lab for all the support and for having a nice work atmosphere. Christina, Nevena, and Ahmed, thank you for being great colleagues inside and outside of the lab. Thank you, Sebastian, for keeping the lab organised and all your help. I wish you all the very best for your future!

I like to thank everyone at the ZMNH for all their help and support in scientific and administrative questions. I value all the interesting discussions during talks, retreats and in between. Thank you to the organisers of the ASMB to offer this programme to students, I enjoyed being a part of it.

Thank you Laura, Silvia, and Christina for our daily lunch routine that helped me through the day, and all the Stammtisch action outside of work! I also appreciated all the other lunches, first floor kitchen rounds, dinners, barbecues, beer evenings, summer and Christmas parties that were always a lot of fun to be at!

Meiner Familie möchte ich im ganz Speziellen danken! Mama, Papa, Berni, vielen Dank, dass ihr immer ein offenes Ohr für mich hattet und mit mir über wissenschaftliche und andere Dinge diskutiert habt. Mama und Papa, ohne euer Interesse an Wissenschaft hätte ich vermutlich nie damit angefangen und auch noch meine kleine Schwester dazu motiviert. Ich danke euch für Alles!

Ein großes Dankeschön geht auch an meine Freunde in Hamburg, Hannover oder anderswo. Vielen Dank für all eure Unterstützung und die schöne Zeit, in der man die Arbeit mal beiseite legen konnte!

Last, but not least, I want to thank my husband James. Without you I would not have made it. Thank you for being by my side!

Eidesstattliche Versicherung

Hiermit versichere ich an Eides statt, die vorliegende Dissertation selbst verfasst und keine anderen als die angegebenen Hilfsmittel benutzt zu haben. Die eingereichte schriftliche Fassung entspricht der elektronischen Version. Ich versichere, dass diese Dissertation nicht in einem früheren Promotionsverfahren eingereicht wurde.

Hamburg, den _____   Unterschrift: _____